N 73-28529

NASA CONTRACTOR REPORT

NASA CR-2243

NASA CR-2243

DESIGN, FABRICATION, AND PERFORMANCE OF FOIL JOURNAL BEARINGS FOR THE BRAYTON ROTATING UNIT

by L. Licht and M. Branger

Prepared by
AMPEX CORPORATION
Redwood City, Calif. 94063
for Lewis Research Center

NATIONAL AERONAUTICS AND SPACE ADMINISTRATION • WASHINGTON, D. C. • JULY 1973

1. Report No.	2. Government Accession No.	3. Recipient's Catalog No.
NASA CR-2243		

4. Title and Subtitle	5. Report Date
DESIGN, FABRICATION, AND PERFORMANCE OF FOIL JOURNAL BEARINGS FOR THE BRAYTON ROTATING UNIT	July 1973
	6. Performing Organization Code

7. Author(s)	8. Performing Organization Report No.
L. Licht and M. Branger	RR 72-25
	10. Work Unit No.

9. Performing Organization Name and Address	11. Contract or Grant No.
Ampex Corporation 401 Broadway Redwood City, California 94063	NAS 3-15341
	13. Type of Report and Period Covered
12. Sponsoring Agency Name and Address	Contractor Report
National Aeronautics and Space Administration Washington, D.C. 20546	14. Sponsoring Agency Code

15. Supplementary Notes

Project Manager, William J. Anderson, Fluid System Components Division; Technical Advisor, James H. Dunn, Power Systems Division; both of NASA Lewis Research Center, Cleveland, Ohio

16. Abstract

Foil bearings were designed and manufactured to replace pivoted-shoe journal bearings in an existing Brayton Cycle turbo-alternator-compressor. The design of this unconventional rotor support was accomplished within the constraints and space limitations imposed by the present machine, and the substitution of foil bearings was effected without changes or modification of other machine components. A housing and a test rig were constructed to incorporate the new foil-bearing support into a unified assembly with an air-driven rotor and the gimbal-mounted thrust bearing, seals, and shrouds of an actual Brayton Rotating Unit. The foil bearings required no external pressure source, and stable self-acting rotation was achieved at all speeds up to 43,200 rpm. Excellent wipe-wear characteristics of the foil bearings permitted well over 1000 start-stop cycles with no deterioriation of performance in the entire speed range. Salient aspects of foil-bearing design and manufacture and of assembly and alignment procedures are reported in considerable detail. A full account is given of rotor and bearing dynamics in the vertical attitude during starting, stopping, and traversing the region of resonances and of temperature measurements in the course of a slow transient to thermal equilibrium. The performance during a 100-hour run is reported and documented, and the state of journals and foils is examined upon completion of 1027 start-stop cycles.

17. Key Words (Suggested by Author(s))	18. Distribution Statement
Journal bearings Gas bearings Foil bearings Turbomachinery	Unclassified - unlimited

19. Security Classif. (of this report)	20. Security Classif. (of this page)	21. No. of Pages	22. Price*
Unclassified	Unclassified	110	$3.00

* For sale by the National Technical Information Service, Springfield, Virginia 22151

CONTENTS

ILLUSTRATIONS

ILLUSTRATIONS (cont)

ILLUSTRATIONS (cont)

ILLUSTRATIONS (cont)

ILLUSTRATIONS (cont)

LIST OF SYMBOLS

A_f, A_g, A_{fg}	Constants involving bearing geometry (Appendix 2)
B_e	Bearing span
b	Distance between lines of contact of tangent plane to journal and guide
C_1, C_2	Integration constants (Appendix 2)
E	Modulus of Elasticity
F	Displacement of foil at center of wrap
G_A, G_B	Displacements of gimbals at monitoring stations
h*	Clearance in region of uniformity (Appendix 2)
h	Clearance, measured at center of wrap
h'	Apparent clearance at center of wrap (Appendix 3)
J	Displacement of journal along bisector of wrap (parallel to F)
L	Length of rotor
ℓ	Length of foil sector between lines of tangency to 2 guides (Fig. 46)
N	Rotor speed in rps (or rpm)
P	Distance between monitoring planes of journal probes
Q	Ratio (eq. 21, Appendix 2)

R	Radius from center of bearing to center of fixed guide (Fig. 46 , Appendix 2)
r_o	Radius of journal
r_g	Radius of guide
S	Distance between outer edges of seals
T	Tension per unit width of foil
t	Foil thickness
$U = r_o \omega$	Surface speed of journal
u	Velocity component of fluid in clearance parallel to journal surface
u_C, u_T	Imbalances referred to compressor and turbine balancing planes
W	Weight of rotor
X, Y	Orthogonal components of journal displacement in monitoring planes
x, y	Cartesian coordinates
α	Coefficient of linear thermal expansion
α_C, α_T	Angular locations of imbalance referred to compressor and turbine balancing planes and measured from arbitrary reference line
$\beta = \theta/6$	Angle (Fig. 46 , Appendix 2)
Δ , δ	Increment (e.g. of temperature, length etc.)
δ	Width of annulus between foil and guide-support (Fig. 44)

$\theta = \pi/2$	Angle of wrap (Fig. 46)
$\Lambda = \alpha/\alpha_j$	Normalized coefficient of thermal expansion
λ	Thermal conductivity
μ	Viscosity
ν	Poisson's ratio
τ	Temperature (τ_o - Reference Temperature)
$\varphi = \Delta\tau/\Delta\tau_j$	Normalized temperature increment
$\omega = U/r_o$	Angular velocity of rotor

SUBSCRIPTS

a	Ambient
C	Compressor (Compressor end)
c	Copper
f	Foil
g	Guide (Guide-support of foil)
h	Housing interior (Bearing cavity)
j	Journal
s	Steel
T	Turbine (Turbine end)

1.0 INTRODUCTION

The present report is an important milestone in the development of foil bearings. Its contents, supplemented by earlier NASA publications, CR-1157, CR-1563, and CR-72864, furnish a thorough review of purposefully applied research, which produced a new technology and resulted in the development of a superior, gas-lubricated rotor support. This program was initiated to provide an alternative method of rotor support for the NASA Brayton Cycle Unit (BRU), at a time when several turboalternators, supported on gas lubricated, pivoted-shoe journal bearings, were being subjected to a series of tests at the Lewis Research Center.

It is well known that the most severe handicaps encountered in the application of gas-lubricated bearings to high-speed turbomachinery are due to hydrodynamically induced instabilities of motion and to the absence of boundary lubrication. The instability limits the speed and mass of the rotor, while the inability of gaseous films to furnish effective boundary lubrication exposes the bearing surfaces to damage during starting, stopping and high-speed contacts. Such difficulties are further compounded by poor tolerance of particles entering the bearing gap, limited accommodation of misalignment, and sensitivity of dynamic performance to changes in clearance caused by differential expansion and temperature gradients.

Some of the problems encountered with fixed, rigid-surface gas bearing were partly resolved in the Brayton Cycle Unit by resorting to pivoted-

shoe journal bearings. Stability in the operating range of the machine was eventually secured by increasing the preload of a flexibly mounted shoe, but starting and stopping could only be achieved with the aid of a cumbersome method of external pressurization via the pivots. This means of support required stable motion of the rotor and of six shoes in both the pressurized and self-acting modes of operation. The semi-flexible system was capable of accommodating misalignments and rotor excursions within the clearance-limit of seals, but did not completely resolve the problem of high-speed rubs and scoring of bearing surfaces by particles and debris. Added to complexity of construction and the need of external pressurization was the problem of friction and wear at the pivots.

Without assigning an order of importance to various considerations, the following advantages may be expected from foil bearings. Rotors supported in foil bearing have been shown both analytically and experimentally to be free from whirl-instability and from resonances at excitation of frequency equal half the rotational speed. The inherent flexibility allows the foil bearing to tolerate both geometrical and thermal distortions and makes it also relatively immune to abrasive particulates entering the bearing gap, because the clearance is bounded on one side by an easily deformable surface. Since contact during starting and stopping is distributed over a multiplicity of points on the conforming foil-surface, the bearing is endowed with excellent wipe-wear and longevity characteristics. The prognosis based on the present series of tests is for a likely extension of useful foil-bearing life to several thousand start-stop cycles, without deterioriation of performance in the entire speed range. Needless to say that this may be accomplished without the aid of external pressurization, which represents a most attractive simplification with respect to the present journal bearings of the BRU. Not to be overlooked is the superiority of foil

bearings over flexible-reed bearings with regard to stiffness, ease of starting, assembly, and simplicity of construction.*

The substitution of foil bearings for pivoted-shoe bearings within the space limitations and constraints imposed by the existing Brayton Cycle Unit (BRU) presented a formidable task. The initial difficulties were compounded by the stipulation that an acceptable design should involve only minimal changes in existing machine components, and that the foil journal-bearings be fully compatible with the gimbal-mounted thrust bearing and the rotor assembly, for which no changes of configurations were permitted. Added to tasks of foil-bearing design and fabrication was the construction of a test rig, in which all bearings, shrouds, seals, and the rotating assembly were to be combined into a unified structure.

The construction of operable gas bearings for a high-speed turbomachine requires both skill and considerable effort. Even when the development of gas bearings is initiated simultaneously, and coordinated with the design and construction of the entire system, the complexity of problems and the difficulties to be overcome may be enormous. For the Brayton Rotating Unit, approximately 45% of contents of the Final Report [1]** were devoted to the pivoted-shoe journal bearings and the gimbal-mounted thrust bearing. This ratio undoubtedly reflects the magnitude of

*Comparison with a flexible-reed bearing, of dimensions very similar to the present-foil bearing, shows that the foil bearing is at least 4 times stiffer and has a frictional starting-torque that is smaller by an order of magnitude. (See Swenson, K.R., Hughes, N.M. and Heuer, D.F., "Evaluation of Gas Lubricated Hydrodynamic Bearings in a Gas Turbine Environment," AiResearch Manufacturing Division, the Garrett Corporation, Technical Report AFAPL-TR-72-41, prepared under Contract No. F33615-71-C-1376, Air Force Aero Propulsion Laboratory, Air Force Systems Command, Wright-Patterson Air Force Base, Ohio 45433).

**Numbers in square brackets refer to references.

effort, the complexity of the problem, and the obstacles in development encountered by the manufacturer.*

In view of the foregoing, the successful application of foil bearings to the existing BRU represents a significant achievement. In our endeavors, we have relied and capitalized on new technology, developed under the sponsorship of NASA and thoroughly documented in a series of NASA CR-reports and ASME publications [2 to 7,9]. The present report contains a detailed description of design, and of methods of manufacture, assembly, alignment, and testing. Results are presented with regard to rotor dynamics during starting and stopping and throughout the operating speed range.

Specifically, and in addition to a complete set of engineering drawings furnished under separate cover to NASA, the report contains numerous photographs, illustrations and schematic drawings of foil-bearing components and assemblies. Experimental data is presented in the form of oscillograms of rotor orbits, and of frequency scans of rotor and gimbal amplitudes. The motion of the rotor axis ("conicity") is assessed from oscillograms of time-base displays of outputs from parallel probes, one probe in each monitoring plane, and the variation of foil-bearing clearance with increasing and decreasing speed is documented. Coastdown curves are furnished and compared at various temperatures and states of wear. Measurements of foil and foil-support temperatures are made during slow transients, in the process of attaining thermal equilibrium.** The histories of a continuous 100-hour run at rated speed and of 1000 start-stop cycles are documented by data recorded at suitable time intervals.

---

*AiResearch Manufacturing Company of Arizona (Division of the Garrett Corporation)

**Thermal equilibrium conditions, with fluid friction in the bearing clearance as the heat source. It is to be noted that temperature differences and gradients associated with such tests may be as large, or greater than during hot runs [1].

2.0 DESIGN, FABRICATION AND ASSEMBLY

2.1 General Considerations and Specific Requirements

The location and configuration of the pivoted-shoe journal bearings in the Brayton Rotating Unit, coupled with the imposed constraints, required that the foil bearings retain the diameter, length and span of their predecessors. Furthermore, the only structural components available for the support of bearing carriers were the ingot iron end-bells, which constituted not only integral parts of bearing assemblies to be replaced, but also essential components of the magnetic circuit of the alternator (Fig. 2 and Fig. 26 of ref. [1]). The present design, therefore, involved the construction of new end-bells of virtually unchanged configuration, to which the new foil-bearing supports and guides were to be securely fastened. Aimed at was the highest degree of accuracy of position, and of parallelism of foil guide-supports with the rotor axis.

The mounting of carrier assemblies by means of flexure beams was modified and adapted to present requirements. The components, however were fastened and secured by means of precision press-fits of flexure beams, rather than by brazing [1]. The foil bearing guide-supports and the ingot iron end-bells were joined in this manner into single assemblies, interchangeable with the existing carriers. These units were made fully compatible with the gimbal thrust-bearing and other components of the BRU, so that the replacement of pivoted shoes with foil bearings could be accomplished with ease.

In addition to constraints of size and space, consideration had to be given to possible conflicts with sequence and procedure in the assembly of the entire machine. Provision was made for alignment and redoweling of the foil-bearing assemblies in a BRU housing, and for centering of the rotor after insertion and tensioning of foils. Alignment, assembly, and tensioning tools and fixtures were constructed for this purpose. A comprehensive outline of assembly procedure is given in Appendix 1 of this report.

The basic foil-bearing arrangement, described in considerable detail in references [2] through [7], was retained, but integration of the concept into the present design involved many changes and innovations. Included among the latter were the foil guide-supports, which combined the function of sturdy carriers with that of nearly continuous and concentric envelopes and exterior heat equalizers. This type of construction made it possible to dispense with clusters of individual pins and to mill cylindrical guide-surfaces at adjacent extremities of supporting sectors. Thus, with the addition of only two free guides and clamps, and of a foil-lock integral with the structure, simple means were provided for completing the foil-loop, equalizing the preload, centering the journals, and securing the foils.

Although the effects of thermal expansion on changes of foil-bearing clearance are moderated by the ability of the foil to extend, or to contract with accompanying changes in tension, careful attention was given to the relative expansion of bearing components within limits of anticipated temperatures, and to the subsequent selection of foil and foil-support materials.* Metals with suitable coefficients of thermal expansion were selected on the basis of the simplified analysis given in Appendix 2,

*The expansion of the journal containing the press-fitted copper shunt was fixed by the existing rotor.

which preceded the more comprehensive numerical work reported in reference [9]. Since suitable foil materials span a range of coefficients of thermal expansion from at least 4×10^{-6} to 10×10^{-6} in/in/°F (7.2×10^{-6}–18×10^{-6} m/m/°C), an additional degree of freedom may be gained by simply replacing a foil of one expansivity with another. This requires no changes in bearing dimensions and geometry and provides versatility that is not attainable with rigid-surface bearings.

The BRU rotor cannot be installed as a single unit after balancing, and the remanent imbalance is unavoidably increased in the process of reassembly, particularly at the compressor end. At resonance, the motion was generally quasi-conical and danger of contact between the rotor and stationary components was greatest at the compressor-end seal. In order to provide a maximum margin of safety at large rotor excursions, great care was exercised to ensure not only the concentricity of journals with reference bores in foil-carrier assemblies, but also the concentric alignment of foil-carrier assemblies and seals.

The foregoing considerations and requirements of design, fabrication and assembly are dealt with in considerable detail in sections (2.2), (2.3) and (2.4).

2.2 Foil-Bearing Configuration and Function of Components-Materials

The foil-bearing configuration is illustrated in the isometric drawing in Fig. 1. The foil-bearing carrier is attached to the ingot iron end-bell of the alternator by means of six, press-fitted flexure beams. The foil-carrier assembly, mounted on the end bell, consists of an inboard and outboard plate and of three foil guide-supports. Each of the three guide-support segments is pinned to the inboard plate by two flexure-beam extensions. The subassembly, consisting of the flexure beams, the inboard plate, and three guide-supports is then joined permanently to the end-bell by means of a simultaneous press fit of six flexure-beam shanks. The

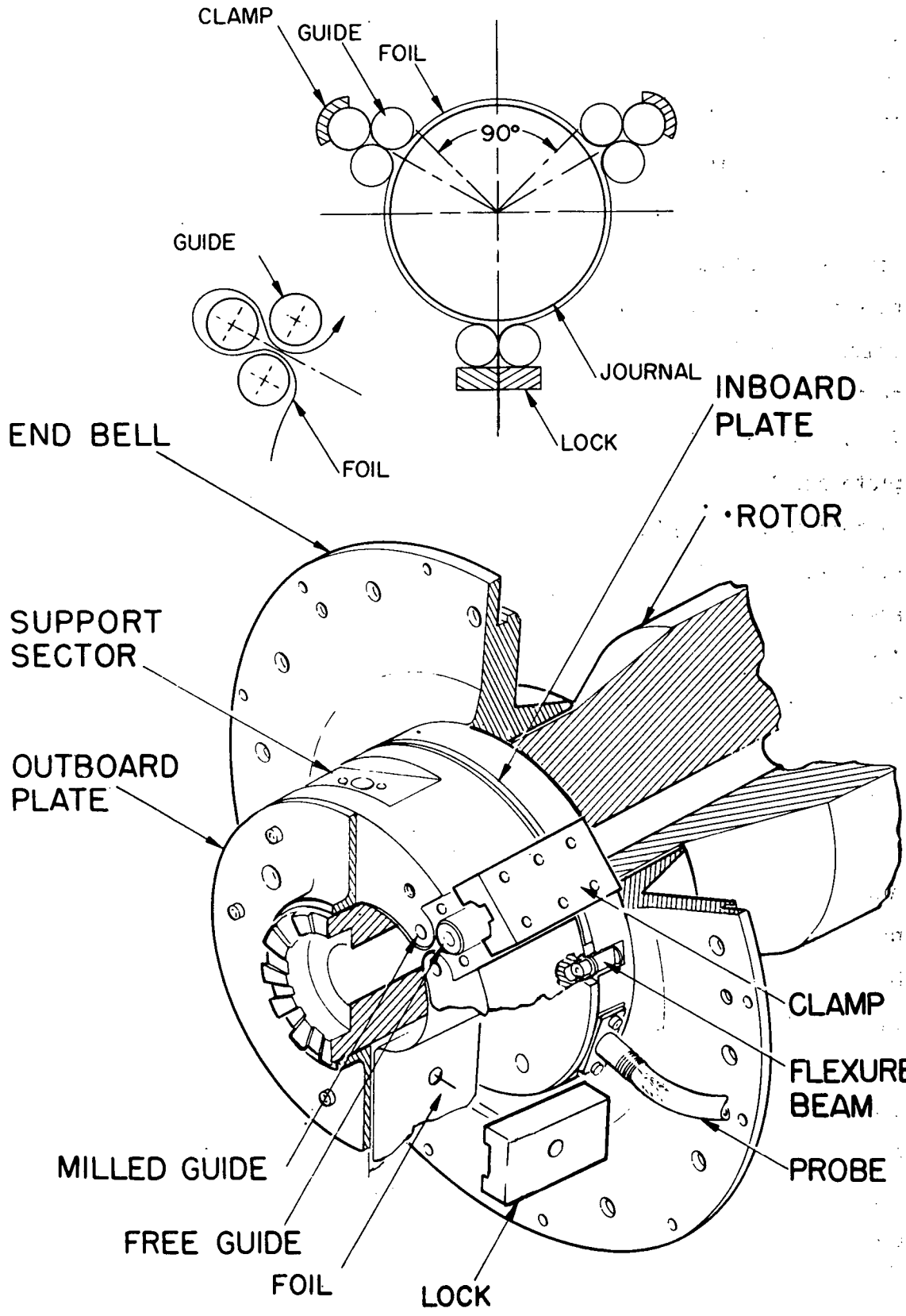

Fig. 1 Isometric Drawing of Foil Bearing Assembly

outboard plate is doweled and fastened with screws to ground end-faces of the foil guide-supports. The plate is removable for the insertion of the foil. A view of a complete foil-bearing carrier, inclusive of end bell and rotor shroud, is shown in Fig. 2.

Essential components of a foil-bearing carrier are illustrated in the photograph of Fig. 3. In the background is the ingot iron end-bell, the face of which contains six holes and slots to accommodate the flexure beams. On the right hand side of the photograph is the outboard plate, and on the left hand side the inboard plate, surrounded by the flexure beams. The lower shanks of the flexure beams are press-fitted into the inboard plate and into the foil guide-supports, and the upper shanks are then forced into corresponding holes in the end-bell. In the center of Fig. 3, arranged in a manner of an exploded view, are three foil guide-supports. Shown also are the free, cylindrical guides and associated clamps and a locking bar. A similar view of foil-bearing components is shown in Fig. 4, alongside a fully assembled foil-bearing carrier. Additional views of assembled foil-bearing carriers, with outboard plate, free guides and clamp removed, are contained in Fig. 5 and Fig. 6.*

As previously stated, the replacement of pivoted-shoe bearings with foil bearings was to be accomplished with minimal changes in BRU components. The end-bells, therefore, retain their initial configuration, and the only modification is a slightly thicker section, reinforcing the region in the vicinity of press-fit holes for the flexure beams. The foil guide-supports incorporate fixed guide surfaces, milled at their extremities, and furnish a sturdy frame for foils under tension. When reinforced by the outboard and inboard plates, and joined permanently to the end-bells, the three segments provide a rigidly integrated unit for clamping the free guides and securing the foil with a foil-lock bar.

*The plate in the foreground of Fig. 5 and Fig. 6 is a spare inboard plate.

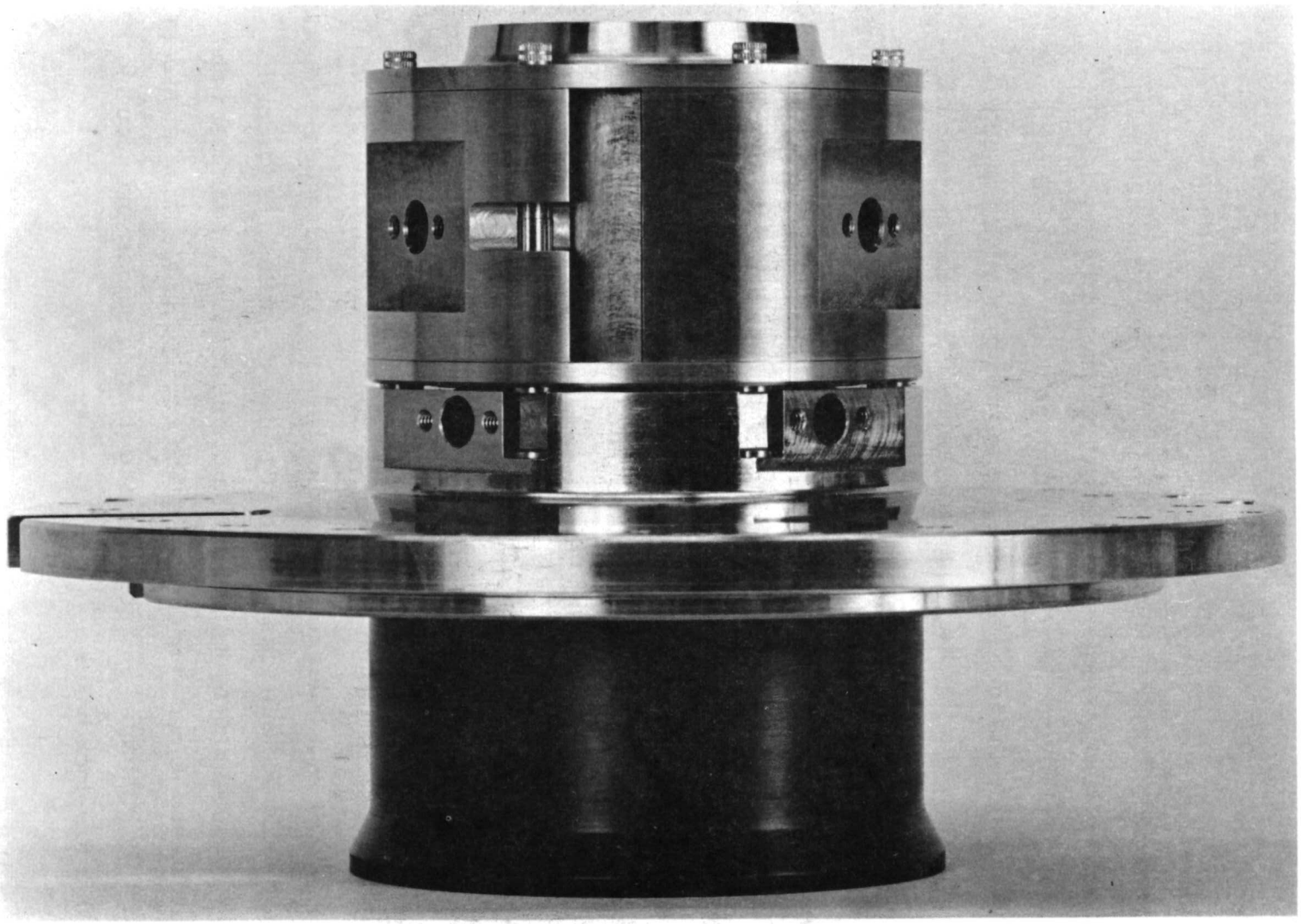

Fig. 2 Foil-Bearing Assembly. - Foil Carrier and End Bell with Rotor Shroud Attached

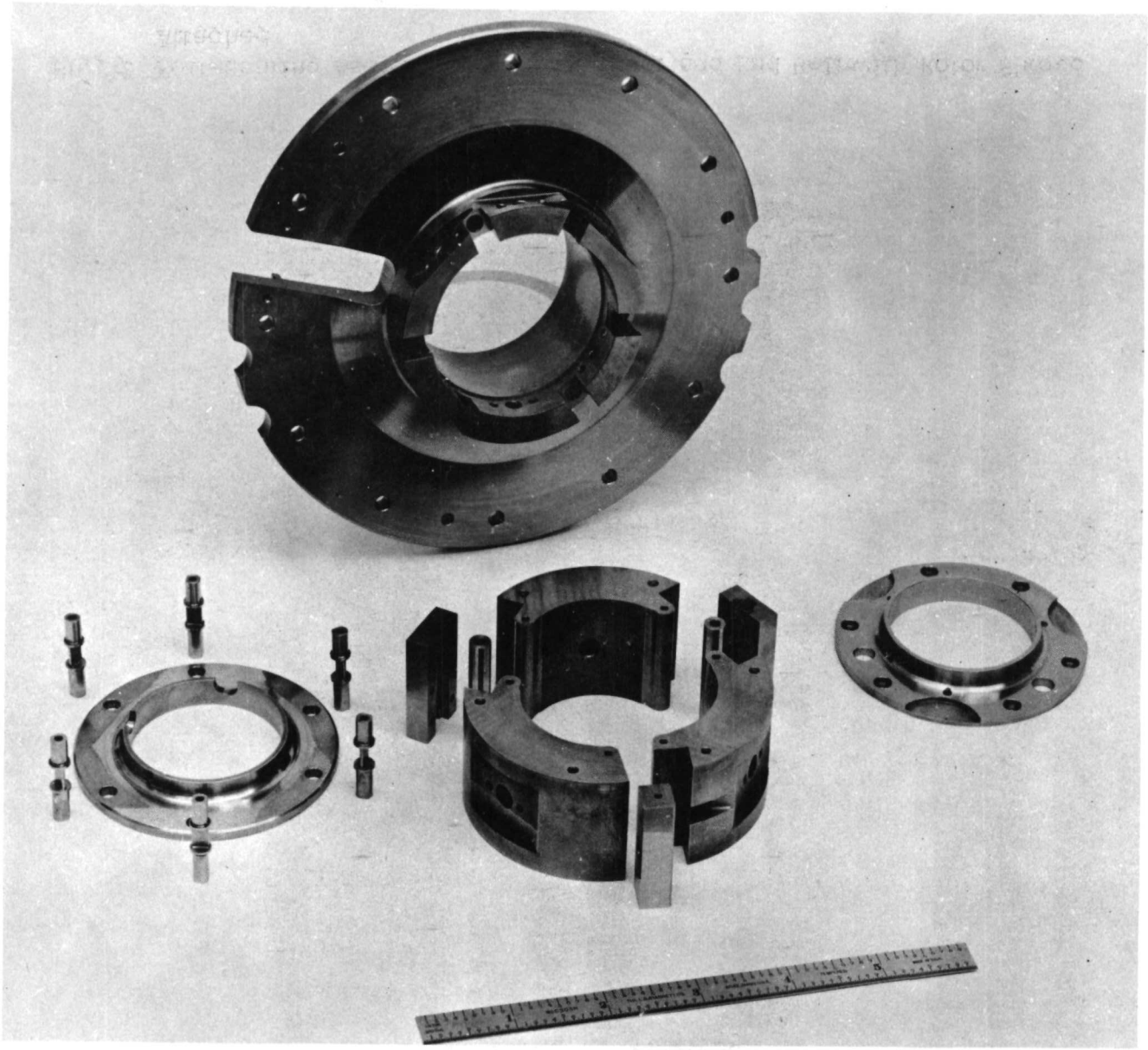

Fig. 3 Components of Foil Bearing Prior to Assembly

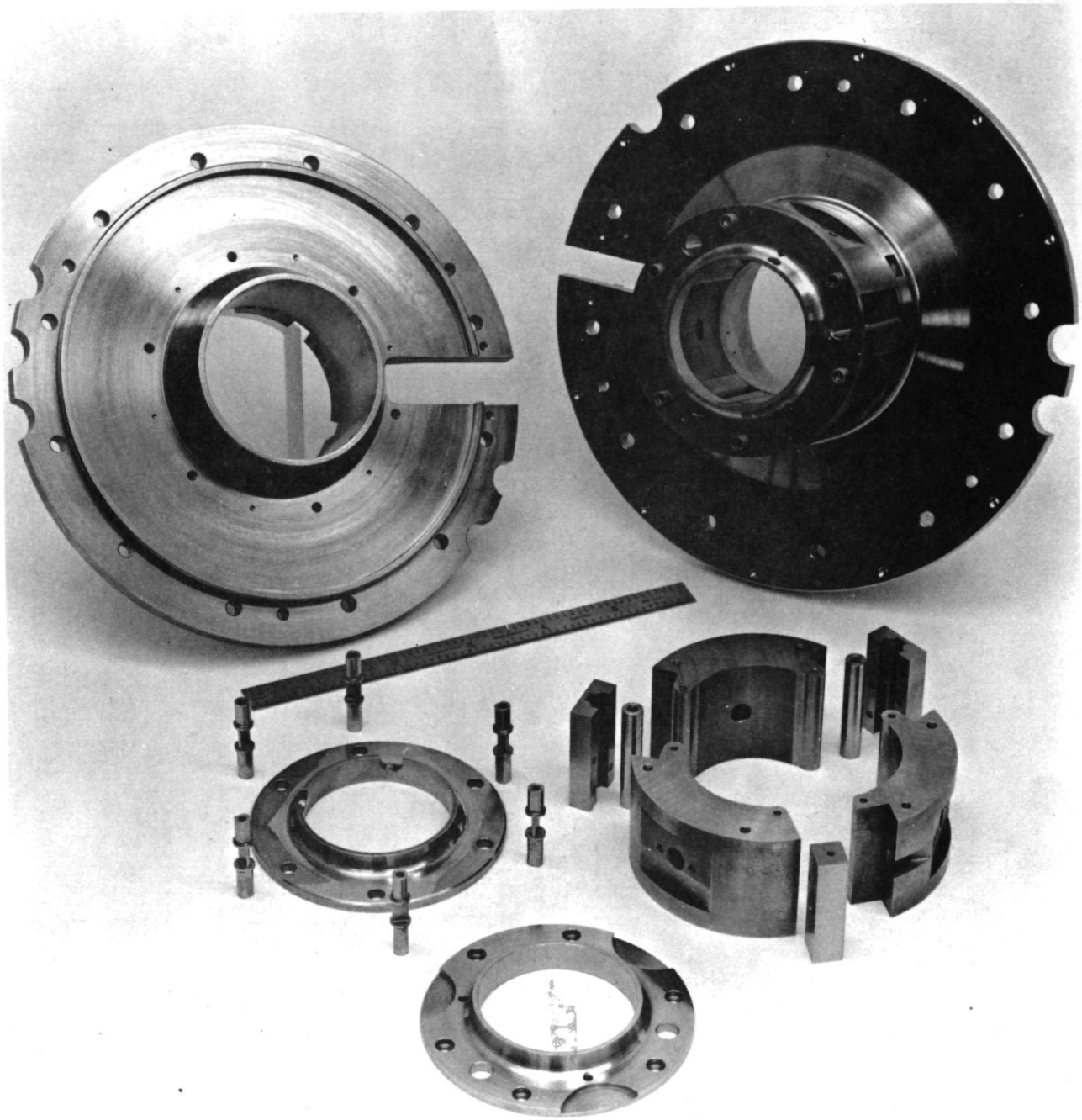

Fig. 4 Components of Foil Bearing and Assembled Foil-Bearing Carrier

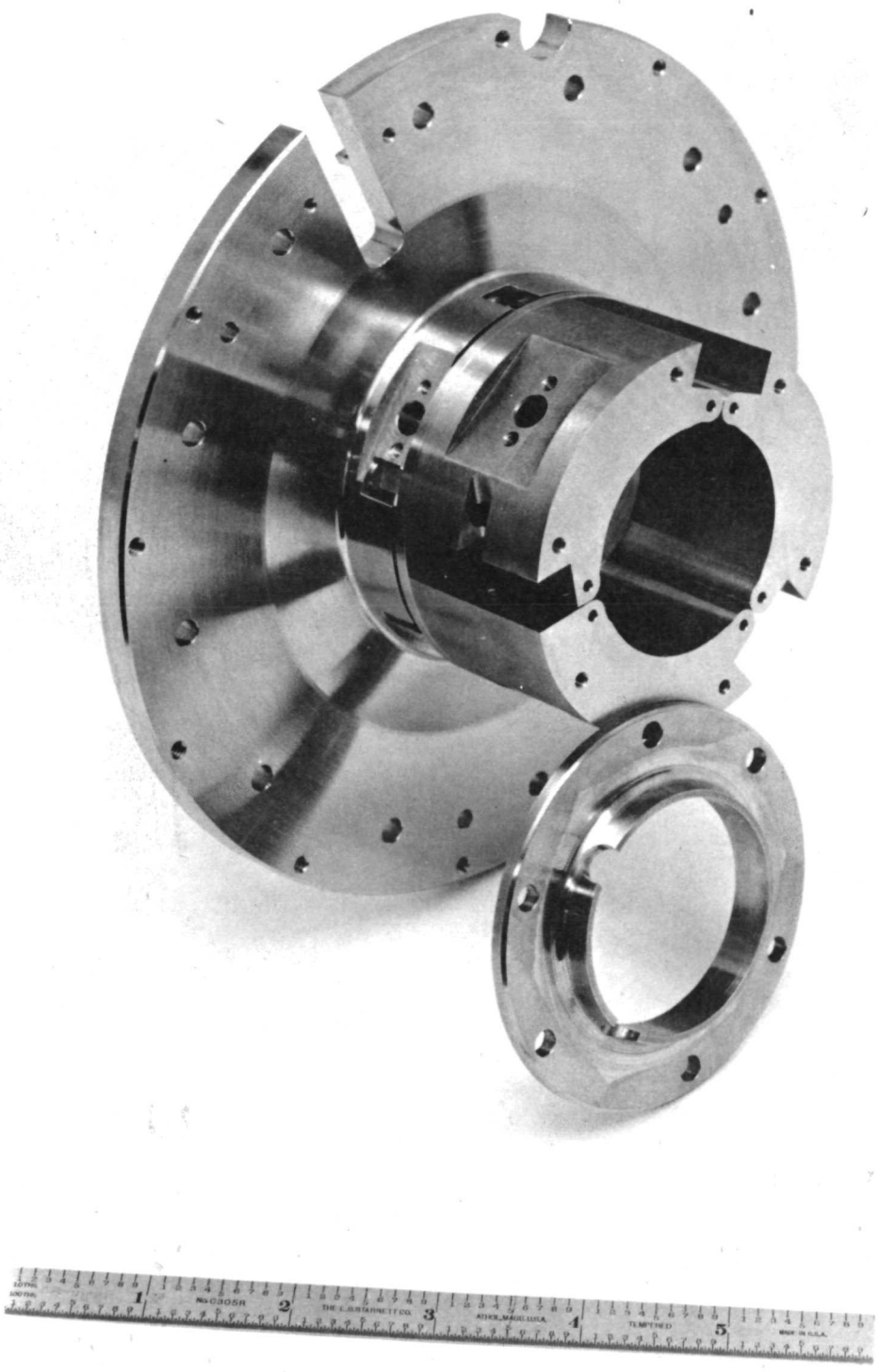

Fig. 5 Foil-Bearing Carrier Assembly with Outboard Plate Removed.- Side View

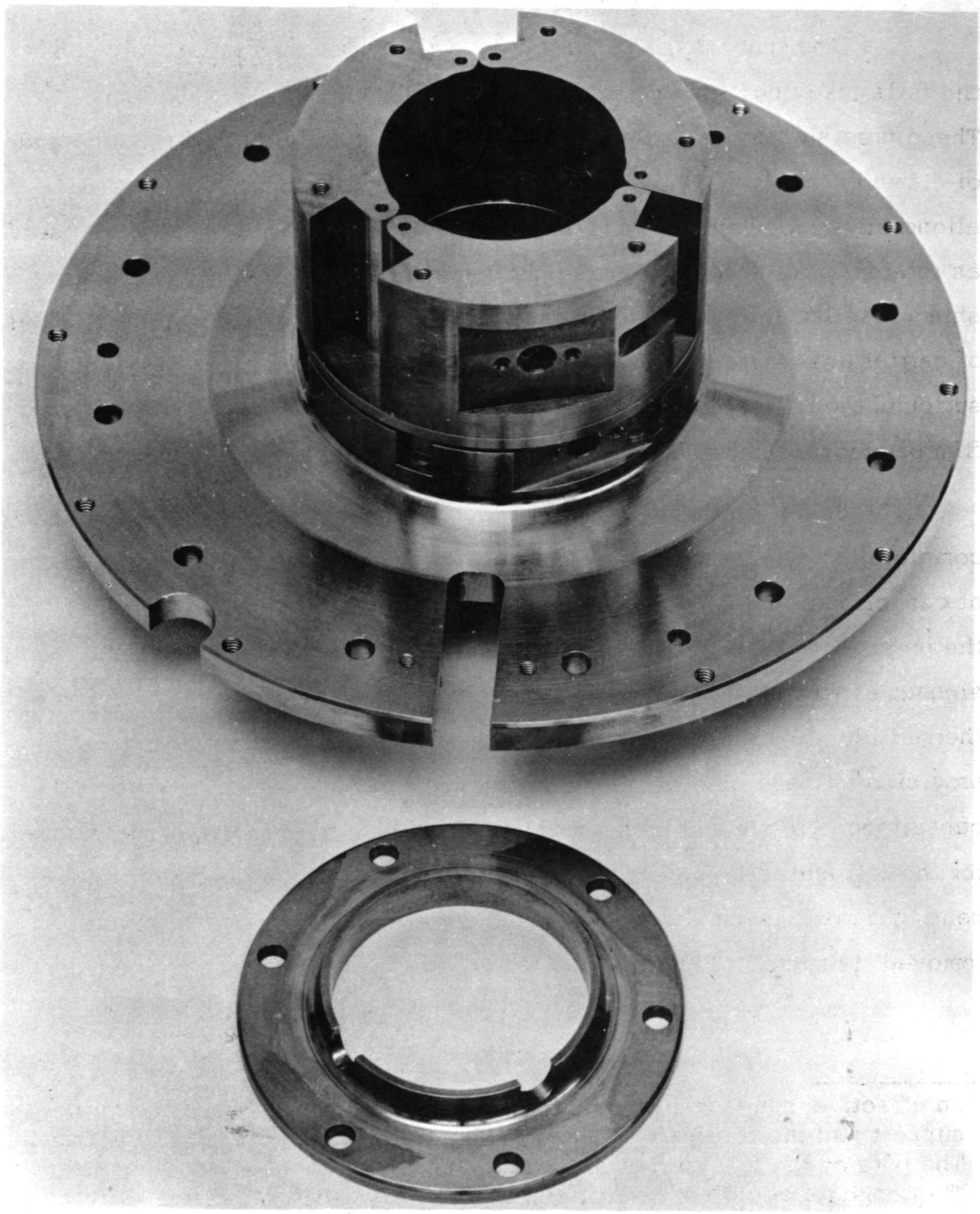

Fig. 6 Foil-Bearing Carrier Assembly with Outboard Plate Removed - Top View

The inner bores of the carriers accommodate the journals and the foils, leaving a "cold" clearance of 0.0053 in. (1.35×10^{-4} m). These precision bores accept an alignment arbor, 12 in (.305 m) long and of diameter barely 0.0002 in (5.08×10^{-6} m) smaller, for the accurate alignment and doweling of foil-bearing carrier assemblies. They also serve as reference bores for the concentric location of the rotor, by means of shims inserted into the annuli between the journals and the outboard plates of carrier assemblies. The foil guide-supports and the adjacent plates surround the journals and the foils with a narrow and nearly continuous film of stagnant gas and form a temperature-equalizing envelope.*

As in the case of their predecessors, the ingot iron end-bells complete the magnetic circuit of the alternator, furnish posts for mounting of capacitance probes to monitor the motion of the journal, and receive the press-fitted extensions of the flexure beams. The flexure beams, an elegant aspect of the previous carrier design, retain their dual function of thermal isolation and accommodation of differential expansion. Finally, provision is made also in the guide-supports to accommodate additional capacitance probes and probe holders, as well as thermocouples to monitor the foil and foil-support temperatures. A comparison between a foil-bearing carrier assembly and a pivoted-shoe carrier (shoes and pivots removed) is made in Fig. 7.

---

*An effective squeeze film could develop, if the gap between the guide-support and the foil were reduced to the order of foil-bearing clearance. The bore of the foil carrier could also serve as a mechanical limit-stop. This concept could not be utilized in the BRU, since the relatively small bearing-span to seal-span ratio permits no protection of seals against large rotor excursions in the conical mode.

The choice of metals used in the construction of foil-bearing assemblies was dictated by several considerations, of which compatibility of thermal expansions was most important (See Appendix 2). The end bells, made of Armco Electromagnet Iron,* have a coefficient of thermal expansion compatible with 416 stainless steel, the free-machining material used in the manufacture of the intricate foil guide-supports and of adjacent plates. Differential expansion is thus minimized and can easily be accommodated by the PH 17-4 flexure beams, press-fitted into the end-bells and into the foil carrier assemblies. Stresses due to interference and expansion, as well as buckling loads, were taken into consideration in the design of parts involved in the press fit.

The foil material, PH 17-4, has a yield strength of 218,000 psi (1.503×10^{9} N/m^{2}) and is coated in the regions of wrap with a 100 to 150 μinch (2.54×10^{-6} to 3.81×10^{-6} m) film of inorganically bonded MoS_2. The high yield strength was dictated not by the preload and the operating tension, but by the requirement of looping the foil around surfaces having relatively small radii of curvature, without producing permanent deformation. The high yield-strength also increases the resistance to damage in handling. The coefficient of thermal expansion of the fully hard, PH 17-4 foil has an average value of 6.3×10^{-6} in/in/°F (11.3×10^{-6} m/m/°C) in the range to 70° to 600°F (21° to 315°C). In addition to three PH 17-4, coated replacement foils, a set of fully-hard Inconel 600 foils is being delivered to NASA. The average coefficient of thermal expansion of Inconel 600, in the same temperature range, is in the order of 7.9×10^{-6} in/in/°F (14.2×10^{-6} m/m/°C). The foils are 0.001 in (0.254×10^{-4} m) thick, 1.375 in (3.49×10^{-2} m) wide, and wrap around 90° arcs along the circumference of 1.750 in (4.45×10^{-2} m) dia. journals.

---

*An improved version of Armco magnetic ingot-iron. Here the choice of material was dictated primarily by the electromagnetic properties of iron since the end bells complete the magnetic circuit of the alternator.

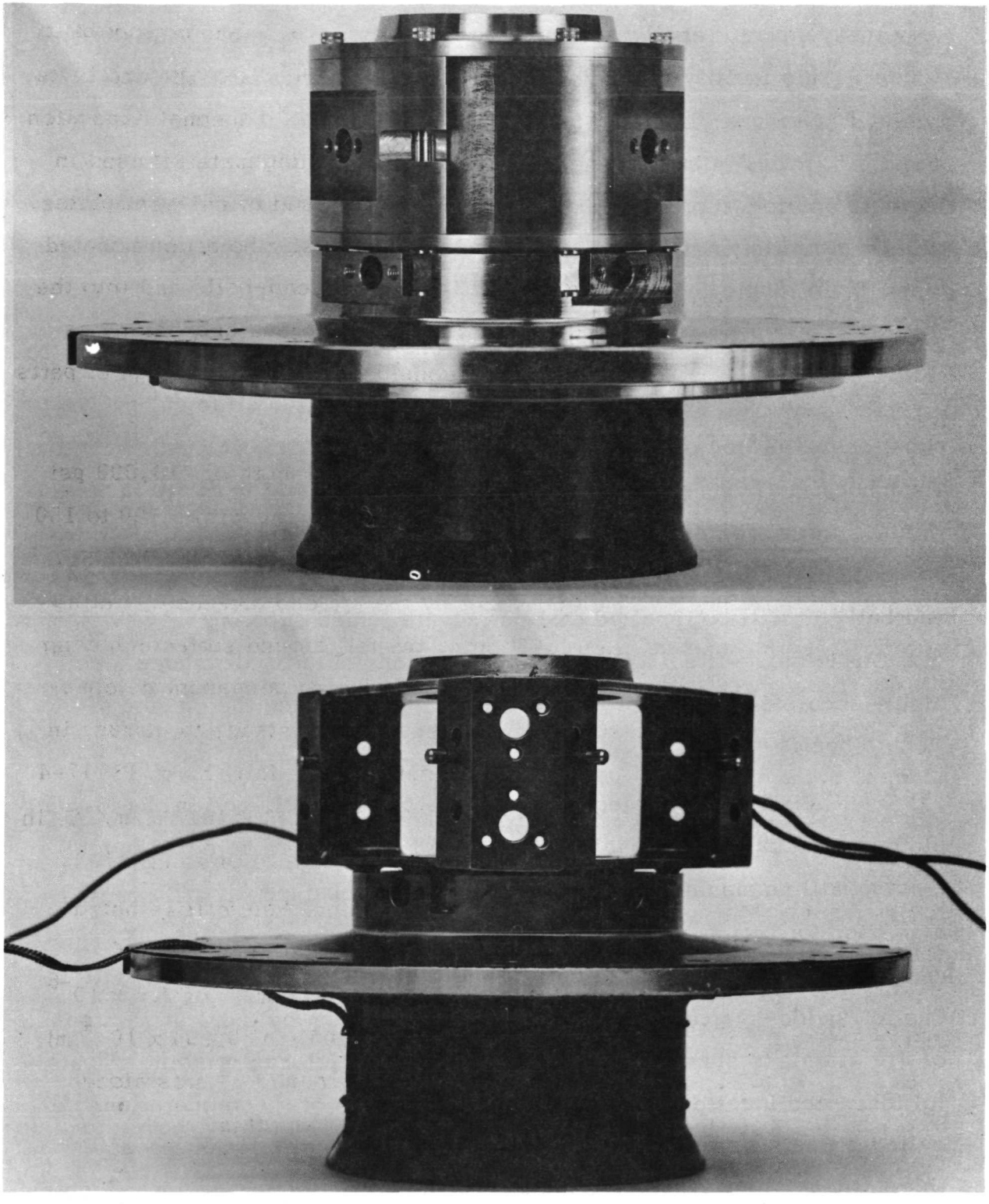

Fig. 7 View of Pivoted-Shoe and Foil-Bearing Carriers

As pointed out in the earlier part of this report, the foil is a very inexpensive, readily available, and easily replaceable bearing component. This facility of choice and replacement is not available with other types of bearings. The calculation in Appendix 2 indicates that both foil materials, PH 17-4 and Inconel 600, are compatible with the expansion of journals and foil supports, and that only a moderate contraction (PH 17-4), or relaxation (Inconel 600) of clearance should be anticipated at operational temperature levels.

2.3 Fabrication. - Crucial Operations and Tolerances

This section furnishes a review and highlights the salient aspects of fabrication of foil-bearing assemblies and test-rig components. The most important, and also the most difficult part of the entire operation was the production of components to a degree of accuracy compatible with perpendicularity of milled foil-guide surfaces to a reference surface on the end bell. It will be recalled that parts were joined successively by means of multiple press-fits, so that ultimate perpendicularity depended also on highly accurate location of interference holes receiving the shanks of flexure beams.

Six locating holes in the ingot iron end-bells and in the inboard plates of the carrier assembly, Fig. 3 and Fig. 4, were bored on a very precise milling machine and rotary table. The same machine tools were also used for boring two interference-fit holes in each guide-support segment, and for milling cylindrical foil-guide surfaces at their extremities. The foil guide-supports were machined in pairs from cylindrical sections of 416 stainless steel, and were stress-relieved prior to grinding of parallel faces and location of holes. Upon completion of these operations, each cylinder was separated into 2 guide-supports, along thin webs spanning the partition slots between the sectors. A pair of sectors (prior to location of holes, partition, and milling of guide surfaces) is shown in the center of Fig. 8, between the foil-bearing assemblies.

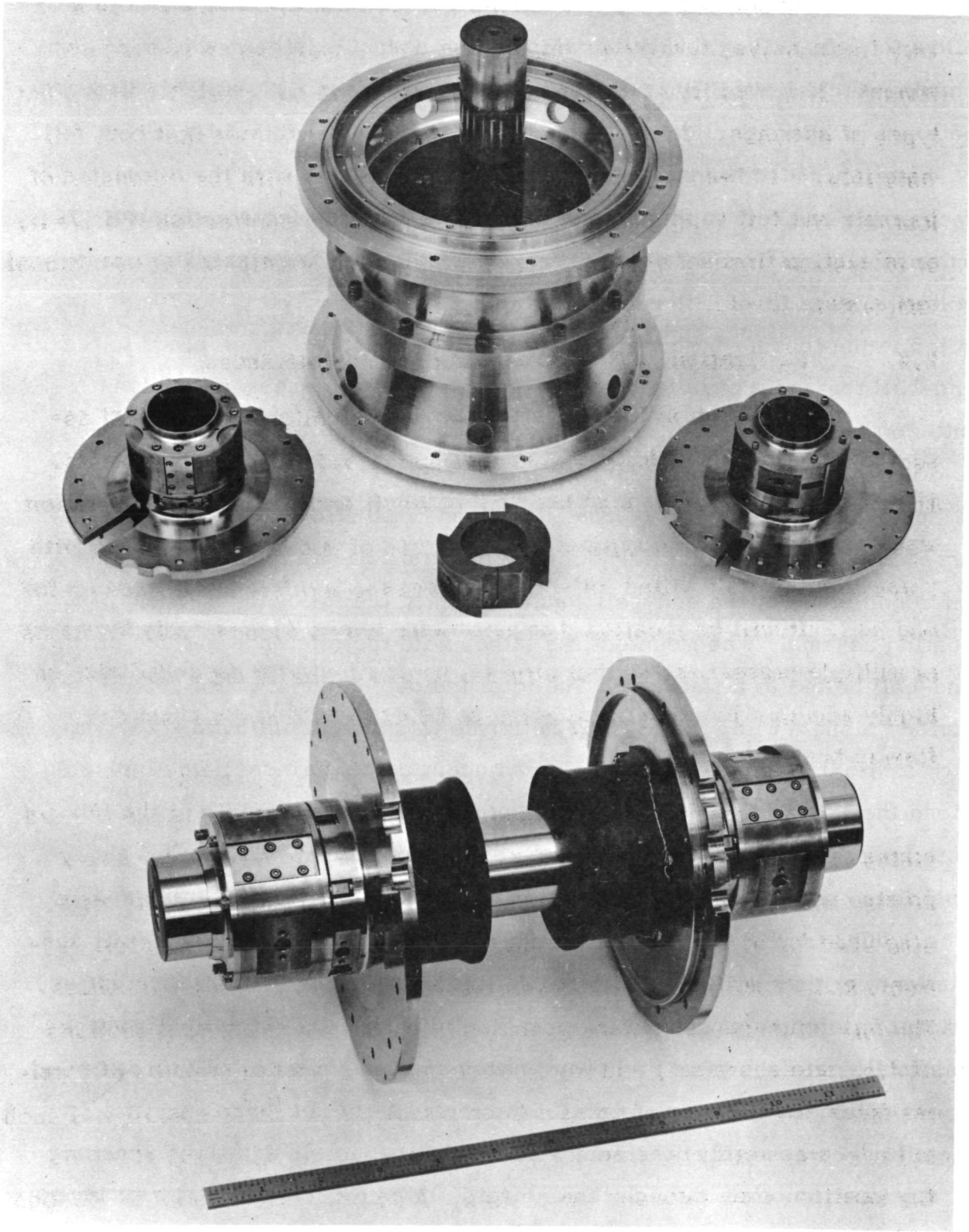

Fig. 8 View of Turbine and Compressor-End Foil Bearings, Housing, and Alignment Arbor

The shanks of 6 flexure beams, Fig. 3, were center-ground to allow for a 0.0003 in (7.6×10^{-6} m) interference fit at either end. The shanks were relieved with flats to facilitate the press fits, and the distance between locating shoulders was held to within 0.0001 in (2.54×10^{-6} m). An equally tight tolerance was imposed on the distance from the reference face of the end bell to the ends of 6 shoulder-locating slots, and also on the thickness and flatness of the inboard plate. The next operation involved a press fit of 6 flexure beams into 3 guide-supports, via 6 matching holes in the inboard plate. The entire subassembly was then joined to the end-bell through a simultaneous press-fit of 6 flexure-beam extensions into corresponding holes. A small, hydraulically actuated press was used to drive 6 flexure-beam extensions into the end-bell, with a terminal force of approximately 2,000 lb (8,896 N). Upon completion of the press-fit assembly, the perpendicularity of 6 cylindrical foil-guide surfaces to the reference plane of the end-bell was checked in the following manner. The bearing assembly was mounted in a lathe, with the reference surface of the end-bell bolted to a flat disc. The total indicated runout of the reference surface along a 6 in. dia. (0.152 m) circle was 0.0002 in (5.08×10^{-6} m). A cylindrical plug gauge, resting on adjacent guide surfaces, was indicated along the 1.375 in (0.035 m) length corresponding to the width of the foil. Both foil-bearing carriers were indicated in this manner in a total of six positions, and the maximum deviation registered in any of six traverses was 0.0003 in (7.6×10^{-6} m), or 60% of the allowance. The outboard plates were then bolted and doweled to the outer faces of the guide supports, prior to machining of central bores to final dimension. The foil-bearing assemblies are shown in the lower portion of Fig. 8 , with both bores accommodating an alignment arbor, of diameter barely 0.0002 in (5.08×10^{-6} m) smaller. On assembly, the annuli between the journals and the extensions of the locating bores through the outboard plates receive shims for centering of the rotor.

In the absence of complexity, the description of fabrication of remaining foil-bearing components, such as free guides, foil lock and clamps, is omitted. It is only noted in passing that the clamps were relieved at the center, to facilitate flexure and engagement of foil and free guides by the cylindrical lands of the clamps. These narrow lands were lapped to a diameter equal to that of the guide plus twice the foil thickness.

The housing, shown in Fig. 8 and Fig. 9 , was rough-machined in two parts, which were bolted together prior to concentric machining of several large diameters to very exacting tolerances. The main objective was to ensure the concentricity and alignment of seals with respect to the reference bores in the foil-bearing carriers. The lathe work involved several setups and stages of machining, in order to effect accurate, slip-fit location of large diameters of seal-and-shroud assemblies in corresponding recesses of the housing. Equally important was the perpendicularity of the housing axis to surfaces mating with the reference planes of the end bells. Upon completion of final machining of the housing, the reference bore of the compressor-end carrier was indicated with respect to the large-diameter bore locating the seal-and-shroud assembly. The carrier end-bell was then firmly bolted to the housing and doweled in the concentric position. The bearing carrier at the turbine end was secured in an identical manner, following indication of the carrier bore with respect to the diameter locating the shroud-and-seal assembly in the housing. The accuracy of mounting of foil-bearing carriers assemblies can be assessed from the fact that an alignment arbor, of diameter barely 0.0002 in (5.08×10^{-6} m) smaller than the reference bores, could be inserted through the outboard plates of both carriers doweled and bolted to the housing. The foil bearing carriers, with the alignment arbor inserted through the reference bores, are shown in the lower part of Fig. 8.

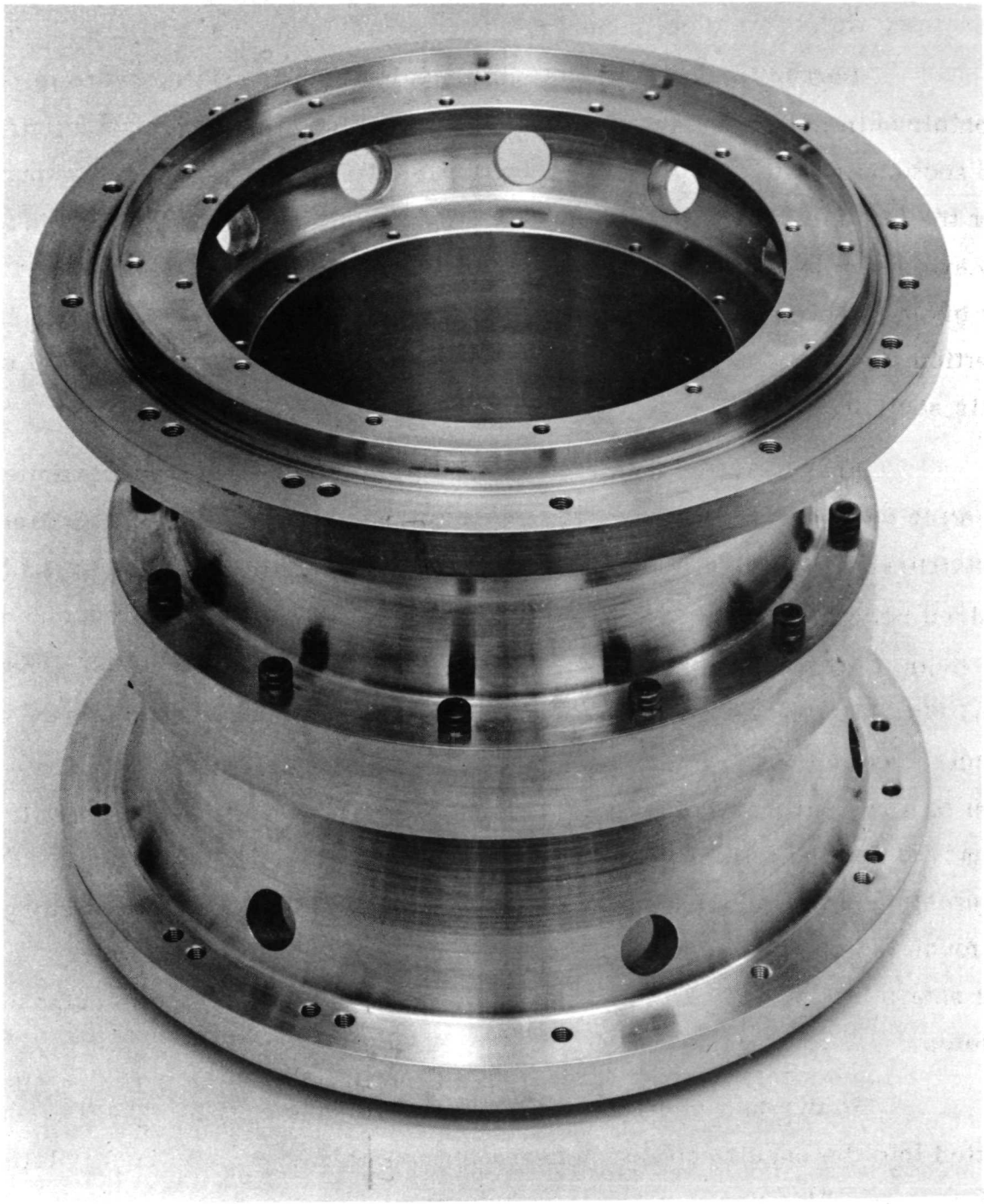

Fig. 9 Housing

2.4 Assembly of Foil Bearings and Centering of Rotor in the Test Rig

Instructions for the assembly of the Brayton Rotating Unit are contained in the Assembly Manual, reference [10]. With the exception of sections pertinent to pivoted-shoe bearings, the assembly instructions for the BRU are also applicable to the present test-rig and are omitted here to avoid needless repetition. A detailed outline of foil-bearing assembly is given in Appendix 1 of this report, and only the essential aspects of insertion and tensioning of foils and centering of the rotor are summarized in this section.*

This narrative begins at the stage of assembly, when both foil-bearing carriers have been bolted to the housing in the concentric position determined by dowels. At this point, the central section of the rotor is contained between the rotor shrouds in the housing, with curvic couplers at journal ends protruding through bores of carriers, as shown in Fig. 10 and Fig. 11. The housing is mounted on a rotatable platform, and the center-section of the rotor is suspended on a threaded rod from the cross-bar of a supporting bracket, Fig. 12. The outboard plates are temporarily removed and the foils are inserted loosely into the annuli between the journals and the guide-supports of the carriers. With foil ends protruding through the open locks, the free foil-guides are inserted through loops, as shown in Fig. 12, before taking up the slack and replacing the outboard plates.

In the next step, the rotor is centered by means of shims, push-fitted into the annular spaces between the journals and the outboard plates of carriers. This position is recorded by means of capacitance probes

*Appendix 1 replaces sections 4.2, 4.4, 4.7, 4.8, 5.2 and 5.4 of reference [10], the Assembly Manual, Brayton Rotating Unit.

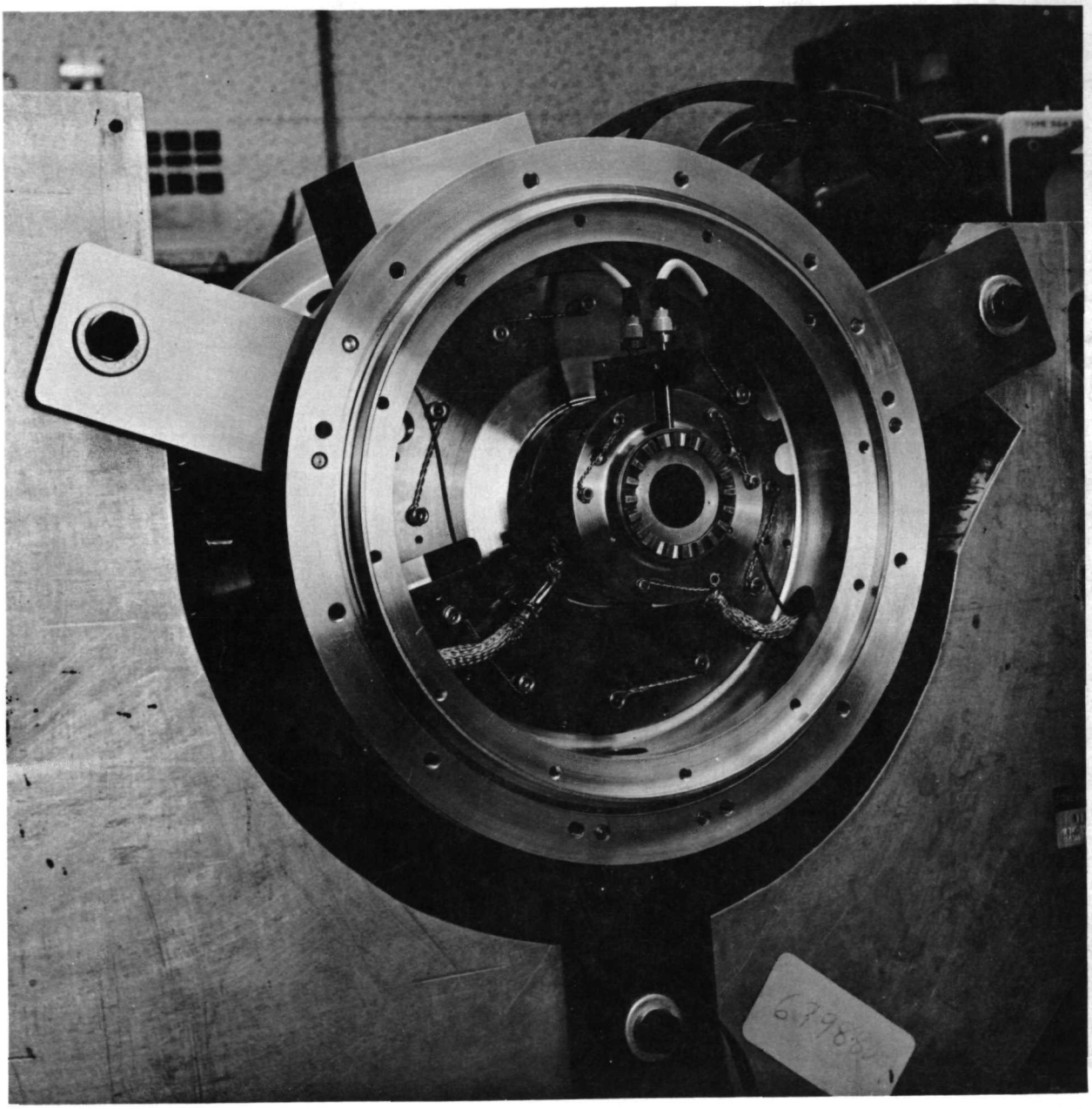

Fig. 10 Foil Bearing in Housing During Assembly of Test Rig (Turbine End)

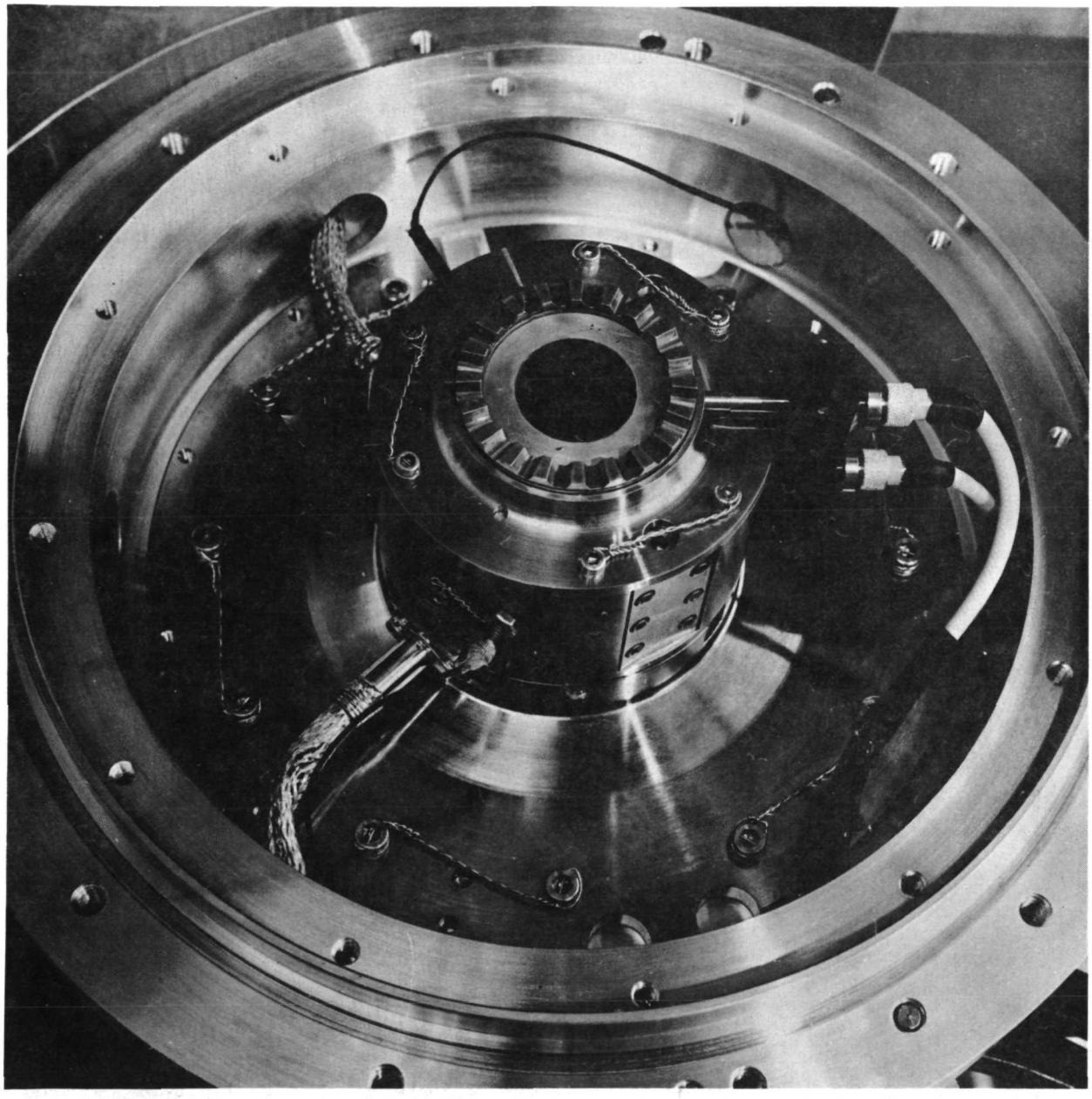

Fig. 11 View of Foil Bearing Carrier with Capacitance Probes and Thermocouples Attached (Turbine End)

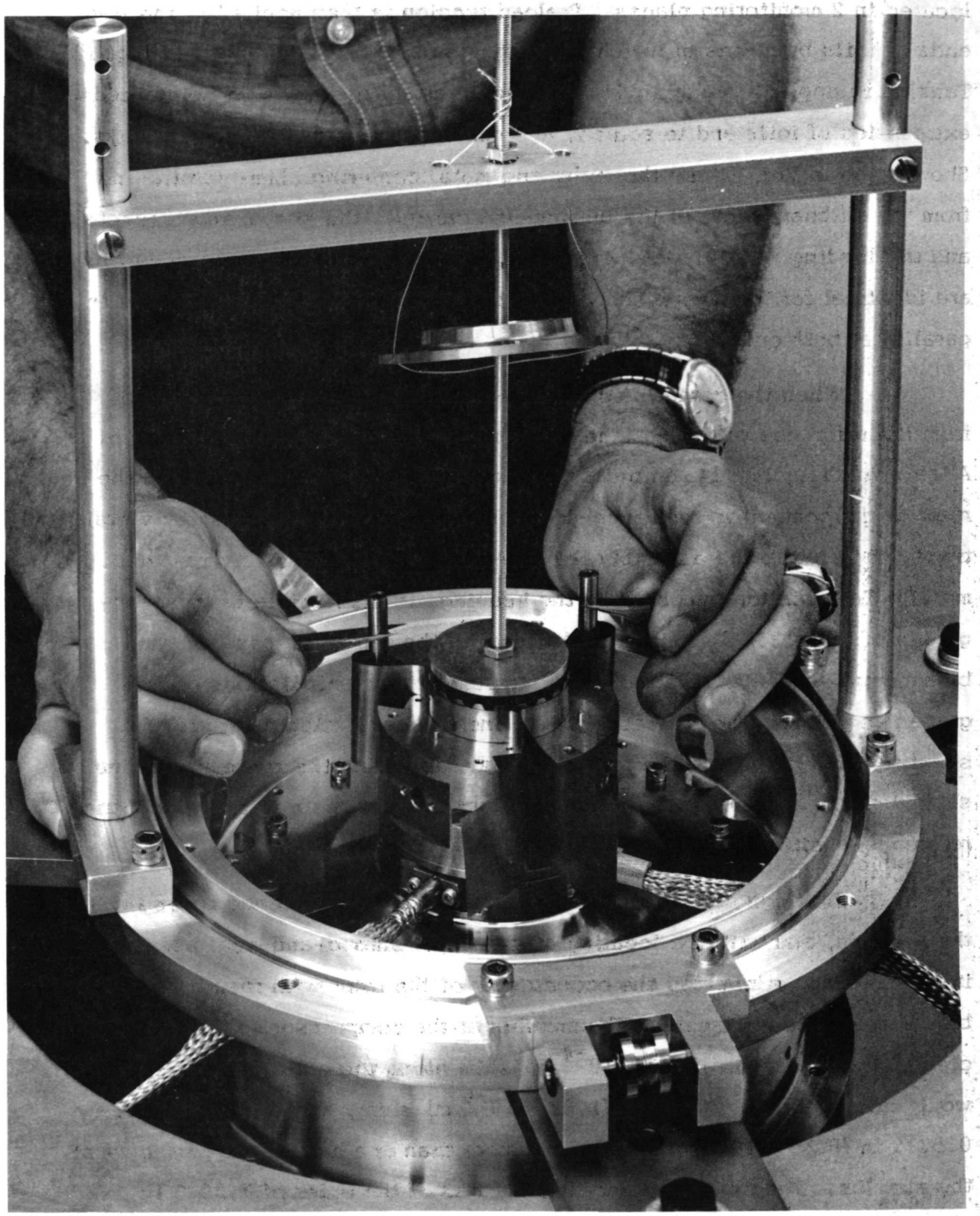

Fig. 12 Insertion of Foil into Foil-Bearing Carrier

located in 2 monitoring planes. Preload tension is then applied to the free ends of foils by means of weights or spring scales, as illustrated in Fig. 13. Tension is applied through nylon filaments, attached to washer-reinforced extremities of foils and to scales, and passing over small loading pulleys. Shown also in Fig. 13 are the mylar and metal centering shims (protruding from the outboard plate of the turbine-end carrier), the supporting brackets, and the loading scales. Foil-insertion, centering and loading procedures are identical for the compressor and turbine bearings and are carried out in parallel at both ends.

When the centering shims are removed, the journals displace from the reference position. The free guides are then rotated by means of Allen wrenches, Fig.14, in order to equalize the tension and to return the rotor to the concentric reference-position. This process is aided by vibrations, imparted to the assembly by an eccentric attached to a small d.c. motor. The vibrator, mounted on the housing, is discernible in the background of Fig. 13. The return of the rotor to the reference position can be accomplished with relative ease by successive manipulations of free guides and vibration of the assembly. The final operation consists of securing the clamps and the foil lock, and subjecting the system to a final shakedown to check that the journals return to and remain in the concentric reference-position.

The high concentricity of journals with the reference bores in the carriers, and with the locating diameters of shroud-and-seal assemblies in the housing, minimized the eccentricity of the rotor with respect to turbine and compressor seals. The annulus at the compressor seal could be cleared by a 0.003 in (0.76×10^{-4} m) shim along the entire periphery, would not receive a 0.004 in (1.02×10^{-4} m) shim, and accommodated a 0.0035 in (0.89×10^{-4} m) shim along more than one half of the periphery of the annulus. The estimated eccentricity was of the order of 0.0003 in

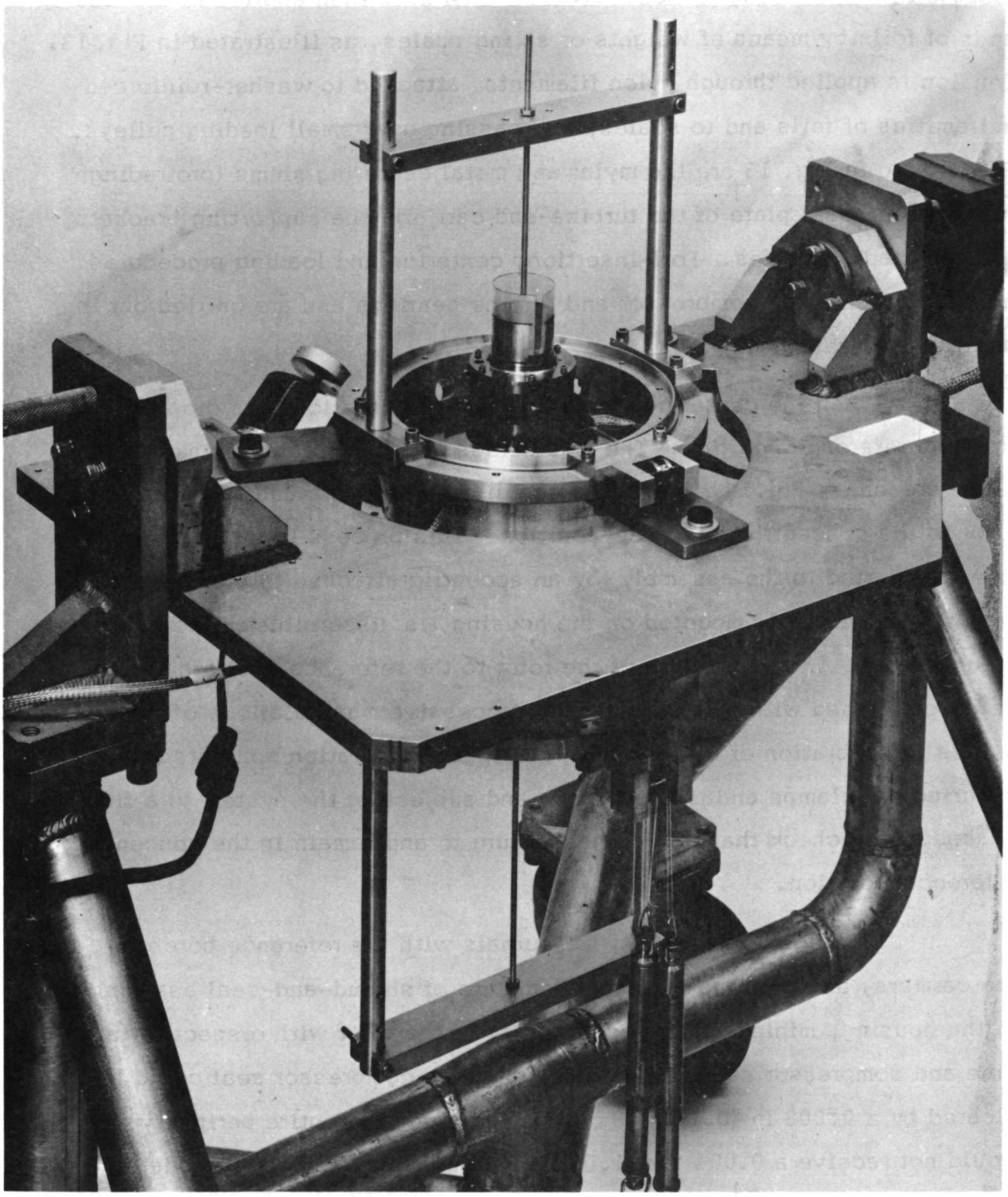

Fig. 13 Centering of Journals by Shims and Tensioning of Foil (Rotor Suspension-Brackets and Loading Pulleys Bolted to Housing)

(7.6×10^{-6} m) and represented less than 9% of the measured, 0.0035 in. (0.89×10^{-4} m) clearance of the compressor seal.

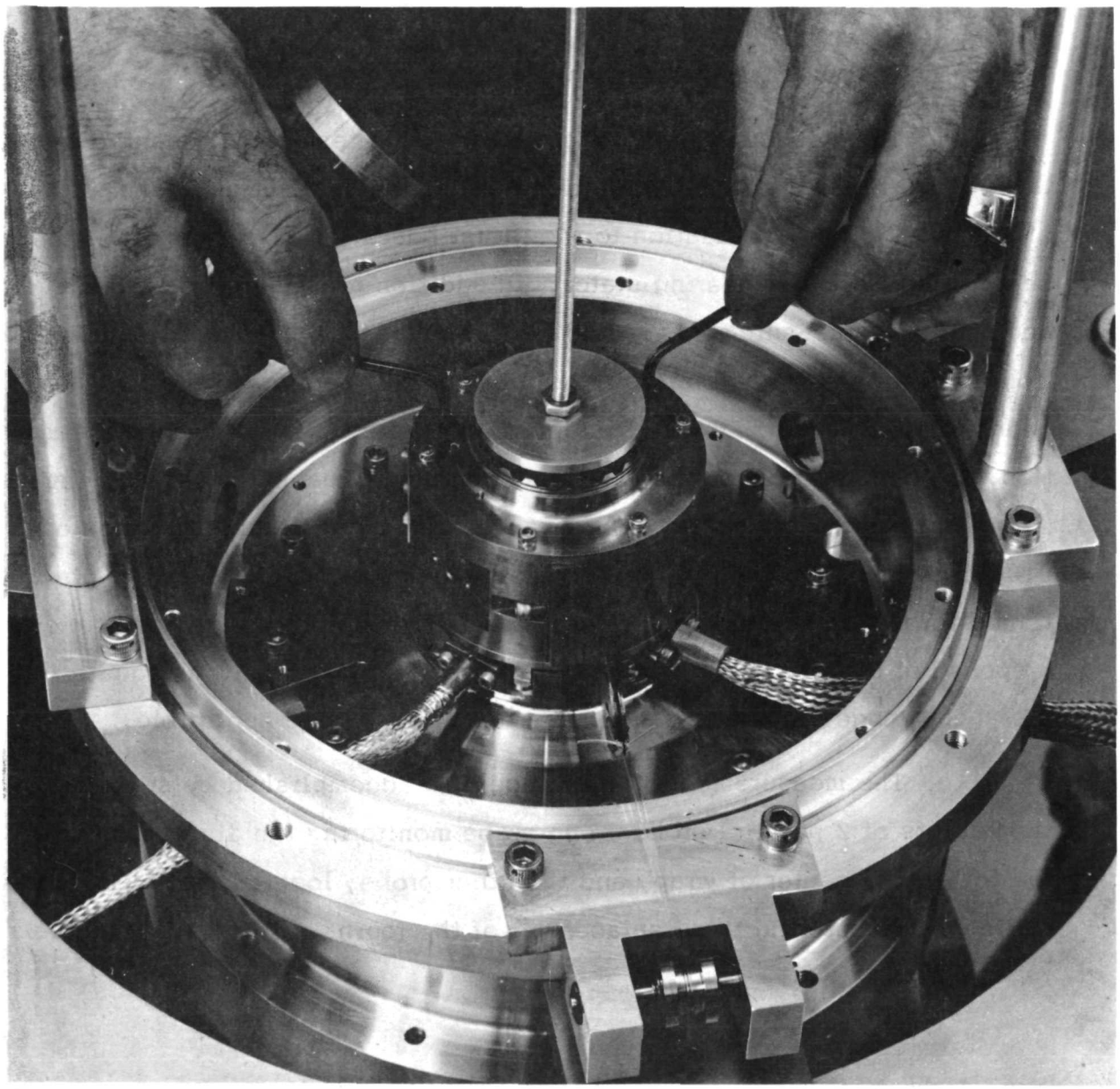

Fig. 14 Manipulation of Free Foil-Guides to Return Journals to Reference Position

3.0 TESTS AND TEST RESULTS

3.1 Measurements and Instrumentation

The measurements associated with the test data presented in this report involved the determination of position and motion of the rotor, of the thrust runner in relation to the thrust bearing plates, and of gimbals supporting the thrust bearing stator. In addition to these displacement and amplitude measurements, provision was made also for the determination of clearance at the center of wrap of one foil sector of the turbine bearing. Wayne-Kerr DM100 Displacement Meters were used in conjunction with capacitance probes, and the accuracy of measurement was estimated to be within 5%. The probes were carefully calibrated in steps of 0.0005 inches (12.7×10^{-6} m) and least-square-fitted curves were obtained for the displacement and for the local sensitivity.* The frequency response of the measuring systems (flat to 2.5 Kc) was quite adequate in the speed range 0-720 rps, and phase differences were negligible.

The measurement of clearance was accomplished by subtracting the outputs of 2 parallel probes; one probe monitoring the displacement of the foil at the center of wrap, and the other probe, located just outside the foil edge, registering the displacement of the journal, Fig. 11. Reliable

*The sensitivity scales appended to various oscillograms of amplitudes of motion, or of journal orbits, represent the average of local sensitivities of the monitoring probes. The estimate of accuracy given above includes differences between probe-meter-filter systems, as well as deviations from linearity in the vicinity of the probe offset points.

clearance measurements were obtained during rapid acceleration and in the course of immediately following coastdown of the rotor. Under these conditions, the effects of differential thermal expansion were quite negligible. On the other hand, the error in clearance measurement (due to the differential expansion of capacitance probes) may have been in the order of 10 to 15% after prolonged runs to thermal equilibrium conditions (see Appendix 3).

Temperatures were monitored at 4 stations. The spherical, hot junction of a chromed-alumel thermocouple, Fig. 15, was brought into contact with the foil at the center of wrap. The junction was coated with a minute quantity of adhesive, and the thermocouple hoop, formed by the 0.003 inch dia. (7.6×10^{-6} m. dia.) wires, was preloaded with a minimal force against the foil to ensure contact. Another thermocuple was embedded in a location approximately half through the thickness of the foil guide-support. The third thermocouple monitored the air temperature of the bearing cavity in the housing enclosure, providing thereby a record of gas temperature in the immediate surroundings of the foil bearing. In addition, a record was also kept of the ambient temperature of the test rig. The thermocouples were calibrated in an oil bath, using a precision mercury thermometer as a reference, and the temperatures were monitored by an Astrodata, Model TDA-121 nanovoltmeter. It is estimated, that in the temperature range relevant to present test conditions, the error due to conduction from the foil via the thermocouple (and subsequent convection) was relatively small. The readings reported herewith may be considered accurate to within 5% of actual foil and guide-support temperatures.

The speed was sensed by a photocell, via a bidirectional, optical fiber-tube, and was displayed on a Hewlett-Packard 523B Electronic Counter. A digital-to-analog converter, integral with a Hewlett-Packard 560A Recorder, was used to convert the output of the counter to a speed-proportional d.c.

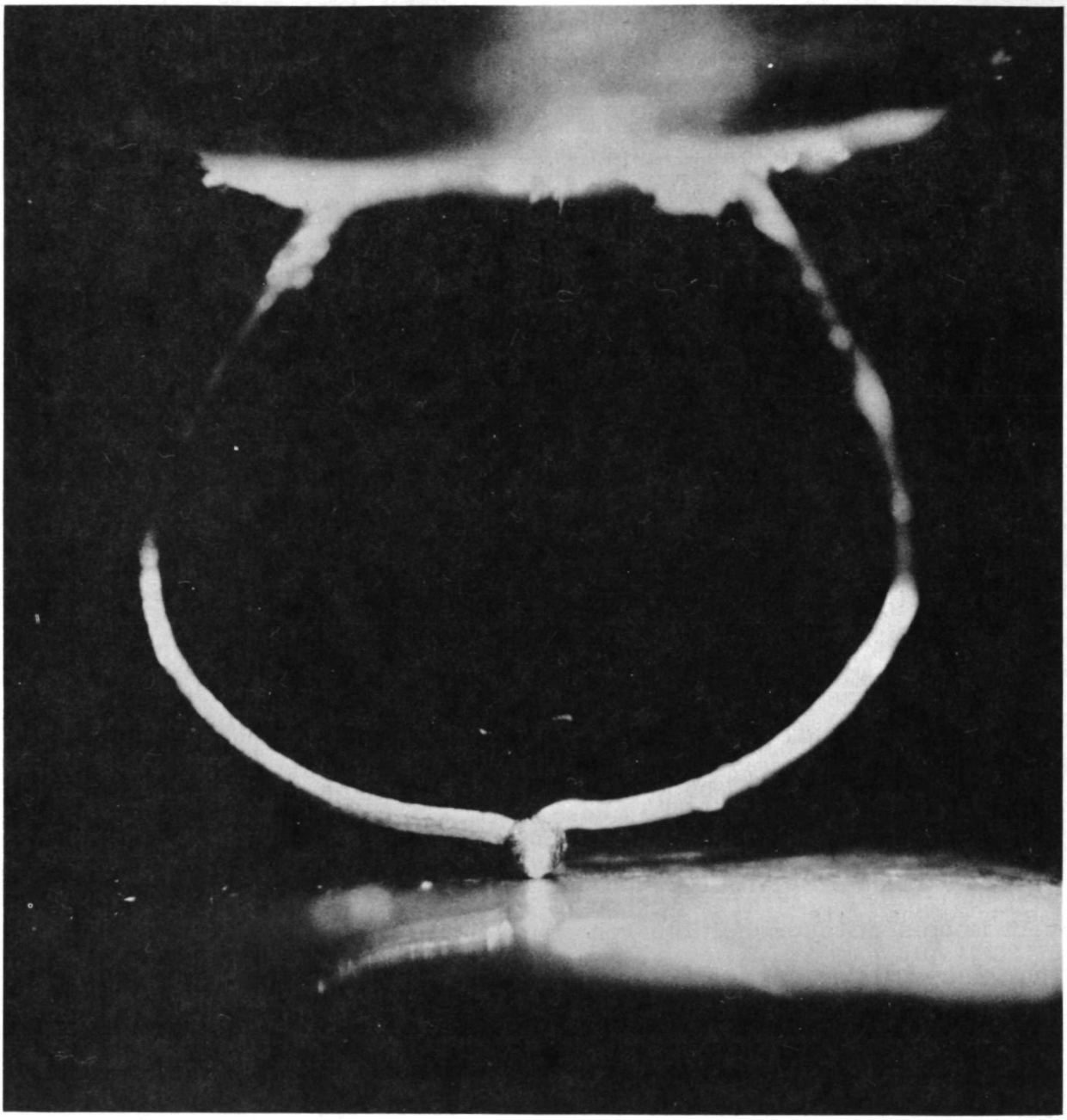

Fig. 15 Magnified View of Thermocouple in Contact with Foil Surface

signal driving the horizontal plates of an oscilloscope. This arrangement permitted photographic recording of simultaneous frequency scans of amplitudes of motion and of variation of clearance. In the oscilloscope records of this report, the maximum absolute error in speed was of the order of 15 rps, and was due mainly to slow drift of the d.c. reference voltage. The horizontal plates of oscilloscopes could also be driven by a time-proportional d.c. output from a precision potentiometer, rotated by a small electric clock. This arrangement furnished means of monitoring and recording of slow temperature transients, in the time interval necessary to attain thermal equilibrium.

The assembled rotor was balanced on a Schenck, Model RS1-b Balancing Machine to better than 100 μin-oz (0.704×10^{-6} m.N) in each balancing plane. The rotor, supported on air bearings in a very light balancing fixture, is shown on the cradle of the balancing machine in Fig. 16.

3.2 Preliminary Tests

The complete rotor assembly consisted of 9 parts,* held together mainly by 3 curvic couplings and a tie bolt. In addition, the assembly of the rotor drive-wheel with a thermal shunt necessitated heating of the wheel to 350°F (177°C) in order to accommodate an interference fit, while cooling of the copper shunt with liquid nitrogen was required to separate the parts [1].

The rotor was received with imbalances of 0.0038 in-oz (26.8×10^{-6} m.N) at 0°, in the balancing plane of the turbine wheel, and 0.0050 in-oz (35.2×10^{-6} m.N) at 10°, in the balancing plane of the compressor wheel, the angular position being taken with regard to a

*13 components, 4 of which were permanently press-fitted, hence a total of 9 separate parts.

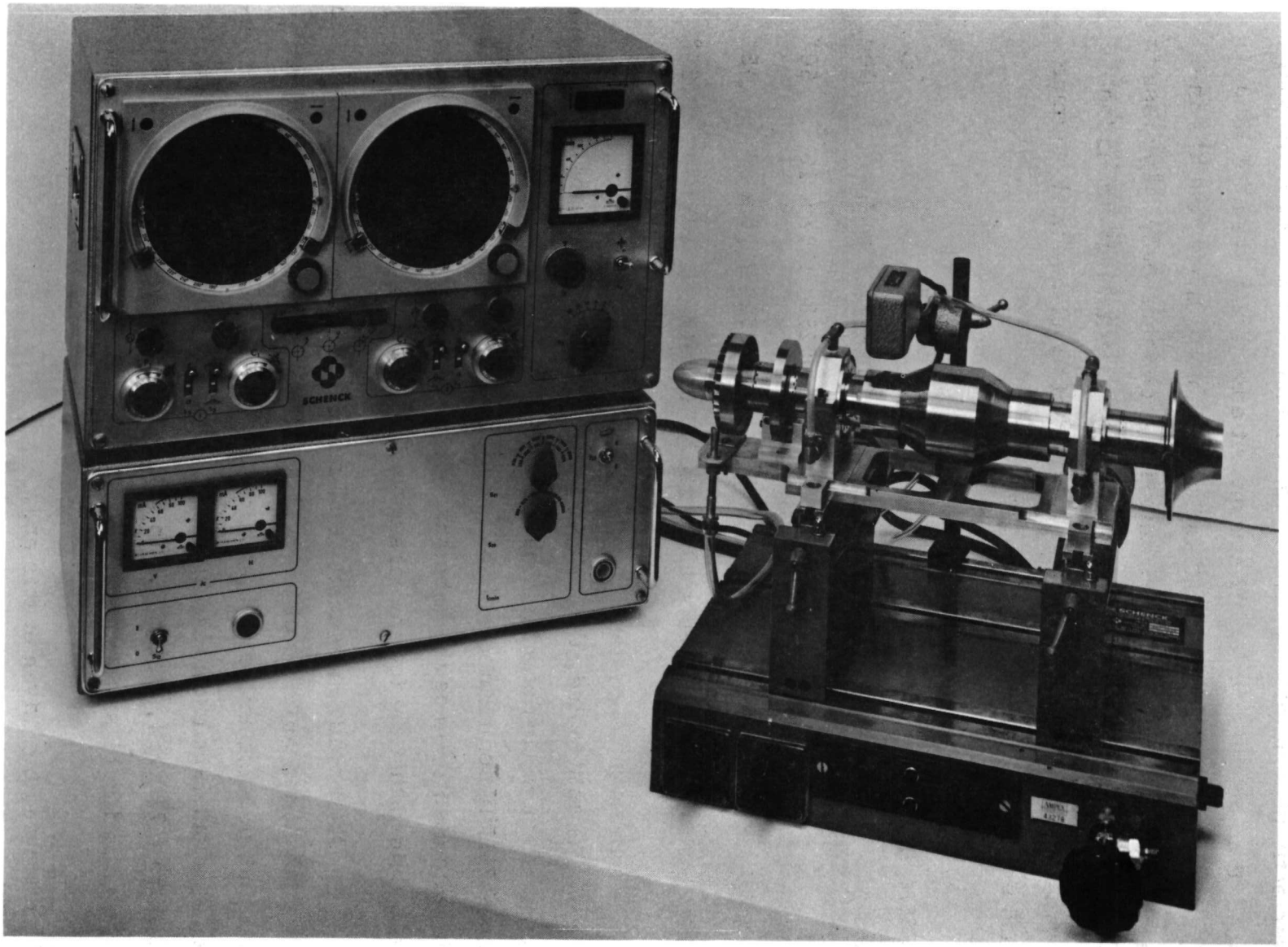

Fig. 16 Rotor in Air-Bearing Fixture on Cradle of Balancing Machine

conveniently chosen reference line. The imbalance of the rotor was then reduced to an entirely negligible amount, at a balancing speed of 3600 rpm. The rotor was disassembled and reassembled 3 times, and the increase of imbalance was checked following each reassembly. The results of these checks are given below in tabular form, with u and α denoting respectively the amount and angular position of imbalance in the turbine (T) and compressor (C) balancing planes:

REASSEMBLY	u_T		α_T	u_C		α_C
No.	in-oz	m.N	Deg.	in-oz	m.N	Deg.
FIRST	0.00061	4.31×10^{-6}	35°	0.00250	17.7×10^{-6}	50°
SECOND	0.00095	6.70×10^{-6}	155°	0.00291	20.6×10^{-6}	115°
THIRD	0.00104	7.34×10^{-6}	110°	0.00175	12.4×10^{-6}	35°

As anticipated, the major imbalance reappeared at the compressor end,* at which mating of a large number of separate components of the rotating assembly contributed to imbalance through slight deviations from the initial alignment. Since the imbalance remained well within specifications, it was decided that the fourth reassembly be final prior to testing.

Other preliminary tests conducted during the assembly of the simulator involved the variation of foil preload-tension; adequate for sufficient constraint, yet compatible with starting-torque requirements, as well as acceptable excursions excited by friction [6,7]. A preload of approximately 2.73 lb/in (477 N/m), that is 7.5 lb (33.4N) applied to the free ends of the foil, appeared to be satisfactory. It is of interest to note the displacement

*The rotor was air-driven at this end.

of the 21.9 lb (97.5 N) rotor from the reference position; first in the vertical attitude, following removal of centering shims, and then upon changing the rotor attitude to horizontal. The displacements in the planes of the monitoring probes are illustrated in the oscilloscope photographs of Fig. 17, in which (a) corresponds to a preload of 3.64 lb/in (636 N/m) and (b) to the operational preload of 2.73 lb/in (477 N/m). The lowermost points in each oscillogram correspond to the orientation of foil-bearing sectors with respect to the load vector indicated in diagram (I), while the uppermost points refer to the orientation depicted in diagram (II). It is noted that the displacement decreases with increasing preload and that, as may have been anticipated, orientation (II) is more favorable. The displacement from the reference position in the vertical attitude (upon the removal of centering shims) can be seen to be of the order of 100 μin (2.54×10^{-6} m). In the horizontal position, and with a preload corresponding to Fig. 17 (b), the mean displacement for orientation (II) is of the order of 420 μin (10.7×10^{-6} m), as contrasted with approximately 650 μin (16.5×10^{-6} m) for orientation (I). The dual purpose of determining the static load-deflection was to assess the magnitude of the upper limit of foil-bearing stiffness, and also to consider eccentricities and offsets relevant to operation in the horizontal attitude.

The frictional starting-torque at 2.73 lb/in (477 N/m) preload was determined from an average of 10 measurements, following the same sense of rotation after each breakaway. The average value was 4.82 in-lb (0.545 m.N), which decreased by 11.4% to 4.27 in-lb (0.482 m.N) upon the conclusion of all experiments, including 1027 "dry" start-stops (Section 3.5).

The main concern, of course, was to limit excursions to a safe fraction of seal clearance, and in particular the tighter seal clearance at the compressor end. At this end resided also the major imbalance of the rotor. Although it was initially planned to accelerate slowly, particularly in approaching the region of resonances (and discontinue rotation if orbits

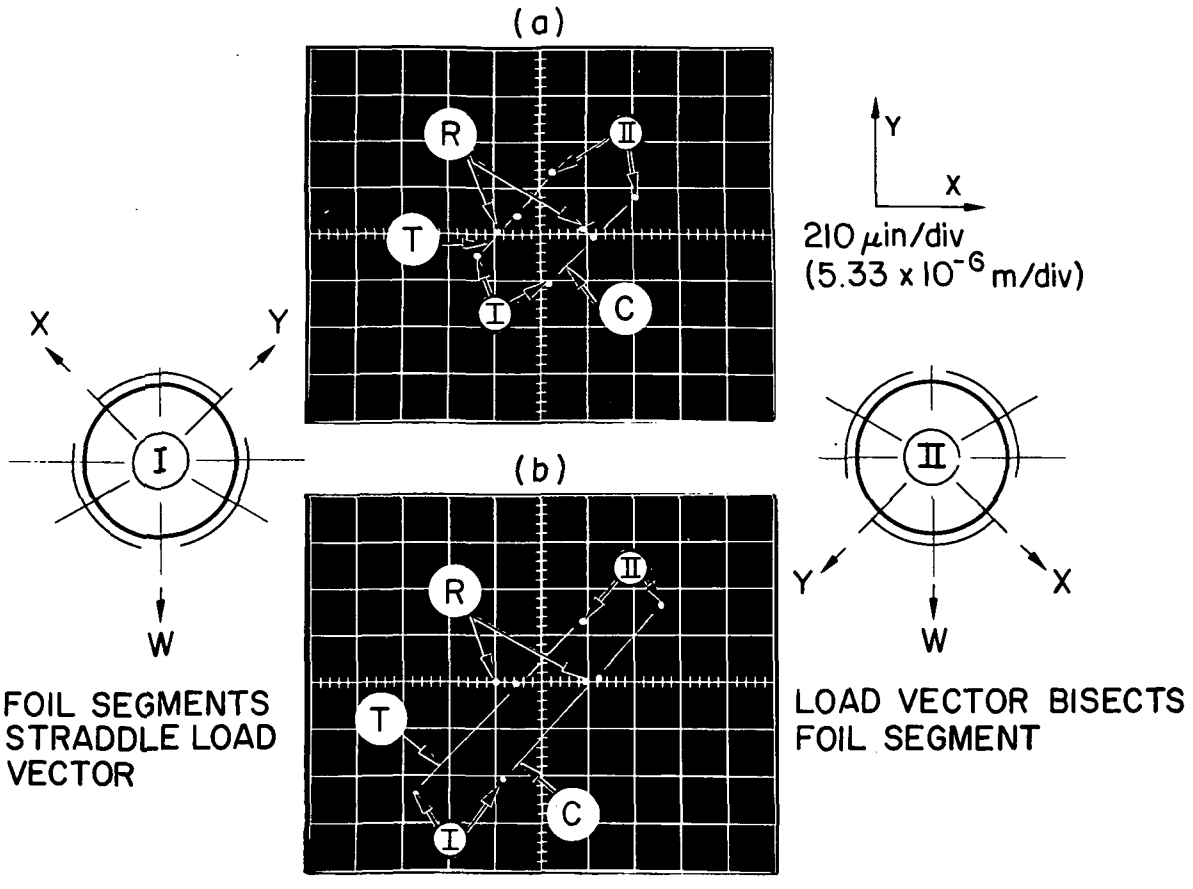

Fig. 17 Static displacements of Stationary Rotor for Two Orientations of Foil Sectors with Respect to Gravity Load-Vector (I and II) and Two Values of Preload (a and b). Lowermost and Uppermost Points Correspond to I and II. Midpoints Correspond to Vertical Attitude of Rotor, Showing Small Displacement from Reference Position (R). Preload T_o = 3.64 lb/in (636 N/m) in (a), and T_o = 2.73 lb/in (477 N/m) in (b) [T = Turbine-End Probes, C = Compressor-End Probes].

appeared to be excessive in size), the manual operation of the turbine air-supply did not allow for a very fine speed control at low rpm. The rotor was consequently accelerated rather rapidly to 600 rps (and then to 720 rps) during the first start, and this was followed by coastdown to standstill. The resonant bandwidth was centered at approximately 121 rps, and the amplitudes remained well within acceptable limits. The friction-excited orbits at very low speeds (less than 20 rps) were initially commensurate with the resonant orbits, but decreased by an order of magnitude in the course of subsequent start-stop cycling. The motion of the gimbals remained also within acceptable limits. It is noted in passing, that the loaded and unloaded side of the thrust bearing were supplied with air at 80 psig (0.552×10^6 N/m^2 gauge) and 20 psig (0.138×10^6 N/m^2 gauge) respectively and that the clearance on the loaded side was approximately 0.001 in. (0.254×10^{-4} m).

The following sections are devoted to the description of test results pertinent to rotor dynamics, thermal effects, extended runs at rated speed, and the performance of the foil bearings in the course of start-stop cycling.

3.3 Rotor Dynamics and Thermal Effects

The present section contains a complete description of dynamic performance of the foil-bearing supported rotor under two thermal conditions. In one case, the rotor was accelerated rather rapidly to rated speed (600 rps), or 20% above rated (720 rps), followed by immediate coastdown. Under these conditions, thermal effects were rather negligible. Alternatively, the machine was operated at rated speed for 2 hours, a time-period more than adequate for the system to attain thermal equilibrium, and data were recorded in the course of subsequent coastdown. Data pertinent to rotor dynamics were supplemented by temperature measurements of foil, foil support, and ambient air temperatures within and without the housing,

providing thereby a record of relatively slow thermal transient at key locations of the foil-bearing assembly and its surroundings. Additional information is also furnished through comparisons of coastdown curves of "cold" and "warm" runs.

Passage through the resonant bandwidth during a cold coastdown is depicted in the series of oscillograms of Fig. 18. As anticipated, the orbits were larger at the compressor end (C) because of imbalance introduced upon reassembly by slight variations in mating of several components at this extremity of the rotor. The largest orbit occurred at approximately 121 rps and was of the order of 900 μin (22.8×10^{-6} m). In the column of oscillograms on the right hand side of Fig. 18 are the corresponding time-base displays of parallel probes Y_C and Y_T. The traces indicate a quasi-conical motion in the resonant bandwidth. A crude estimate, based on location of the monitoring planes of the capacitance probes in relation to the outer edges of the seals, indicates that a peak amplitude of 450 μin (11.4×10^{-6} m) in the plane of the compressor-end probes, and a 180 μin (4.57×10^{-6} m) amplitude in the plane of the turbine-end probes, leave approximately 80% of the compressor seal-clearance as a margin of safety.

At high speeds, the orbits were nearly circular and less than 90 μin (2.28×10^{-6} m) in diameter. The orbits and time-base oscillograms at 600 rps and 720 rps are shown in Fig. 19. Additional information for the same run during coastdown is contained in Fig. 20. Oscillogram (a) is a frequency scan of journal amplitudes in the planes of the monitoring probes, while (b) contains a scan of amplitudes of gimbals of the thrust-bearing stator, and (c) is a scan of the relative motion of the stator and of the thrust runner. Note that the maximum amplitude of the outer gimbal G_B, at 375 rps, is approximately 285 μin (7.23×10^{-6} m), which corresponds to a reduction of clearance at the edge of the runner by 160 μin (4.06×10^{-6} m), leaving a safety margin of nearly 85% at the

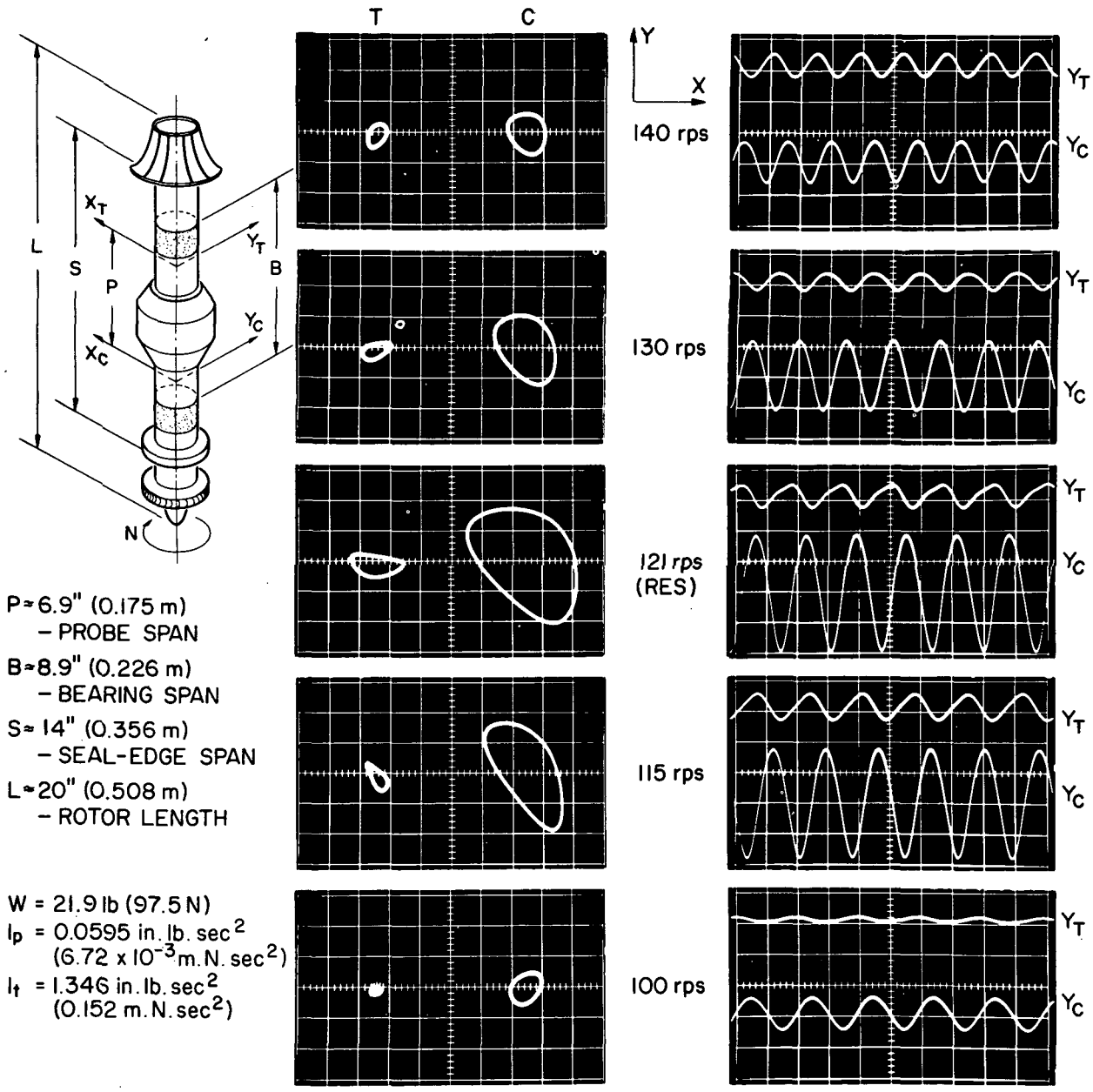

Fig. 18 Motion of Rotor in Resonant Bandwidth. Coastdown after Rapid Acceleration to 43,200 rpm. [210 μin/div (5.33 x 10^{-6} m/div) and 5 ms/div, T = Turbine-End Probes, C = Compressor-End Probes]

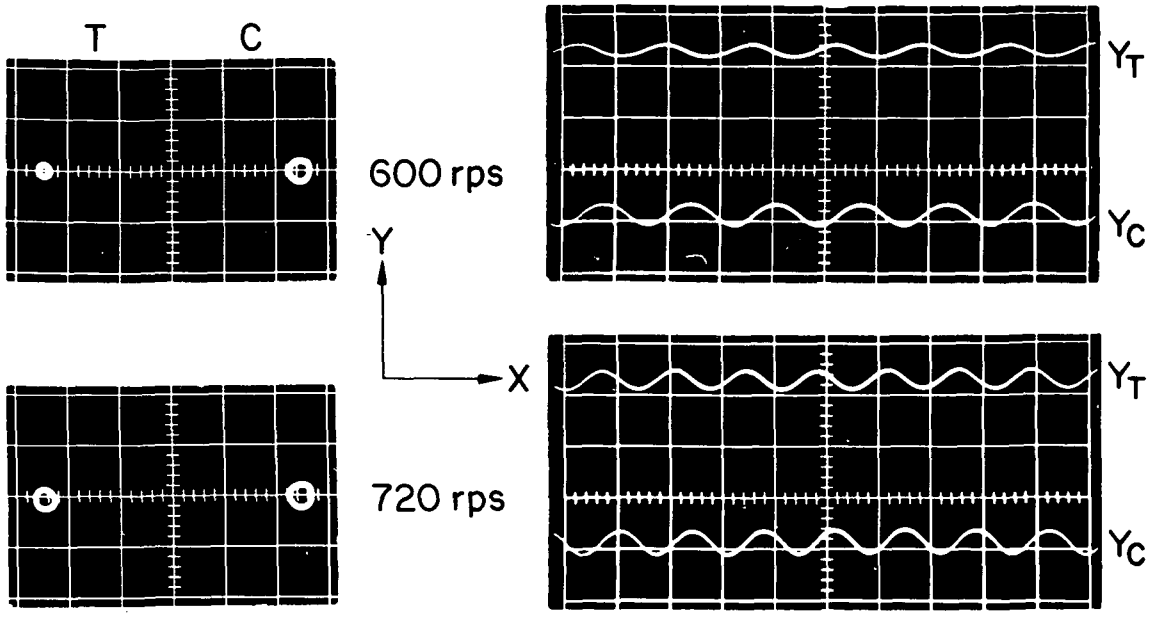

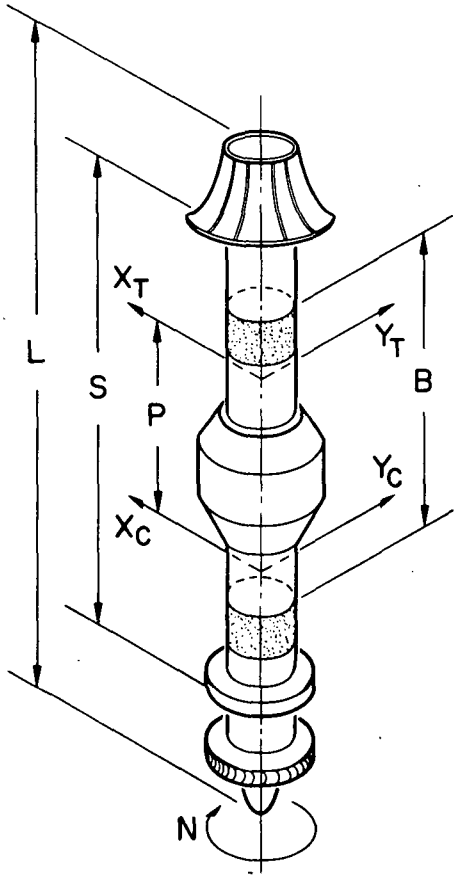

P≈6.9" (0.175 m)
– PROBE SPAN

B≈8.9" (0.226 m)
– BEARING SPAN

S≈ 14" (0.356 m)
– SEAL-EDGE SPAN

L≈20" (0.508 m)
– ROTOR LENGTH

W = 21.9 lb (97.5 N)

I_p = 0.0595 in. lb. sec^2
(6.72×10^{-3} m.N. sec^2)

I_t = 1.346 in. lb. sec^2
(0.152 m.N. sec^2)

Motion of Rotor at Rated Speed (36,000 rpm) and 20% above Rated (43,200 rpm). Coastdown Following Rapid Acceleration. [210 μin/div (5.33×10^{-6} m/div) and 1 ms/div, T = Turbine-End Probes, C = Compressor-End Probes]

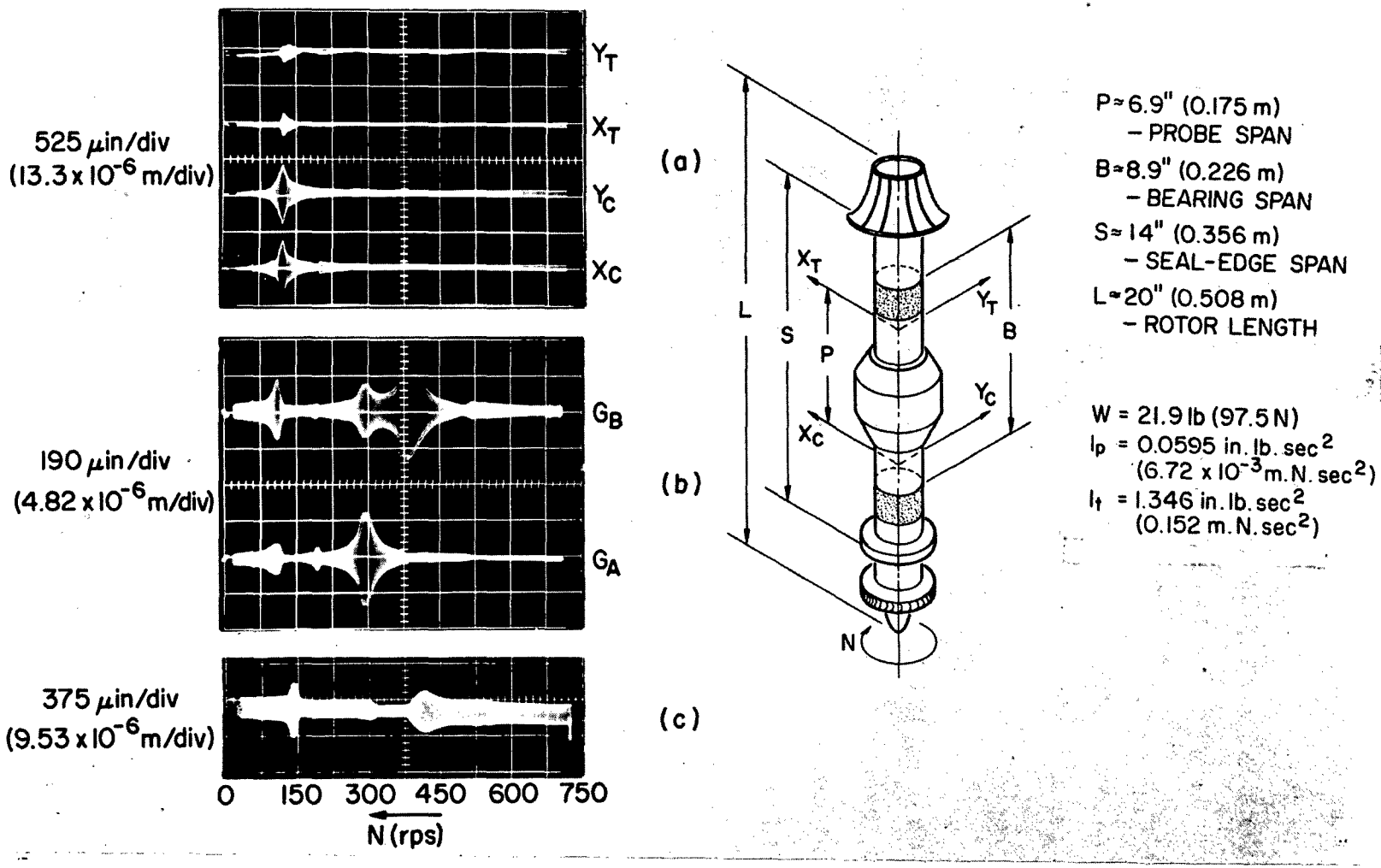

Fig. 20 Scans of Amplitudes of Motion of Rotor (a), Thrust Bearing Gimbals (b), and Thrust Bearing Gap (c). Coastdown Following Rapid Acceleration

loaded side of the thrust bearing. Note also that the resonance of G_A occurs at a lower speed (since it involves the larger, i.e. total stator inertia), and that it is reflected in the motion of G_B because of coupling via a frictional damper.* It can also be seen that rotor-foil bearing resonances are reflected in the motion of the thrust bearing stator. The variation of thrust bearing gap in (c) is more difficult to interpret, since it involves the phase between motions of gimbals, the axial movement of the rotor, and a slight deviation in perpendicularity between the plane of the runner and the axis of rotation. The spike at the beginning of coastdown is caused by the sudden air-supply cutoff and the corresponding step-change in axial thrust. The content of Fig. 21 is identical with that of Fig. 20, except that scans were recorded during acceleration (cold) to rated speed, rather than during coastdown. The differences between corresponding oscillograms in Fig. 20 and Fig. 21 are minor.

The first measurements of journal-bearing clearance are presented in Fig. 22. Oscillogram (a) contains the scan of d.c. outputs of probes F and J (see insert-diagram in Fig. 22), the difference of these outputs being proportional to the clearance h at the center of wrap. Scans of clearance during acceleration and coastdown are presented in oscillograms (b) and (c). The scans were recorded in virtually "cold" condition, and the clearance was of the order of 420 μin to 460 μin (10.7×10^{-6} m to 11.7×10^{-6} m). This is approximately twice the magnitude obtained numerically by means of the computer program of reference [9]. The time-base oscillograms (d) and (e) show the amplitudes of motion at resonance (121 rps) and at high speed (630 rps) of the journal (J) and of a foil sector at the center of wrap (F). The trace of the J-probe in Fig. 22 (e) displays 2 cycles per revolution.

*See reference [1] for illustrations of thrust-bearing configuration. The resonant speeds and amplitudes of the gimbals will, of course, vary with thrust-bearing supply pressures.

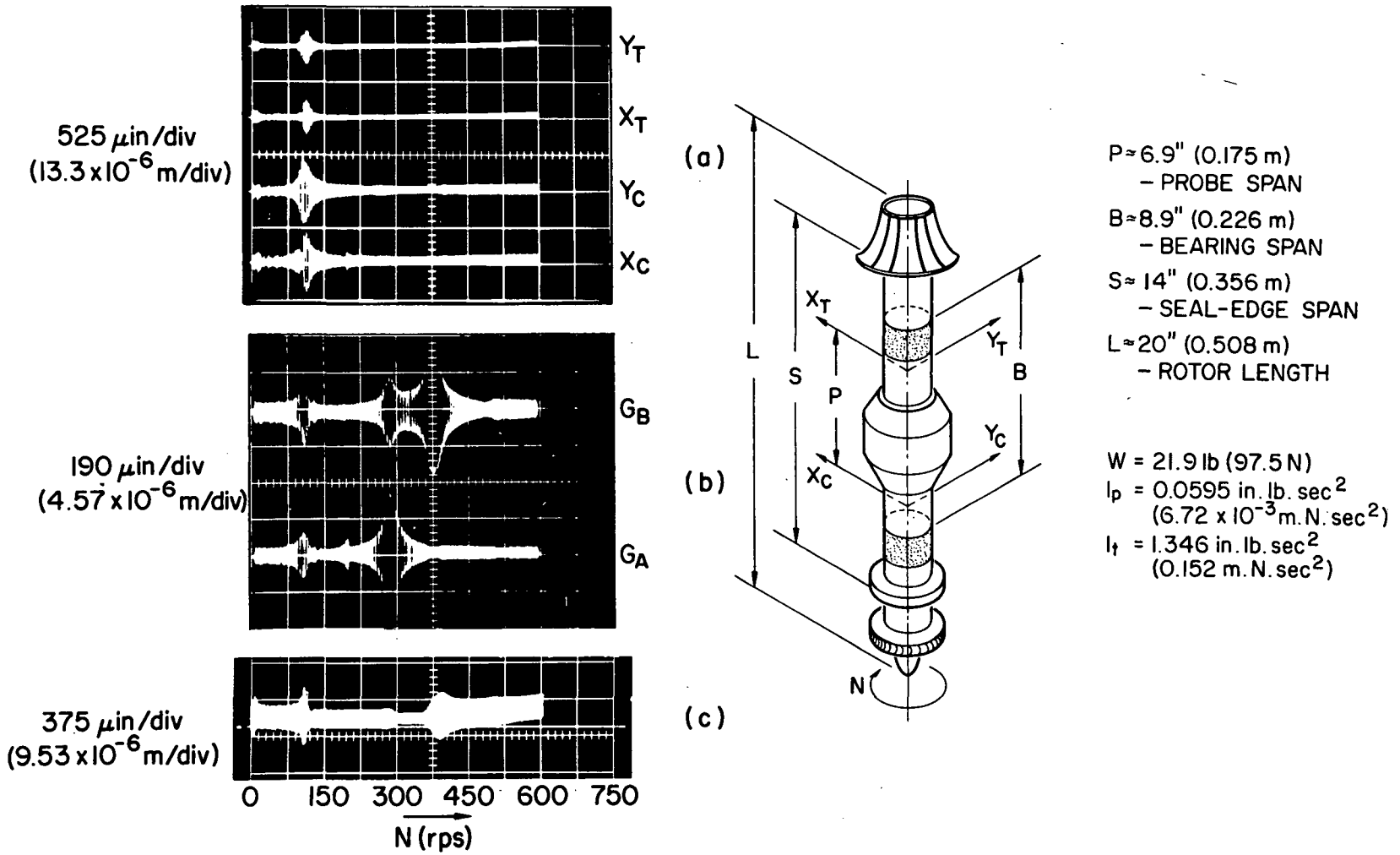

Fig. 21 Scans of Amplitudes of Rotor (a), Thrust Bearing Gimbals (b), and Thrust Bearing Gap (c). Acceleration to Rated Speed (36,000 rpm) from Ambient Temperature Conditions

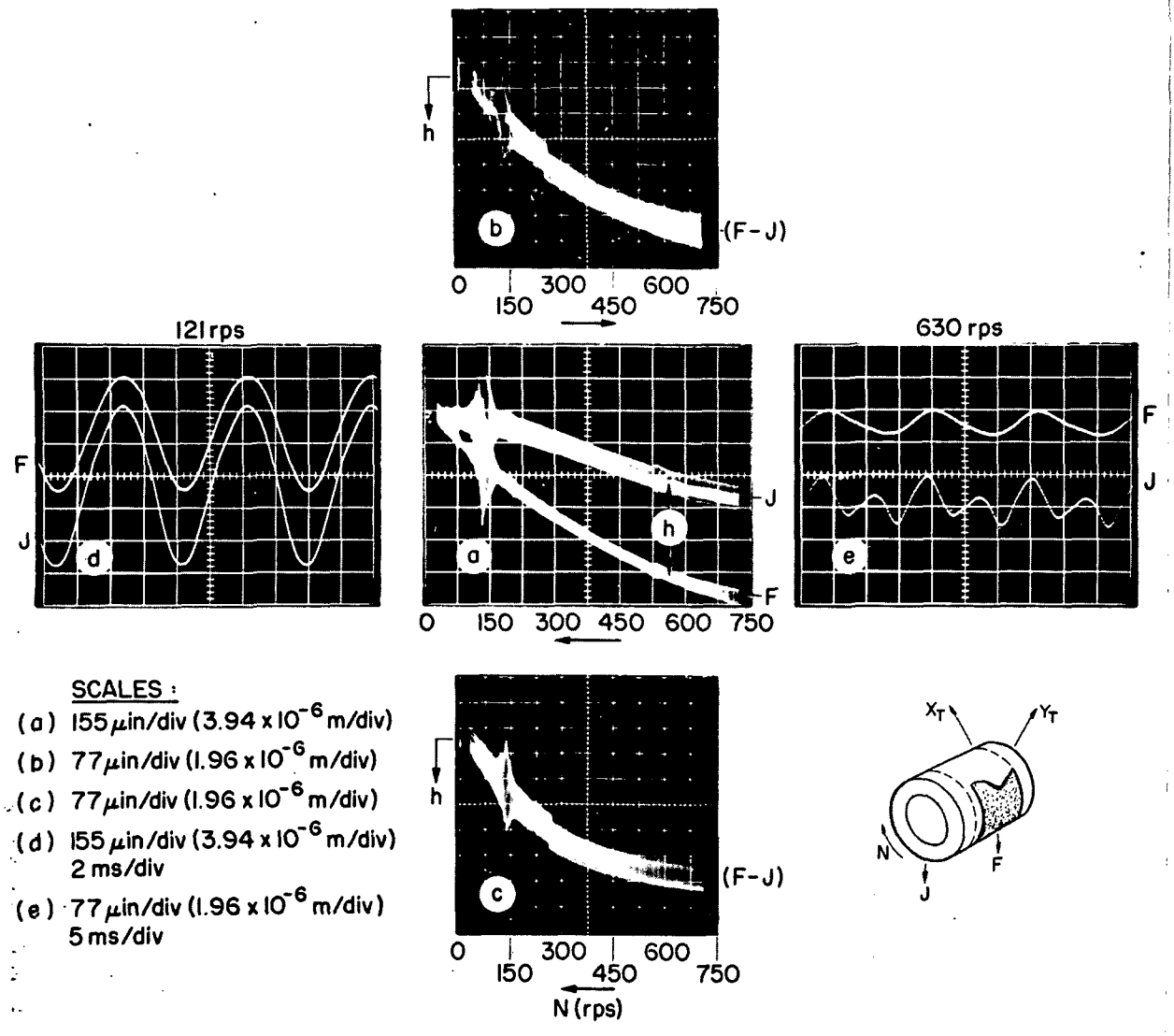

Fig. 22 Displacement and Motion of Journal and Foil (Turbine End). - Scan of Displacements (a), and Gap Width (b,c). Motion of Journal and Foil at Resonance (d), and Rated Speed (e).

This is due to the location of the probe in the immediate vicinity of a curvic coupling. In this region, the local distortion (ovality) of the journal is pronounced, since it adjoins the area where forces are transmitted from the tension bolt through the serrations of the coupling. The time-base displays indicate that the motion of the foil at the center of wrap and that of the journal were nearly in phase, particularly at resonance. Additional data relevant to clearance measurement are contained in Appendix 3.

In the next series of tests, the simulator was operated at rated speed of 600 rps for a period of 2 hours, in order to bring the system to thermal equilibrium prior to recording of data during coastdown. The objective was to observe the effect of temperature rise on high-speed rotor performance, and to determine the influence of differential expansion of system components on rotor dynamics. Such 2-hour runs were preparatory to a continuous 100-hour run, scheduled for a more comprehensive evaluation of foil bearing performance at rated speed.

Temperature variations associated with slow thermal transient are presented in Fig. 23. It can be seen that the temperatures of the foil and of the support-guide leveled off at approximately 218°F (103°C) and 184°F (85°C). This represents a difference of 34°F (19°C) between foil and support-guide temperatures. The foil temperature, which can be assumed to vary but little from the journal temperature (see Appendix 2), rises 85°F (47°C) above the air temperature in the bearing enclosure within the housing, and 149°F (83°C) above the ambient air temperature. Note that the foil temperature rise in 1 hour is approximately 97% of the total increase.

The orbits and time-base displays presented in Fig. 24 were recorded during coastdown from thermal equilibrium, attained at rated speed of 600 rps. A comparison can be made with data in Fig. 18, which corresponds to a cold coastdown. The 10% increase in resonant speed

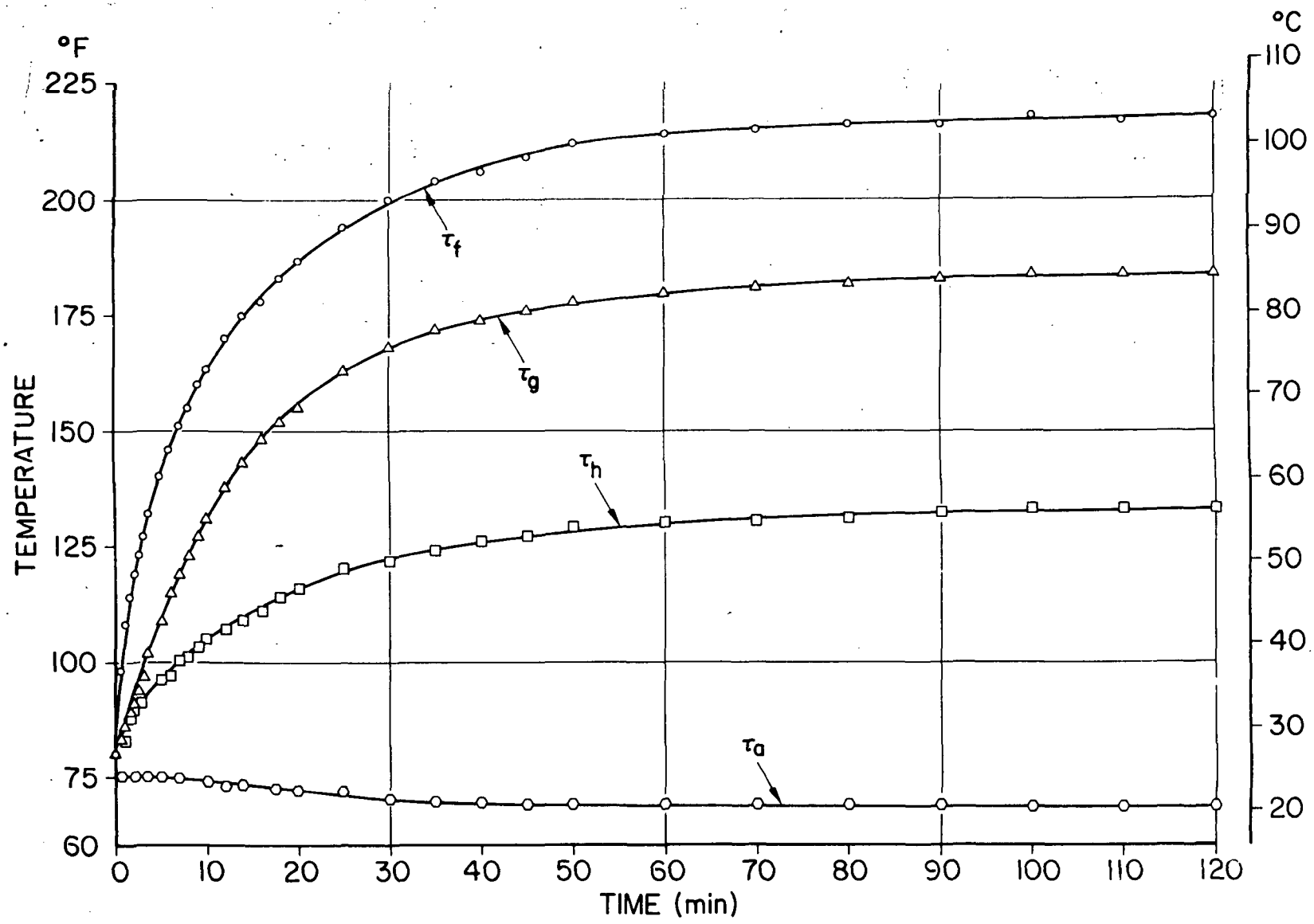

Fig. 23 Temperature Record of 2-Hour Run to Thermal Equilibrium (τ_f = Foil Temperature, τ_g = Foil Guide-Support Temperature, τ_h = Air Temperature in Housing, τ_a = Ambient Air Temperature Outside Housing)

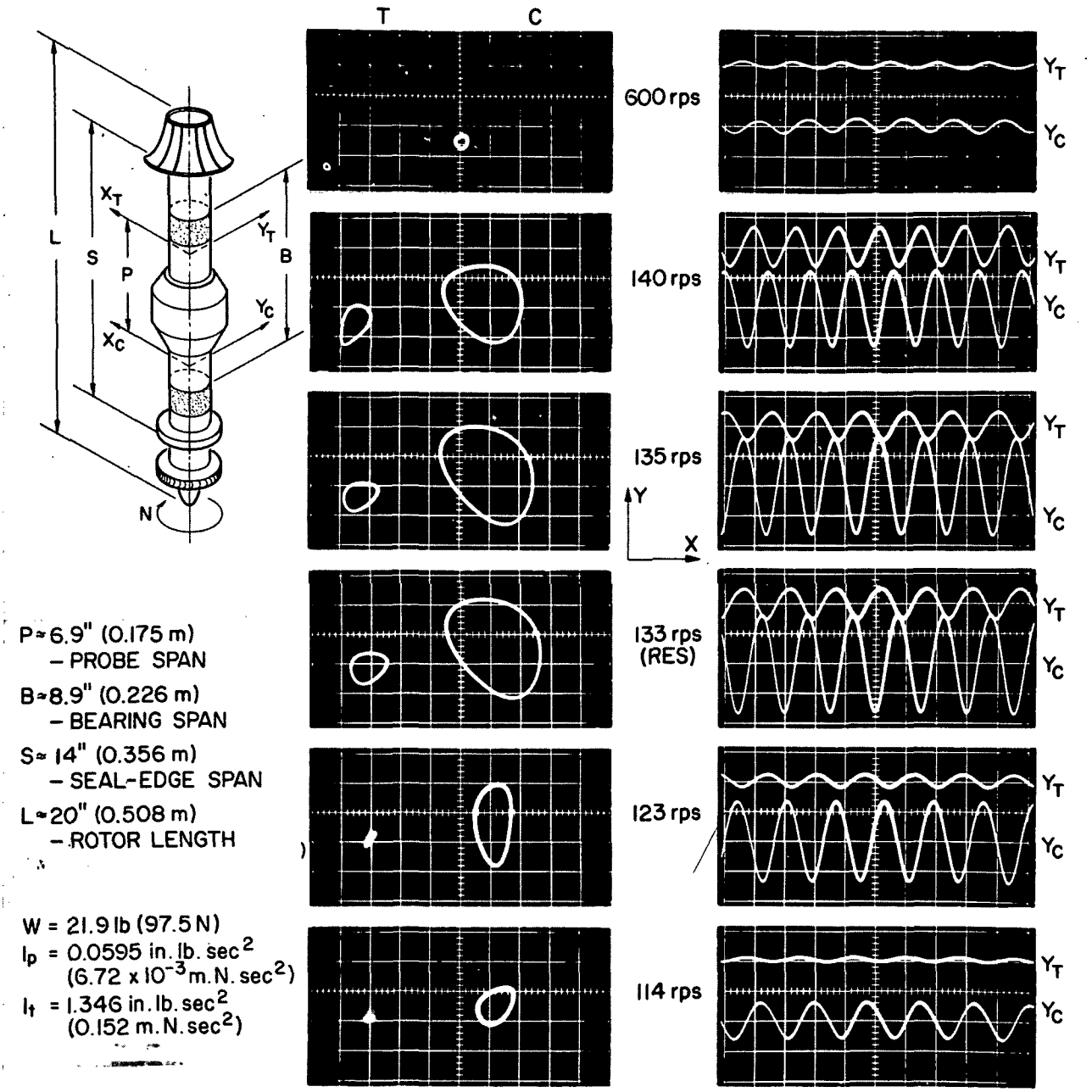

Fig. 24 Motion of Rotor in Resonant Bandwidth and Rated Speed (36,000 rpm). Coastdown from Thermal Equilibrium Conditions after 2-Hour Run. [210 μin/div (5.33 x 10^{-6} m/div) and 5 ms/div (1 ms/div at 600 rps). T = Turbine-End Probes, C = Compressor-End Probes]

(from 121 rps in Fig. 18 to 133 rps in Fig. 24) indicates an increase in bearing stiffness, which may be attributed to a moderate decrease of clearance induced through differential thermal expansion. The maximum orbit dimension of approximately 800 μin (20.3×10^{-6} m) at 133 rps, Fig. 24, is 11% smaller than the resonant orbit in the cold condition at 121 rps, Fig. 18. The foregoing comparison appears to indicate, that for the particular combination of metals and temperature differences, the effect of heating and differential expansion produced an increase in both stiffness and damping of the foil bearing.

3.4 Continuous 100-Hour Run

The 100-hour continuous run at rated speed of 600 rps was quite uneventful. A record of this run is presented for the sake of completeness of this report. The orbital motion, recorded photographically at 13 time intervals, varying in length between 6 and 10 hours, is documented in Fig. 25. The orbits remained identical, with the diameter of the larger, compressor-end orbit the order of 85 μin (2.16×10^{-6} m). A temperature log, maintained in the course of the 100-hour run, is appended in Fig. 26. Temperatures varied within narrow limits and reflected hourly and daily changes at the air intake and at the cooling-water inlet of the reciprocating compressor supplying air to the drive. Minor temperature variations were also due to small deviations from rated speed.

At the end of the 100-hour period, the rotor was accelerated up to 720 rps (20% above rated) and allowed to coast down. Data pertinent to this coastdown is presented in Fig. 27. The column of oscillograms on the left hand side of Fig. 27 pertains to the resonant bandwidth, and the orbits vary but little from those obtained after a 2-hour run, Fig. 24. Shown also in Fig. 27(d) is the inwardly spiralling orbit, associated with frictional excitation prior to stopping. The maximum peak-to-peak excursion occurred at approximately 13 rps and was of the same order of

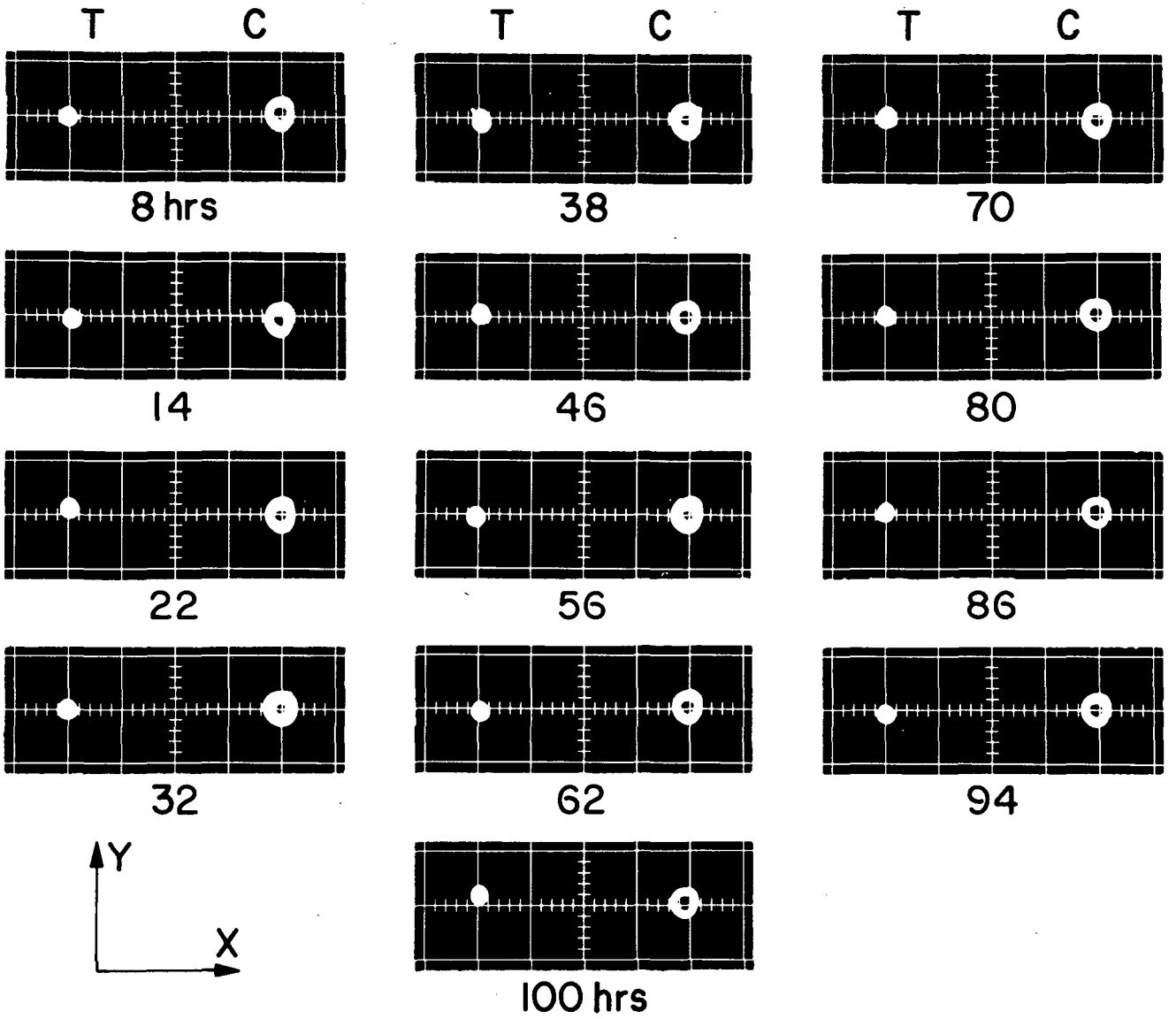

Fig. 25 Record of Orbital Motion at 36,000 rpm During 100-Hour Run. [210 μin/div (5.33×10^{-6} m/div), T = Turbine-End Probes, C = Compressor-End Probes]

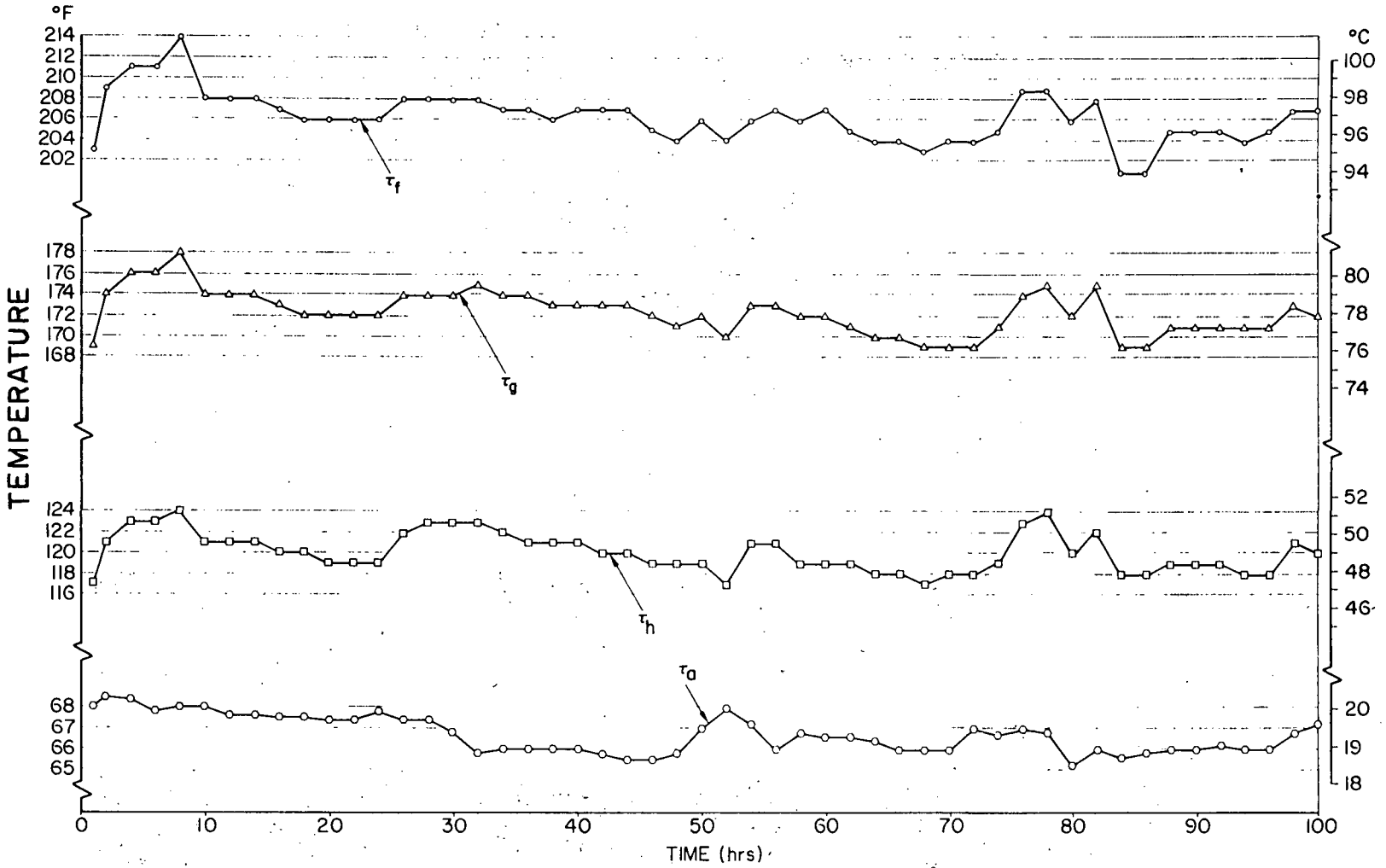

Fig. 26 Variation of Temperatures During 100-Hour Run. (τ_f = Foil Temperature, τ_g = Foil Guide-Support Temperature, τ_h = Air Temperature in Housing, τ_a = Ambient Air Temperature Outside Housing)

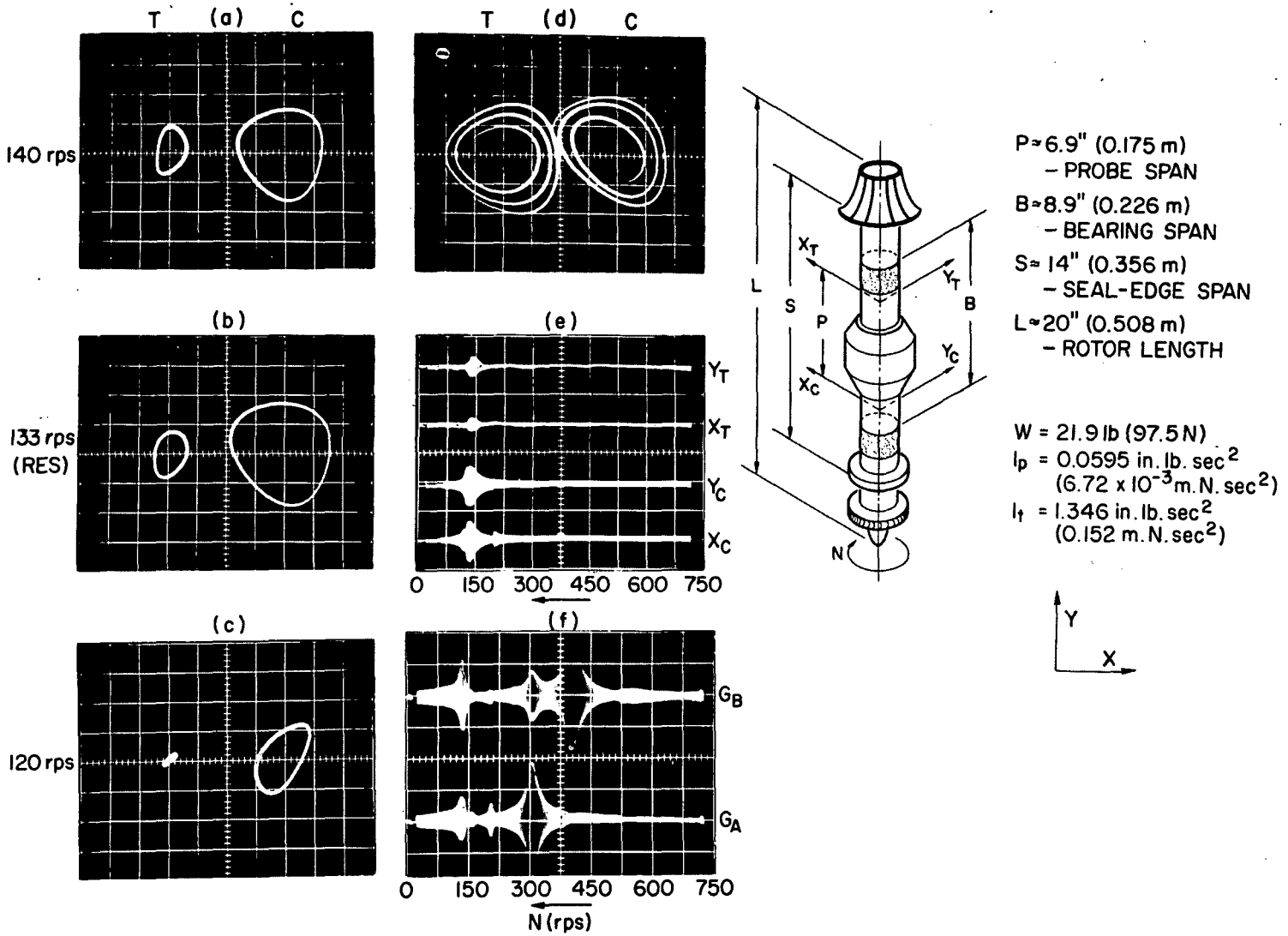

Fig. 27 Motion of Rotor and Gimbals During Coastdown after 100-Hour Run. Orbits in Resonant Bandwidth (a,b,c), and at ~ 13 rps prior to Stopping (d). Scans of Rotor (e) and Gimbal (f) Amplitudes. [Orbits 210 μin/div (5.33 x 10^{-6} m/div), Rotor Ampl. 525 μin/div (13.3 x 10^{-6} m/div), Gimbal Ampl. 180 μin/div (4.57 x 10^{-6} m/div). T = Turbine-End Probes, C = Compressor-End Probes]

magnitude as the orbit at resonance. Scans of journal and gimbal amplitudes are illustrated in the oscillograms (e) and (f) in Fig. 27. The latter are very similar to those previously presented in Fig. 20 and Fig. 21.

At the time of completion of the 100-hour run, the rotor had been started and stopped close to 100 times. The history of start-stop cycling is the subject of the following section, with emphasis on both the dynamic response to frictional excitation and wipe-wear effects on foil-bearing performance.

3.5 Starting and Stopping. - Dynamic Response to Frictional Excitation. Wipe-Wear Effects on Performance of Foil Bearings

At the conclusion of the 100-hour and of several 2-hour runs, and upon completion of various tests and recording of data under "cold" and "warm" conditions, the foil bearings and journals had been subjected to over 125 start-stop cycles.* The largest excursions encountered in the course of testing occurred during coastdown, at speeds less than 20 rps, and were commensurate with the resonant amplitudes, Fig. 27. Maxima of spiralling orbits were attained at approximately 13 to 15 rps, i.e. at speed low enough not to cause significant contact-damage. At no time, however, were the seals contacted by the rotor, and even the largest excursions left a very comfortable margin of safety. Oscillograms of the 90-th start-stop cycle are shown in Fig. 28. Unlike the largest resonant orbits, excited by major imbalance concentrated in the vicinity of the compressor end, the response to frictional excitation was more pronounced at the turbine end. The maximum radius of the rather symmetrical stopping spiral in Fig. 28 was 890 μin (22.6×10^{-6} m). This corresponds to an excursion of approximately 1150 μin (29.2×10^{-6} m) at the edge of the

*The contractual stipulation was a minimum of 10 start-stops, but thorough testing and scrupulous documentation of test results required that this number be exceeded many times.

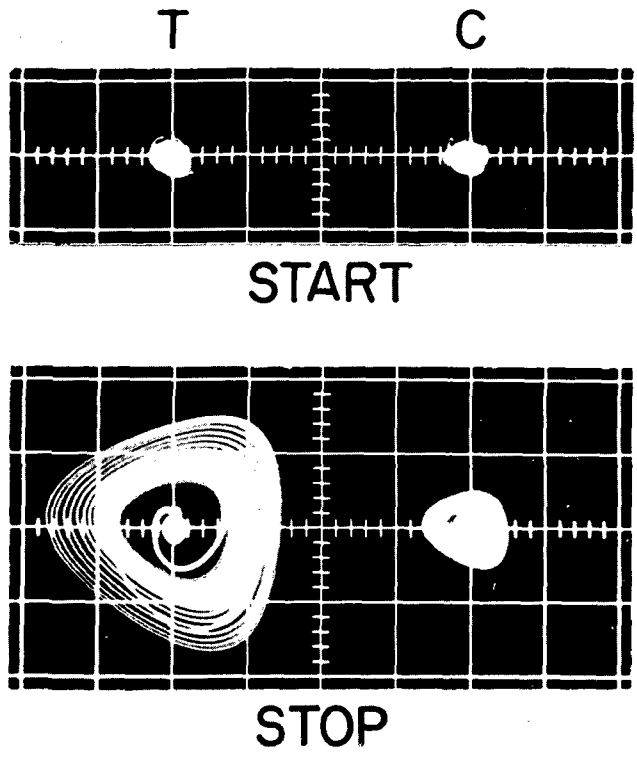

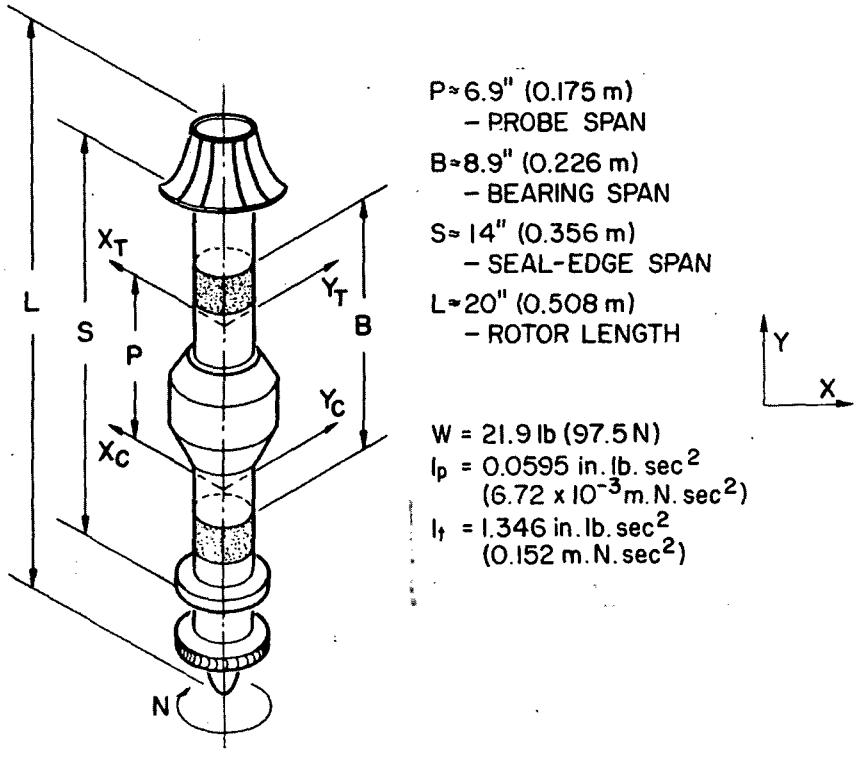

Fig. 28 Orbits of 90-th Start-Stop Cycle. Example of Largest Excursions During First 120 Start-Stops [525 μin/div (13.3 x 10^{-6} m/div). T = Turbine-End Probes, C = Compressor-End Probes]

turbine seal and represents merely 23% of the radial clearance-space. On the other hand, the maximum orbits recorded during relatively fast starting, Fig. 28, are approximately five times smaller in comparison with the largest stopping orbit.

After approximately 100 start-stop cycles, a marked decrease in amplitudes of excursions became quite apparent, particularly during stopping. Records of motion in the span 130 through 200 start-stop cycles, obtained at suitable intervals, are presented in columns of oscillograms in Fig. 29. Note that the largest excursions could be accommodated within a circle of radius smaller than 210 μin (5.33×10^{-6} m). A similar set of oscillograms, in the interval 200 through 400 start-stop cycles, is contained in Fig. 30. Sampling records were obtained at each 50-th start-stop cycle, and during each sampling cycle the rotor was brought up to rated speed of 600 rps prior to coastdown. This procedure furnished a periodic check of rotor performance in the entire speed range, and in the resonant bandwidth in particular. The central column in Fig. 30 contains the oscilloscope photographs of resonant orbits, obtained during coastdowns of sampling cycles. The magnitude of these orbits remained essentially constant and unchanged with respect to those recorded in the initial phase of testing. Furthermore, while the starting orbits (which reflect the excitation from the turbine-drive in addition to frictional excitation) remained practically unchanged, the magnitude of maximum excursions during stopping continued to decrease.

Encouraged by the faultless performance of the foil-bearing support and the absence of any danger signals in the dynamic response of the rotor, the experimenters decided to continue the test up to 1000 start-stop cycles.* Results pertinent to the interval from 400 through 1000 start-stop

*At the time of writing, the cumulative number of start-stop cycles stood at 1027. At this point the simulator was disassembled for the purpose of demonstration of foil-bearing assembly procedure to NASA personnel.

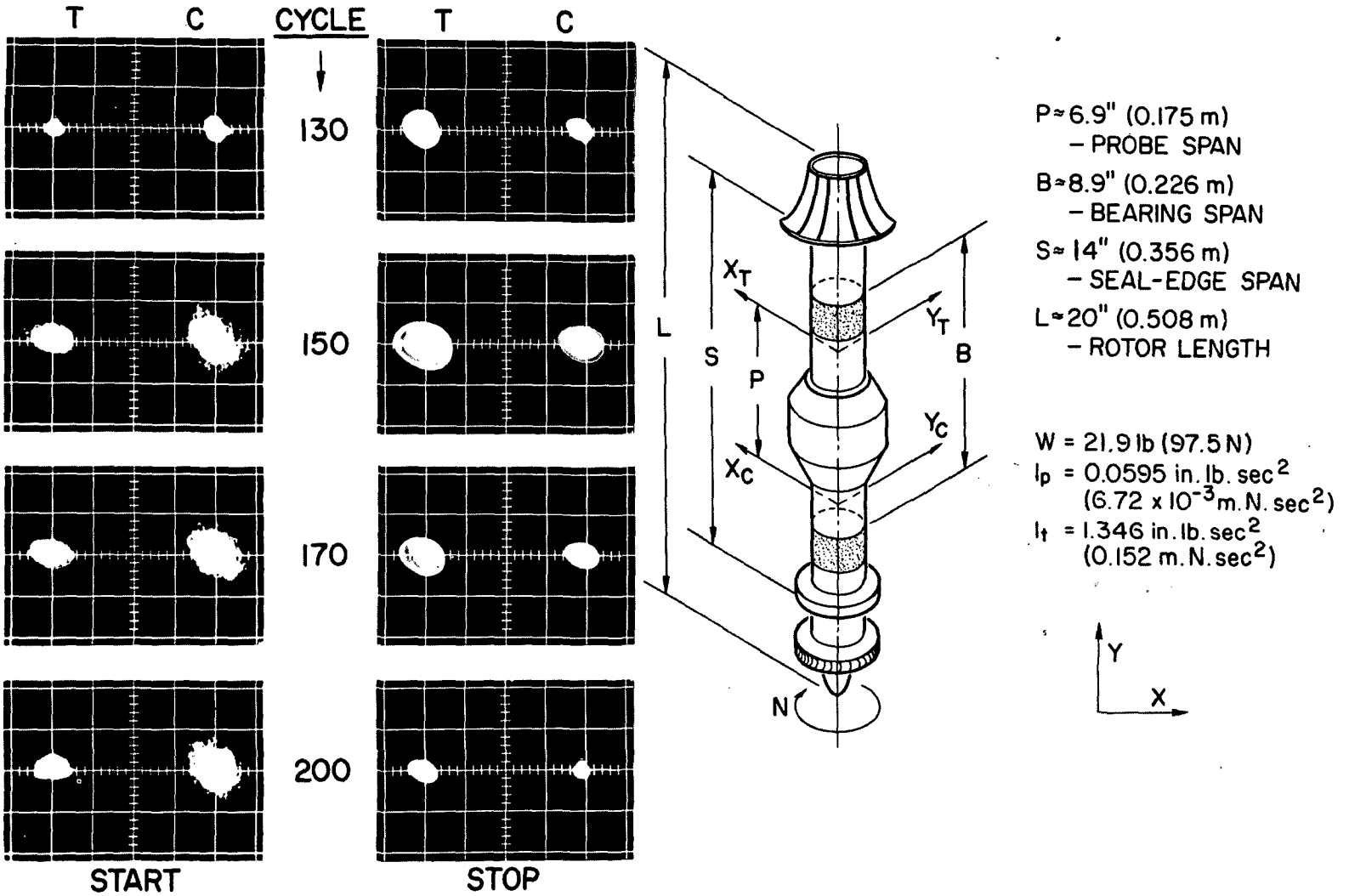

Fig. 29 Orbital Motion in the Interval 130-200 Start-Stop Cycles [210 μin/div (5.33 x 10^{-6} m/div). T = Turbine-End Probes, C = Compressor-End Probes]

cycles, with record-samples of performance now being limited to each 100-th cycle, are illustrated in Fig. 31. The results are similar in all respects to those presented in Fig. 30, and it can be seen that the response to frictional excitation during starting and stopping remained essentially unchanged. Moreover, no adverse effect on rotor performance could be observed, as evidenced by the resonant orbits in the center column of Fig. 31. The only exception was a hitherto unobserved subharmonic motion, in the speed intervals of approximately $240 < N < 255$ rps, and $150 < N < 205$ rps. The phenomenon was only present when the rotor was cold and could not be observed during coastdown from a state of thermal equilibrium.

The subharmonic motion in the interval $150 < N < 205$ rps is illustrated in Fig. 32. The number of revolutions per 1 cycle of the subharmonic motion remained constant at any given speed (i.e. repetitive path of journal center), but varied rapidly with speed in the interval $150 < N < 205$ rps, attaining a maximum ratio of 11 rps/cycle at approximately 167 rps. Initially, the regions of subharmonic motion were characterized by minor, synchronous resonances, with orbits of the same order of magnitude as the motion shown in Fig. 32. The subharmonics began to manifest themselves when the number of start-stop cycles was approaching the 1000 mark. The amplitude of the subharmonic motion remained small, and the interesting phenomenon, which reflects nonlinearities of the system encountered also in the course of previous experiments [2,3,6,7], caused little concern with regard to the operational capability of foil bearings.

Upon completion of the 1000-cycle start-stop test, the 1007-th start of the rotor was followed by yet another 2-hour run, in order to re-examine the system performance in the "warm and worn" condition. The results of this run, recorded during starting, coastdown and stopping, are shown in the oscilloscope photographs of Fig. 33. The maximum excursions at starting, resonance and stopping can be assessed from the upper row of

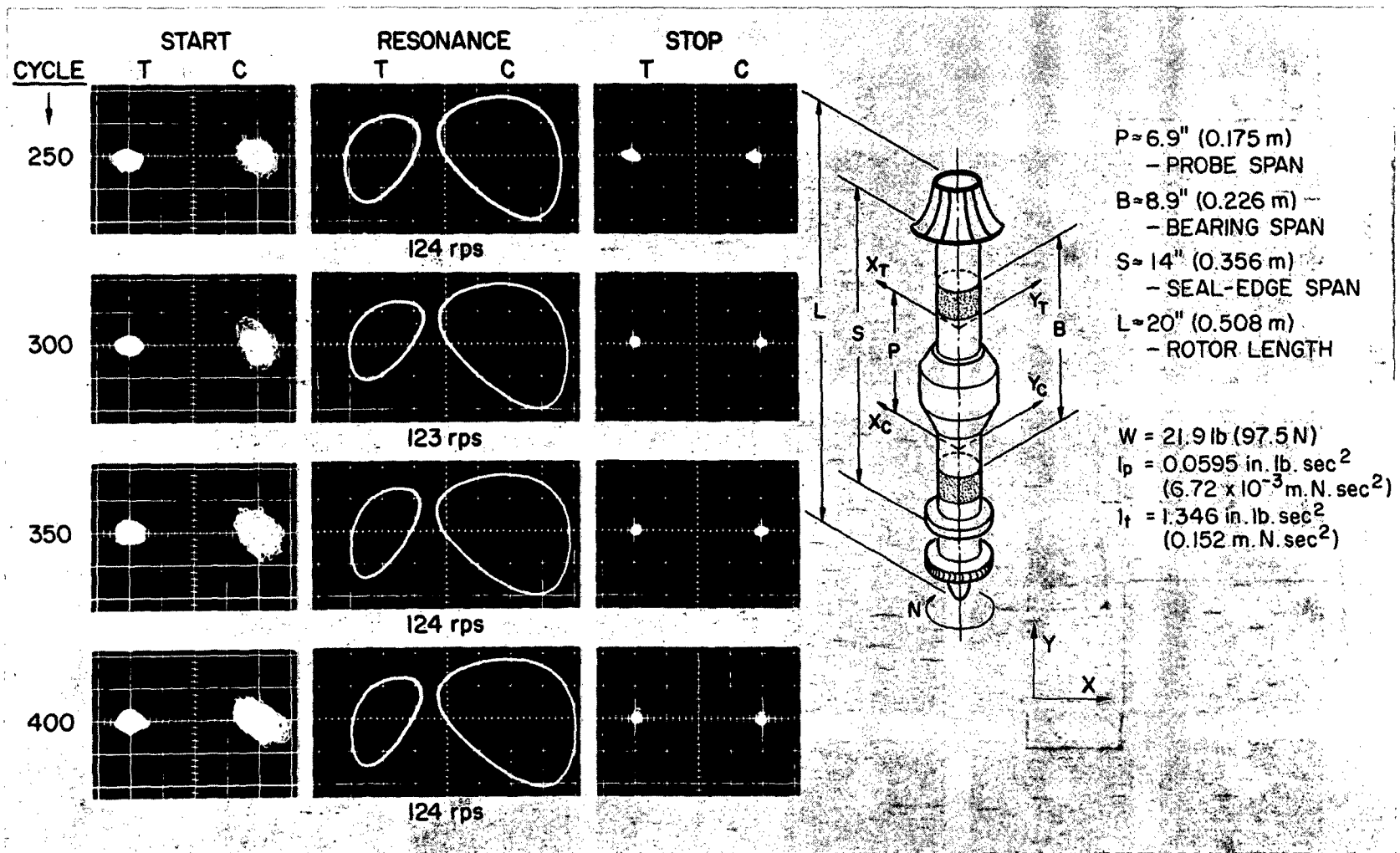

Fig. 30 Start-Stop and Resonant Orbits in the Interval 250-400 Cycles. [210 μin/div (5.33×10^{-6} m/div). T = Turbine-End Probes, C = Compressor-End Probes]

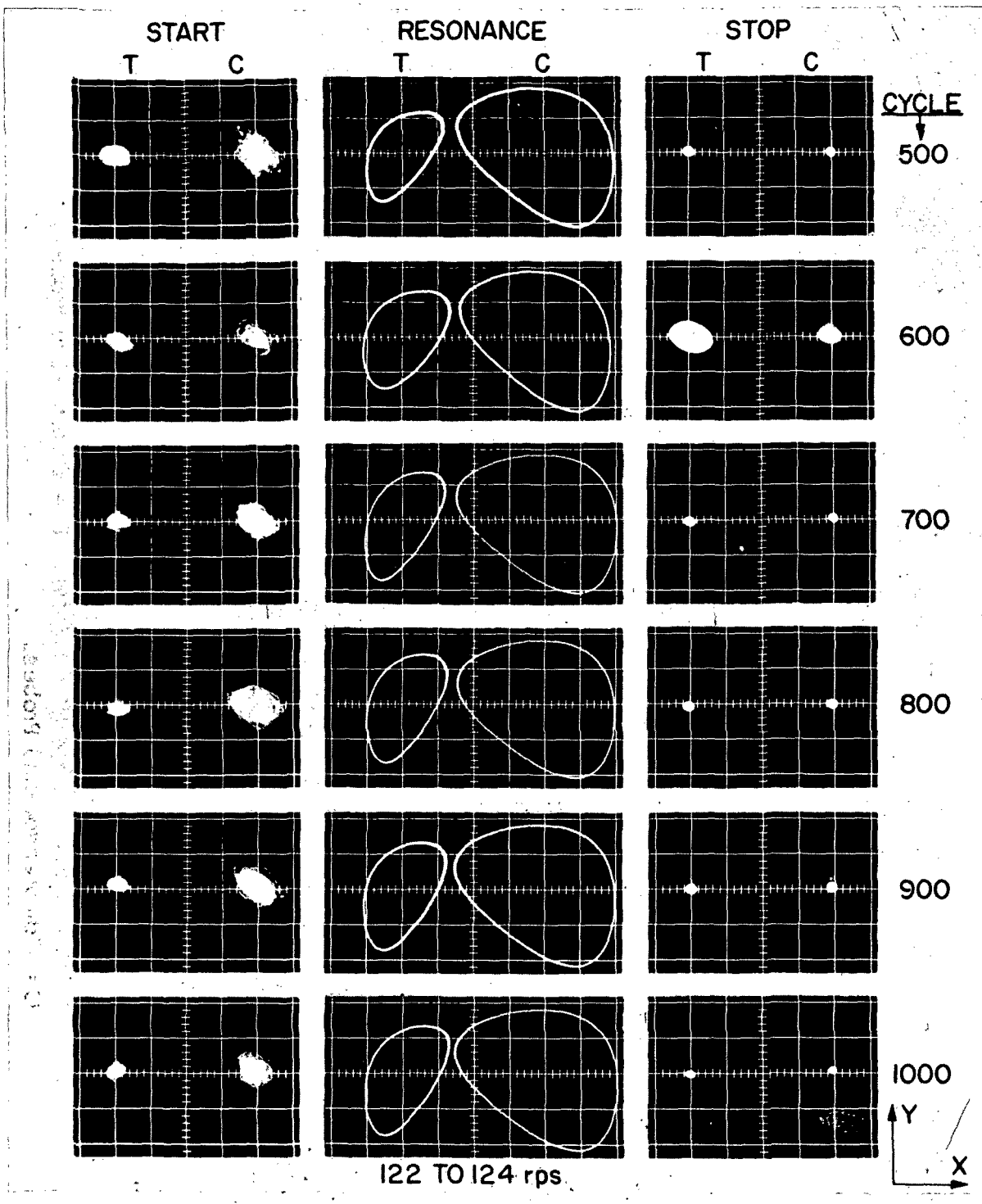

Fig. 31 Start-Stop and Resonant Orbits in the Interval 500-1000 Cycles. [210 μin/div (5.33×10^{-6} m/div). T = Turbine-End Probes, C = Compressor-End Probes]

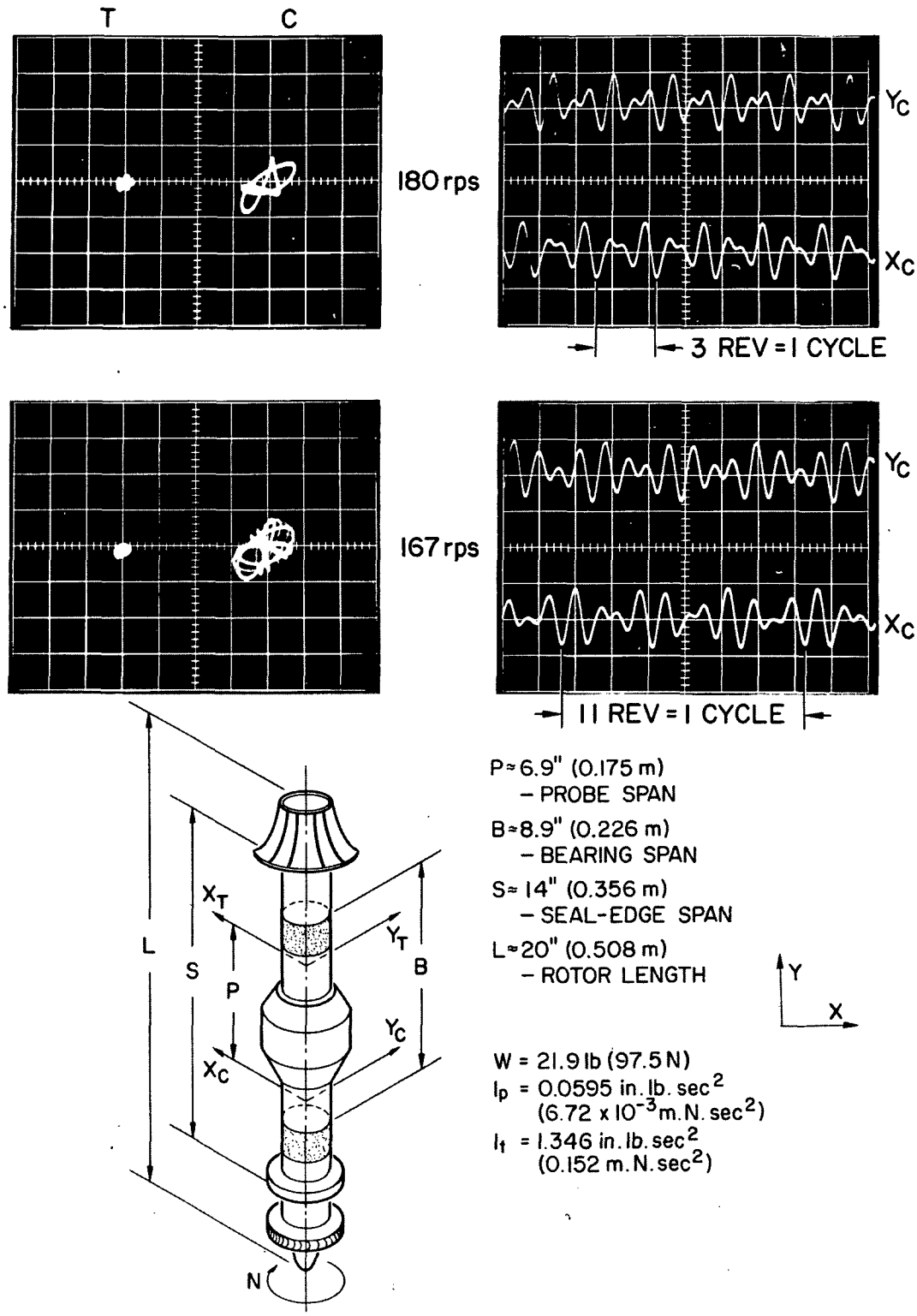

Fig. 32 Subharmonic Motion in the Bandwidth 150 < N < 205 rps During Coastdown, Following Rapid Acceleration from Ambient Temperature Condition. - 1015-th Start-Stop Cycle [210 μin/div (5.33 x 10^{-6} m/div) and 10 ms/div. T = Turbine-End Probes, C = Compressor-End Probes]

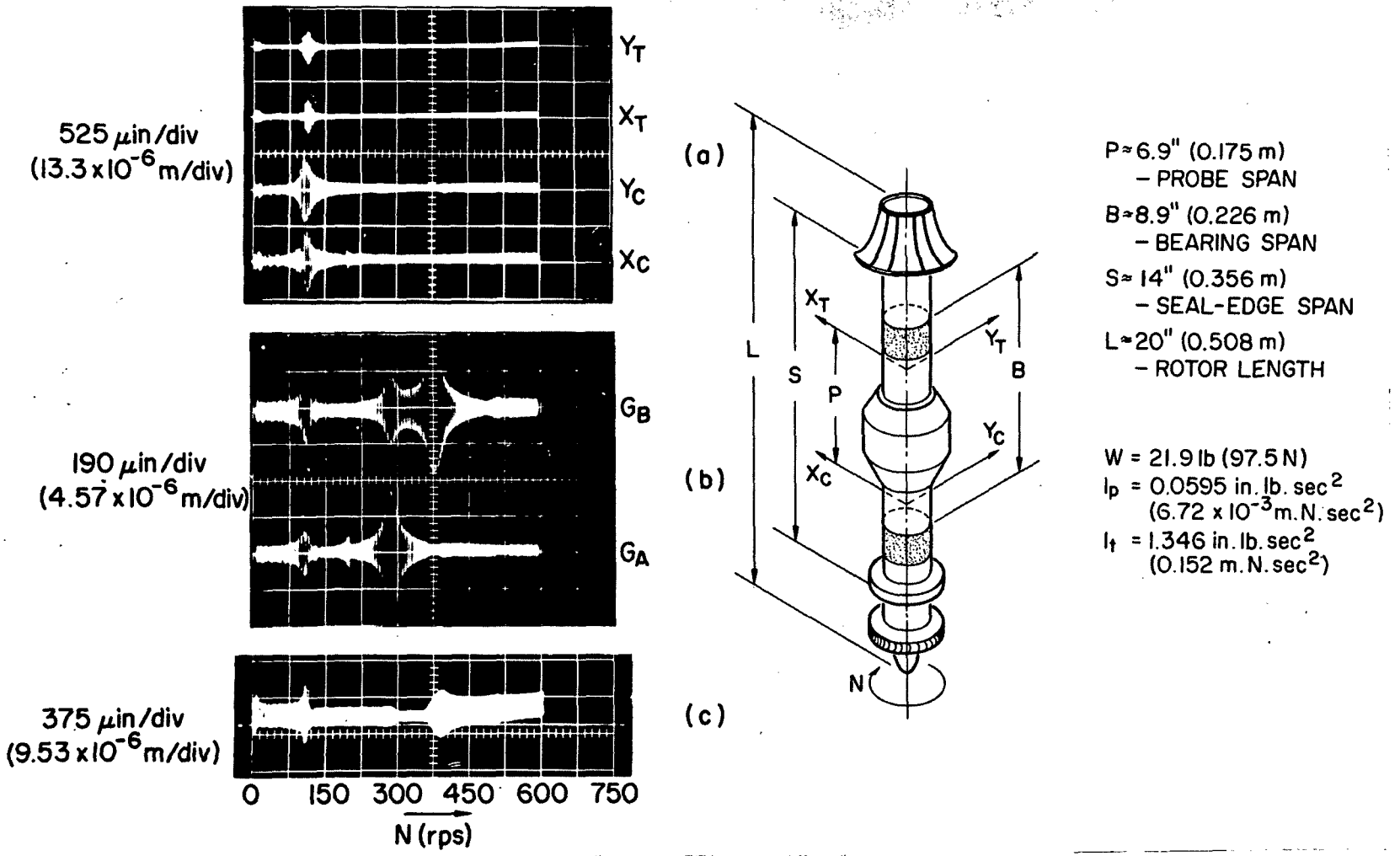

Fig. 33 Motion of Rotor During Coastdown from Equilibrium Temperature Following 2-Hour Run and 1000 Start-Stops (1007-th Cycle). [210 μin/div (5.33 x 10^{-6} m/div), except (d) 525 μin/div (13.3 x 10^{-6} m/div). T = Turbine-End Probes, C = Compressor-End Probes]

photographs in Fig. 33, while the remaining oscilloscope photograph contains a scan of amplitudes, similar to those presented in previous figures, e.g. Fig. 20. It can be seen that the 1007-th coastdown, following a 2-hour run to thermal equilibrium, was characterized by a resonant speed and orbit which differed but little from those recorded in the course of a similar run , in the early stages of start-stop cycling (Fig. 27). The subharmonic motion could not be observed during coastdown in the warm condition.

Although but a fraction of high-speed losses due to fluid friction can be attributed to viscous dissipation in the journal bearings, some conclusions can be drawn from the lower portions of coastdown curves of speed versus time presented in Fig. 34 and Fig. 35. A comparison is made in Fig. 34 between deceleration in the cold and in the warm condition, both having been recorded at, or near the 80-th start-stop cycle. The curves are nearly congruent and their slopes are almost identical, even in the low-speed range (although, as anticipated, the "warm" curve is slightly steeper). Another comparison is made in Fig. 35, which emphasizes the effect of wear, rather than of temperature. The coastdown curves compared in this case were obtained under cold conditions, one following the 80-th and the other the 1000-th start-stop cycle. The curves are congruent, down to approximately 150 rps. Thereafter, with the mean clearance decreasing to less than 100 μin (2.54×10^{-6} m) and foils coming progressively into contact with the journals, deceleration was more rapid during coastdown following 1000 start-stops. This may be due to localized surface roughening, especially along the foil edges [11,12].

The state of the journals and of the foils after 1027 start-stop cycles is illustrated in Fig. 36 through Fig. 39. The photographs of journals in Fig. 36 illustrate wear tracks, mostly along the foil edges, of which only one is of discernible but hardly significant depth. From the appended profilometer traces, it can be seen that the maximum depth of

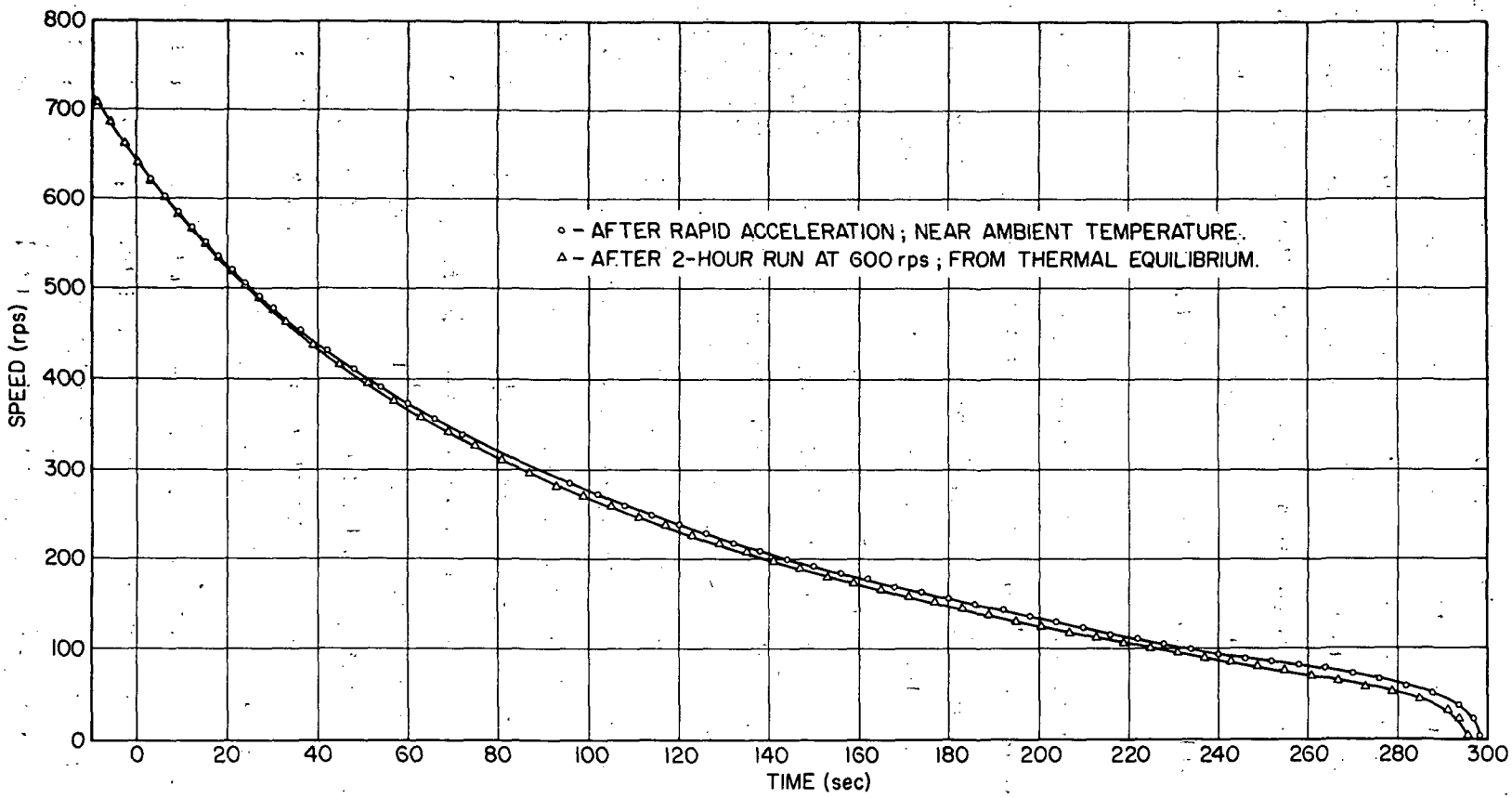

Fig. 34 Comparison of Coastdown Curves at Two Thermal Conditions (Following 80 Start-Stop Cycles)

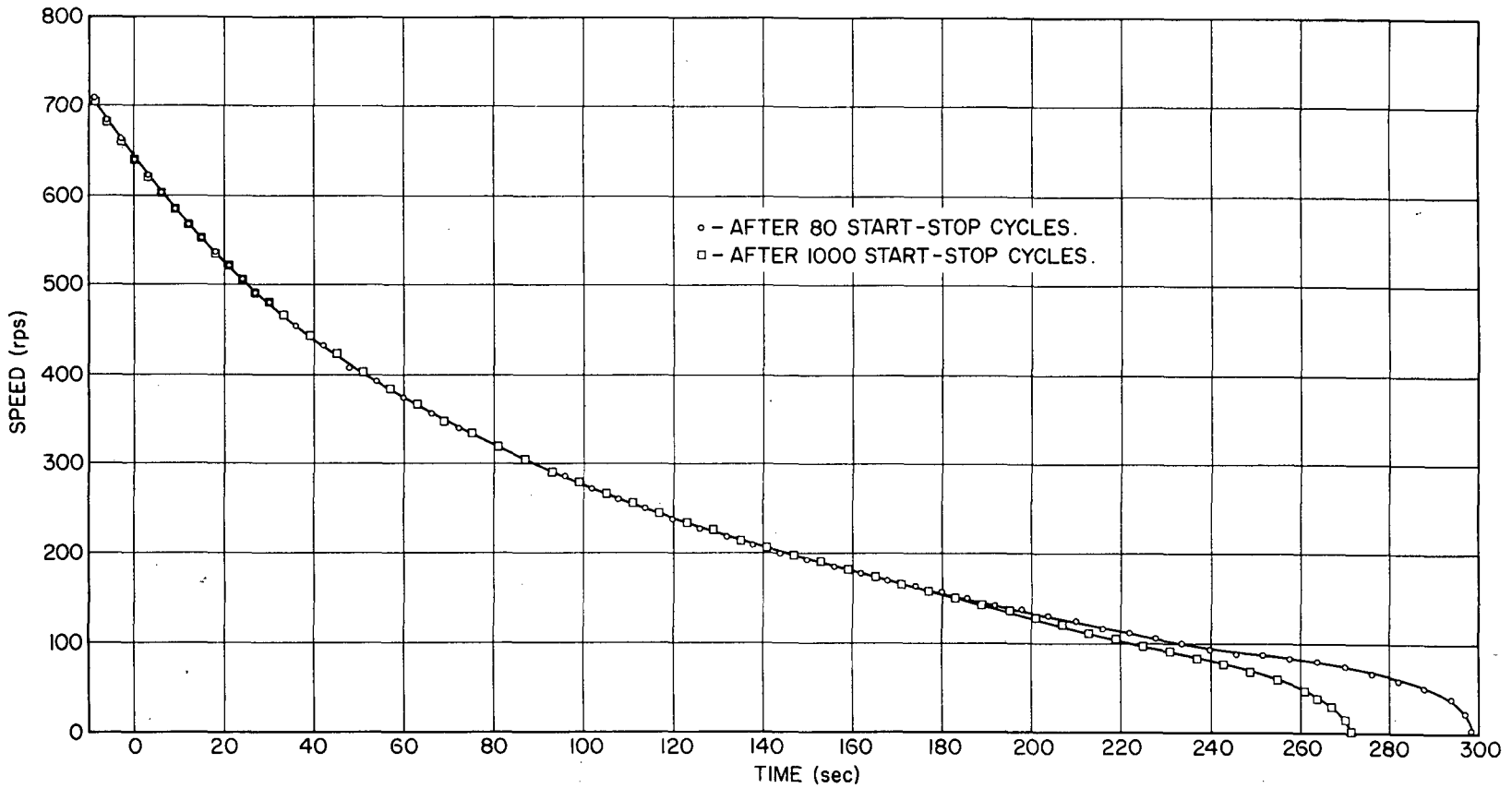

Fig. 35 Comparison of Coastdown Curves at Near Ambient Temperatures in Two States of Wear (Following Rapid Acceleration).

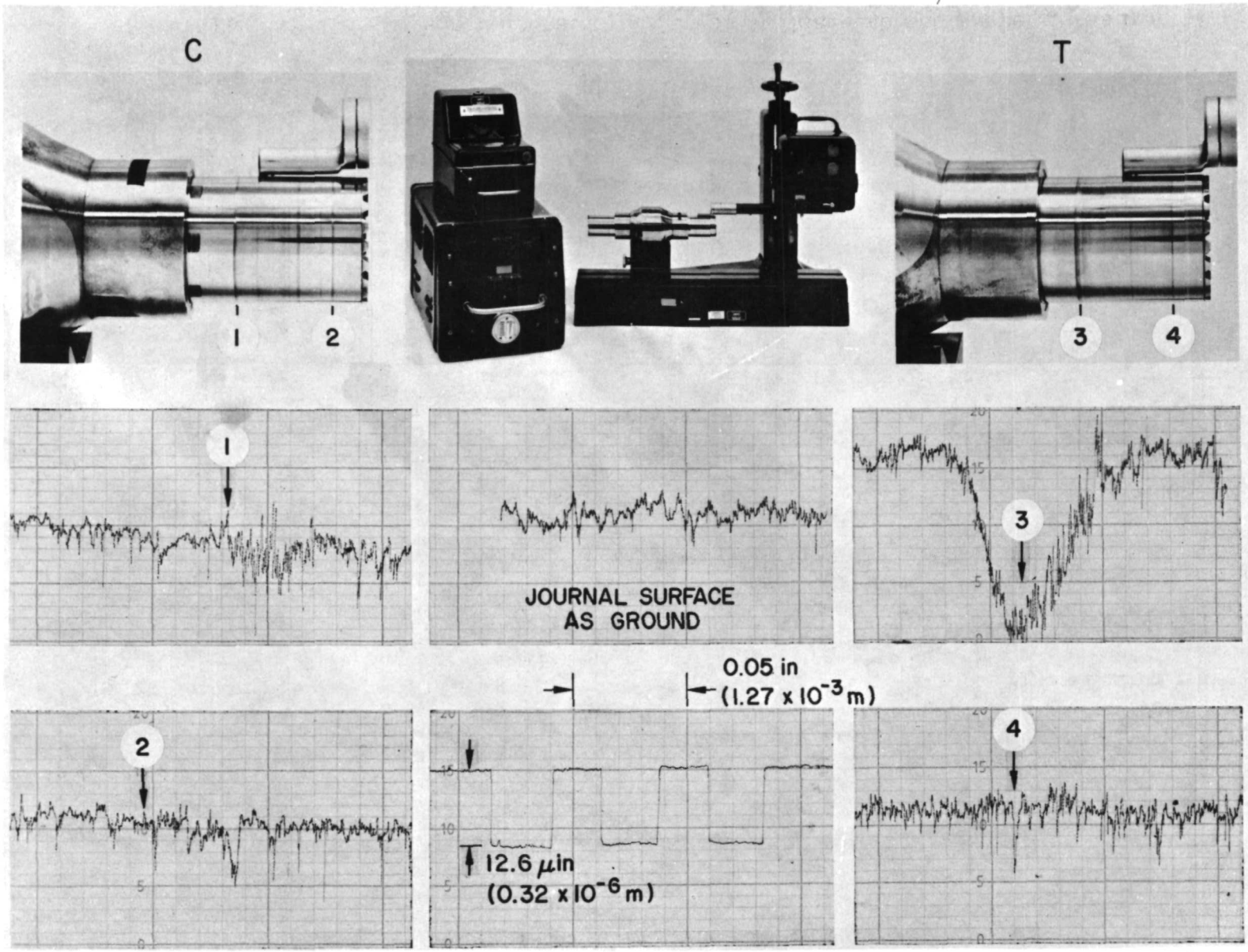

Fig. 36 State of Journals Following 1027 Start-Stop Cycles

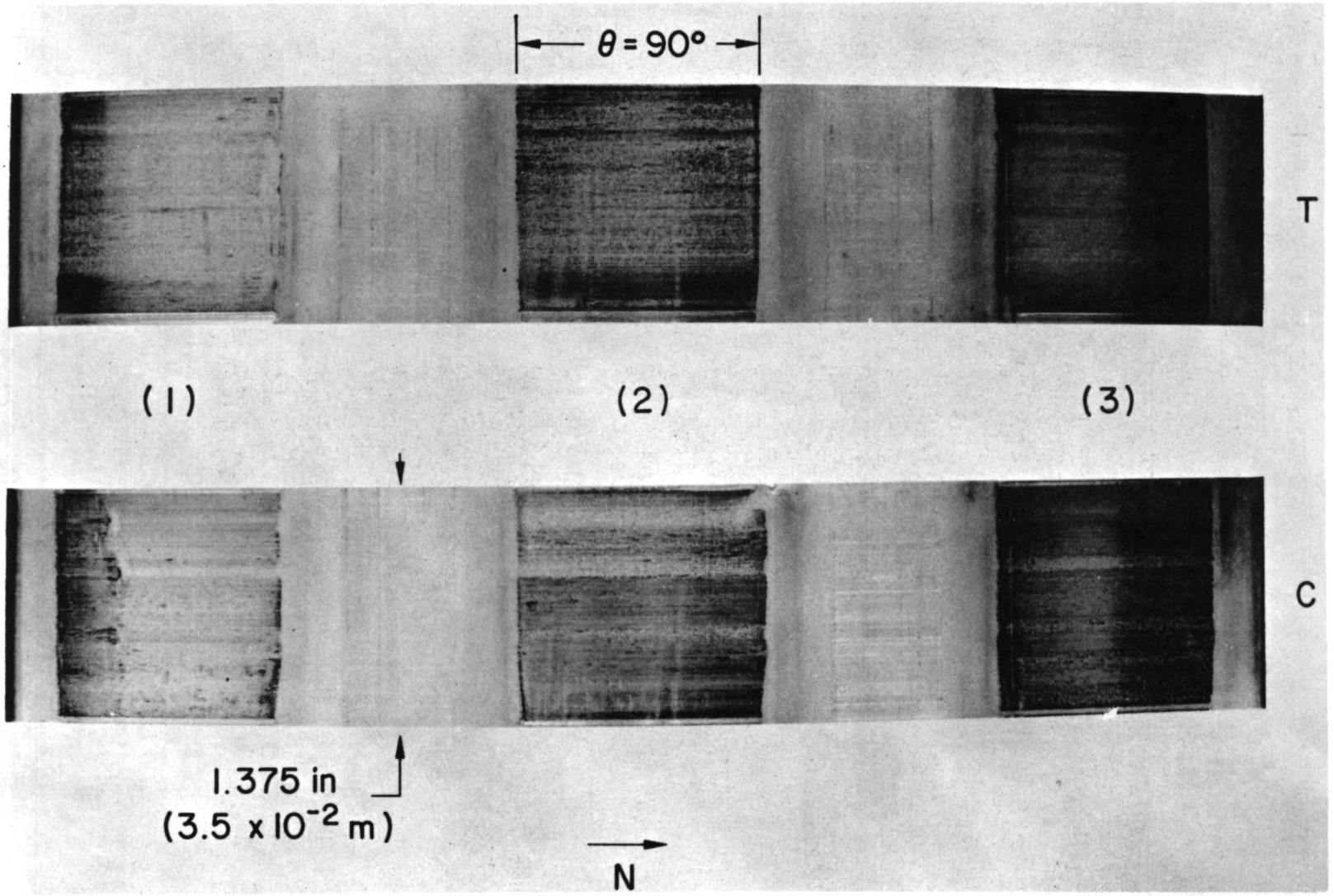

Fig. 37 State of Foils Following 1027 Start-Stop Cycles

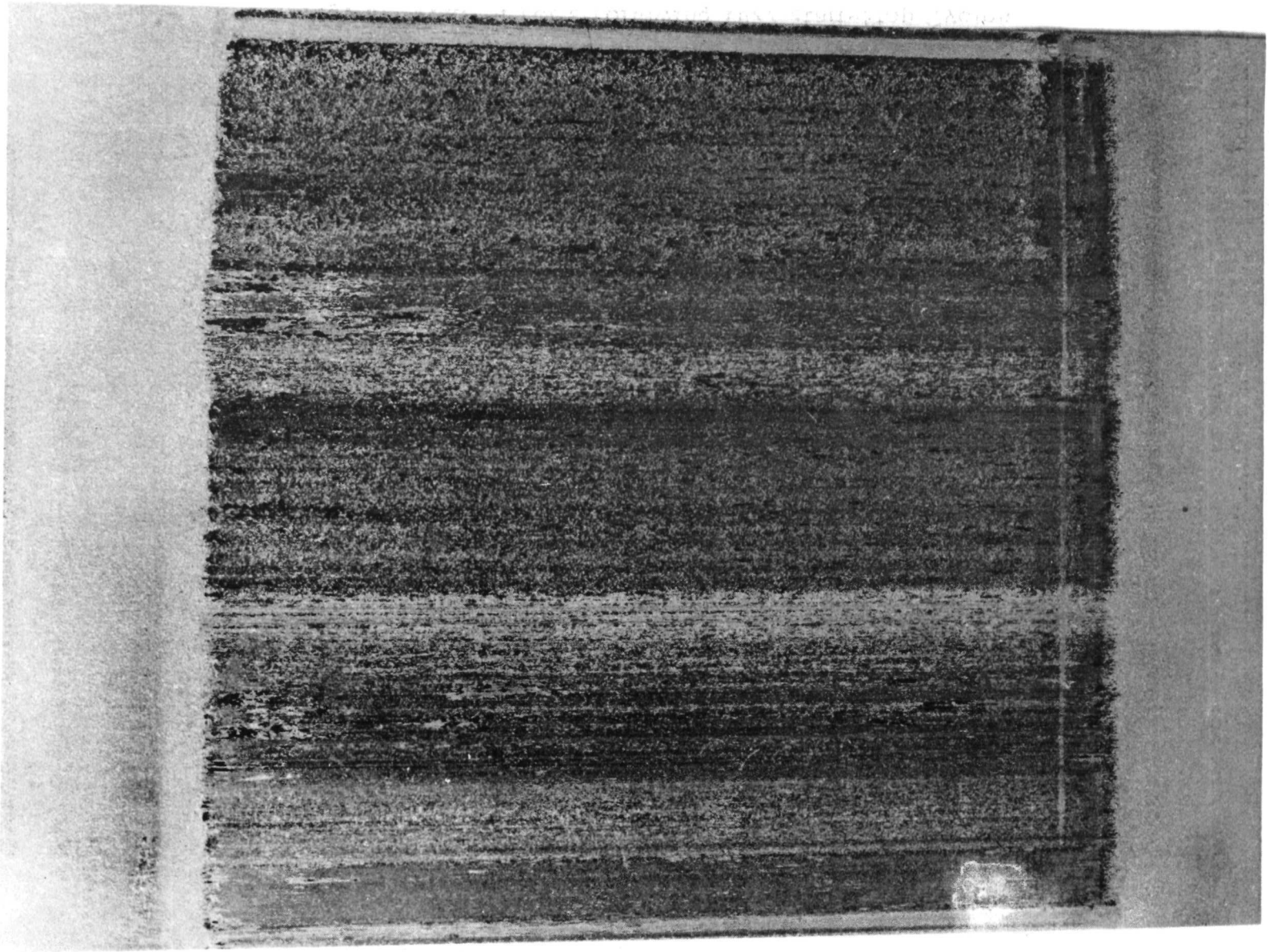

Fig. 38 Enlarged View of Coated Foil-Sector No. 3, Compressor End

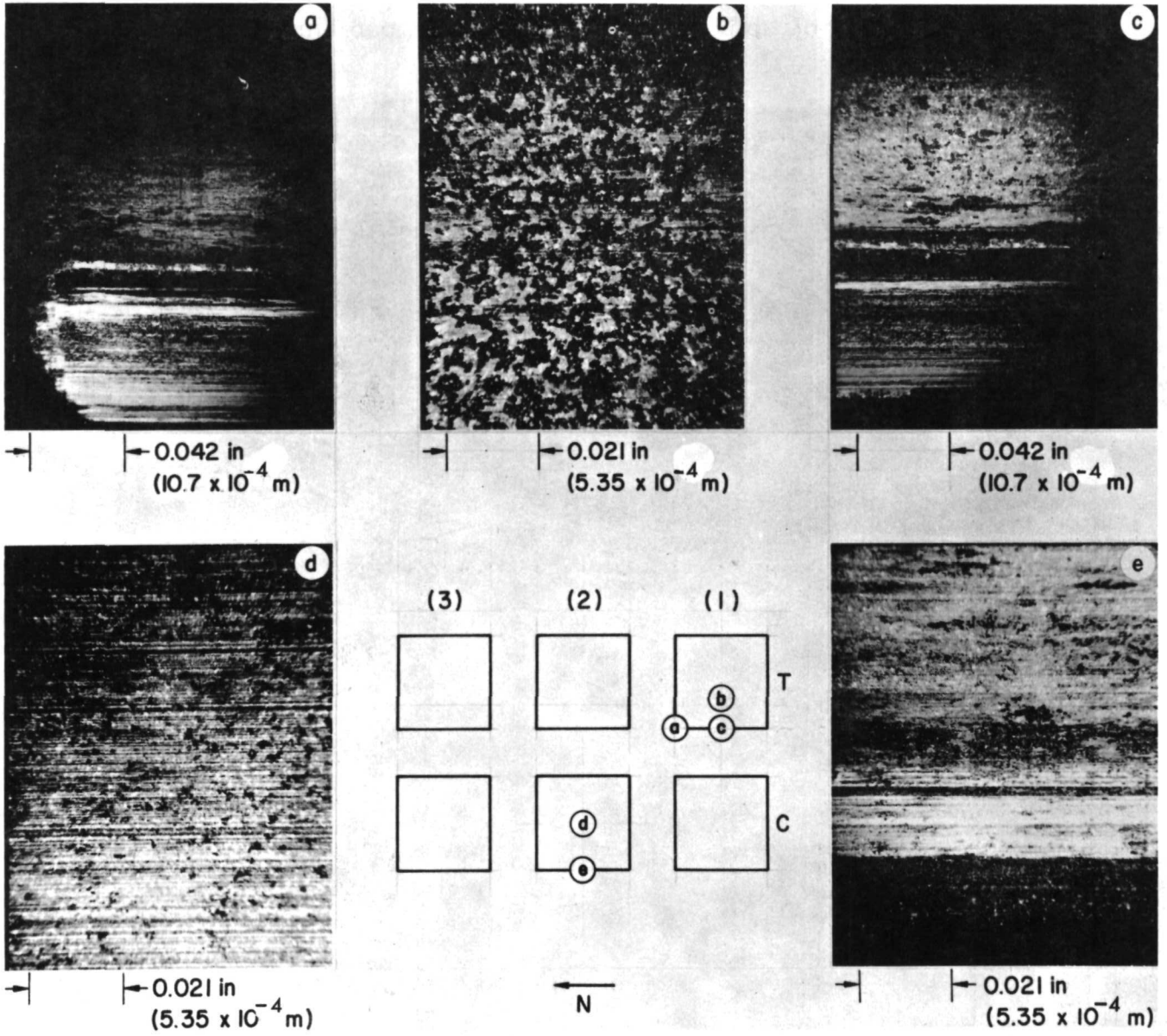

Fig. 39 Microscope Photographs of Coated Foil-Sectors Following 1027 Start-Stop Cycles

this wear track was approximately 30 μin (0.76×10^{-6} m), and that wear of journal surfaces was otherwise limited to polishing of microasperities. The foil photographs in Fig. 37 show broad and highly polished bands of MoS_2 film, separated by narrower and relatively dull strips, along which little film-wear had occurred. Clearly discernible is the bare, narrow strip along the lower edge of the turbine-end foil, which corresponds to the deepest, 30 μin (0.76×10^{-6} m) wear track on the journal in Fig. 36. Because of residual misalignments and nonuniformities of tension, wear was always more prominent at one of the two edges. Also, because of combined anticlastic and side-leakage effects, contact occurs first along ridges in close proximity of the edges [11, 12]. Narrow wear-tracks of this type are clearly discernible in the sector shown in Fig. 38.

The nature of wear of coated foil-sectors is also illustrated by means of microscope photographs in Fig. 39, and the approximate location of each field of view is indicated in the appended diagram. The reader should note that lighter areas (i.e. more reflective regions) correspond to polished MoS_2 film, or to bare foil-metal along the edges. Photographs (a) and (c) show the edge-zone of the foil from the turbine bearing, in which localized wear was more pronounced. Typically polished foil-sectors from both bearings are illustrated in photographs (b) and (d). In (b), the polished islands are beginning to form continuous chains, a process which has progressed further in (e). Both photographs, particularly (b), show dispersed islands of virgin film (black). The last photograph (e) shows a typical wear track through the film, separated from the edge by a strip of virgin coating of approximately equal width. Inward from the wear track is another narrow strip of original coating, followed by broad band of polished film.

4.0 SUMMARY OF RESULTS

Foil bearings were designed and manufactured within space limitations and constraints imposed by an existing, Brayton cycle, turbo-alternator-compressor. Tolerances of components and assemblies remained well within specified limits, and this contributed greatly to the ease of assembly and alignment of the entire test rig. The replacement of pivoted-shoe bearings with foil bearings required no modification of other components of the machine and resulted in a compact, symmetrical, simple, elegant and superior rotor-support.

The series of tests described in the preceding sections substantiated the supportworthiness and superior performance characteristics of foil bearings of the present design. The experimental results, obtained in the course of previous investigations with a realistic simulator [6,7], were confirmed with a full-fledged foil-bearing assembly, completely interchangeable with the present BRU rotor-support. Specifically, it was shown that stable operation in the vertical attitude, that is in the radially-unloaded mode, could be maintained at all speeds to 43,200 rpm, and that the maximum rotor excursions at resonance, or during starting and stopping, were limited to less than 25% of compressor-seal clearance.* Although trouble free performance in the course of a continuous, 100-hour run was anticipated, the long run certainly did not detract from the reliability as-

*In the absence of the constraining clearance-circle of a rigid-surface bearing, the danger of first contact is transferred to the seals, especially the tighter, compressor-end seal.

pect of foil bearings, especially since an additional 25 hours were logged under variable and extreme operating conditions. Of particular significance, however, was the insensitivity of the amplitude response to temperature changes, a good omen with regard to forthcoming, full-performance testing.

The entire series of intensive testing was crowned by the ability of the foil bearings to withstand well over 1000 start-stop cycles, with no change in operational characteristics and no adverse effect on high-speed performance. Furthermore, examination of journals and foils upon completion of all tests showed that wear was both minimal and benign, so that the useful life of foil bearings is by no means limited to 1000 start-stops and can probably be extended to several thousand cycles.

It is most encouraging to note that excursions of the rotor during starting and stopping remained within acceptable limits and continued to decrease with the number of cycles. Also, the frictional starting-torque of approximately 5 in-lb (0.565 m.N), and the bearing stiffness the order of 18,000 lb/in (3.15×10^6 N/m), compare most favorably in relation to flexible-reed bearings of similar dimensions.

5.0 CONCLUSIONS AND RECOMMENDATIONS

The significance of activities reported herewith resides in the fact that accumulated knowledge was used purposefully and embodied in the construction of a unique bearing. Moreover, the results contained in this and other reports [2,4,6] suggest the utilization of NASA-sponsored research and development in areas extending well beyond the limits of specific application to space-power turbomachinery.

With regard to the Brayton Cycle Unit, it is felt that the present foil-bearing was proved superior to other rotor supports hitherto considered and tested. It should, therefore, be designated as the prime candidate for journal bearings in this class of turbomachines. Specifically, the foregoing conclusions and recommendations are based on the following combination of excellent characteristics of this foil-bearing type:

(a) Stability.

(b) High tolerance of geometrical and thermal distortions and misalignment.

(c) Relative immunity from effects of abrasive particulates entering the bearing clearance.

(d) Sensibly low starting torques.

(e) Excellent wipe-wear, start-stop, and longevity characteristics.

(f) Insensitivity of high-speed performance and rotor dynamics to large numbers of start-stop cycles, as well as to relatively wide, temporal and spacial temperature variations.

(g) Simplicity of basic construction and extremely wide tolerance with regard to nominal dimensions of journals.*

It is also concluded that this type of foil bearing may be eminently suited for a variety of applications in environments other than characterized by weightlessness, such as aircraft, terrestrial, and submarine auxiliary power units. A logical complement of this investigation, therefore, would be an extension of the present series of tests to operation in the horizontal attitude.

Furthermore, a variety of applications are envisaged for this type of foil bearing, ranging from very high-speed, fractional horsepower turbo-generators and turbo-compressors, to cryogenic pumps and expanders. In the area of instrumentation, foil bearings may be incorporated in systems requiring the use of rotating mirrors, such as high-speed photography and laser recording. Since speeds up to 500,000 rpm are not uncommon in such devices, they represent definite areas of application, in which the inherent stability of foil bearings could be capitalized on.

Finally, since preliminary tests indicate that excellent performance may be expected with liquid lubricants and greases, the utilization of foil bearings in pumps, lubricated by both clean and contaminated, particle-laden process fluids, represents an attractive possibility. Since the present design was specialized to gas-lubricated bearings and to a very definite machine, it is recommended that the base of applications be widened by extending the development to liquid-lubricated foil bearings.

---

*Some intricacies of the present construction were dictated by the existing BRU, and many features of the present design were hereditary and a consequence of interfacing constraints. On the other hand, deviations of several mils from nominal dimensions of journals are of no consequence, as long as the latter remains sensibly round and cylindrical.

REFERENCES

1. Davis, J.E., Gildersleeve, R.B. and Pietsch, A., "The Design and Fabrication of the Brayton Rotating Unit (BRU)," AiResearch Manufacturing Company of Arizona, Final Report No. APS-5334-R, May 15, 1971, prepared under Contract No. NAS3-9427, NASA Lewis Research Center, Cleveland, Ohio 44135.

2. Licht, L. and Eshel, A., "Study, Fabrication and Testing of a Foil-Bearing Rotor Support System," NASA CR-1157, November 1968, prepared by the Ampex Corporation under Contract NASW-1456, NASA, Washington, D.C.

3. Licht, L., "An Experimental Study of High-Speed Rotors Supported by Air-Lubricated Foil Bearings - Part 1: Rotation in Pressurized and Self-Acting Foil Bearings and Part 2: Response to Impact and to Periodic Excitation," Journal of Lubrication Technology, Trans. ASME, Vol. 91, Series F, No. 3, July 1969, pp. 477-505.

4. Licht, L., "Design, Fabrication and Testing of a Foil Gas-Bearing Test Rig," NASA CR-1563, May 1970, prepared by the Ampex Corporation under Contract NAS3-11826, NASA Lewis Research Center, Cleveland, Ohio.

5. Eshel, A., "Dynamic Analysis of Three-Foil Rotor Support System in Zero Gravity Environment," Journal of Lubrication Technology, Trans. ASME, Vol. 92, Series F, No. 4, October 1970, pp. 617-629.

6. Licht, L., "Studies of Foil Journal-Bearings for Brayton Cycle Turbomachinery," NASA CR-72864, February 1971, prepared by the Ampex Corporation under Contract No. NAS3-13482, NASA Lewis Research Center, Cleveland, Ohio 44135.

7. Licht, L., "The Dynamic Characteristics of a Turborotor Simulator Supported on Gas-Lubricated Foil Bearings. - Part 1: Response to Rotating Imbalance and Unidirectional Excitation, Part 2: Operation with Heating and Thermal Gradients, and Part 3: Rotation in Foil Bearings of Reduced Length, with Starting and Stopping Unaided by External Pressurization," Journal of Lubrication Technology, Trans. ASME, Vol. 92, Series F, No. 4, October 1970, pp. 630-660, and Vol. 94, Series F, No. 3, July 1972, pp. 211-222.

8. Eshel, A. and Licht, L., "Foil Bearing Design Manual," Ampex Corporation, Report No. RR 71-18, September 1971, prepared under Contract No. Nonr-N00014-71-0001, Office of Naval Research, Arlington, Va. 22217.

9. Eshel, A., "Study of Thermal Effects on the Clearance and Stiffness of Foil Journal-Bearings for a Brayton Cycle Turboalternator," NASA CR-2113, September 1972, prepared by the Ampex Corporation under Contract No. NAS3-15341, NASA Lewis Research Center, Cleveland, Ohio 44135.

10. Spragins, W.W., Gildersleeve, R.B., et al, "Assembly Manual, Brayton Rotating Unit 699700," AiResearch Manufacturing Company of Arizona, Engineering Report No. APS-5339-R, March 1970, prepared under Contract No. NAS3-9427, NASA Lewis Research Center, Cleveland, Ohio 44135.

11. Eshel, A. and Elrod, H.G., Jr., "Finite Width Effects on the Self-Acting Foil Bearing," Columbia University, Lubrication Research Laboratory, Report No. 6, August 1966.

12. Licht, L., "An Experimental Study of Elastohydrodynamic Lubrication of Foil Bearings. - Part 1: Displacement in the Central Zone and Part 2: Displacement in the Edge Zone," Journal of Lubrication Technology, Trans. ASME, Vol. 90, Series F, No. 1, January 1968, pp. 199-220.

13. Schlichting, H., "Boundary Layer Theory," McGraw-Hill, 1960, p. 307.

14. Wang, C., "Applied Elasticity," McGraw-Hill, 1953, pp. 57-58.

APPENDIX 1

ASSEMBLY PROCEDURE FOR FOIL JOURNAL-BEARINGS

Note: All 6-digit numbers 699xxx refer to BRU parts.
All 4-digit numbers 58xx refer to foil-bearing parts.

(a) Attach 3 brackets,* P/N 699799, to main housing, P/N 699713, using 6 screws, P/N 699235-10, torqued to 25-30 in-lb (2.82-3.39 m.N). Mount assembly on stand, P/N 699880, and connect flex-lines to the housing-mounted filters.

(b) Install rotor shroud, P/N 699778-2, on compressor-end carrier, P/N 5823. Install rotor shroud, P/N 699778-1, on turbine-end carrier, P/N 5822. Twelve screws, P/N 699231-104, torqued to 3-5 in-lb (0.339-0.564 m.N) are required.

(c) Install turbine-end carrier in housing, using 12 screws, P/N 699233-10, torqued to 12-14 in-lb (1.37-1.59 m.N).

(d) Position assembly stand, so that compressor end of engine faces upward. Using polyethylene gloves, carefully insert the shaft assembly, P/N 699721, into the housing, letting it rest against the turbine-end rotor shroud.

*Modify one bracket to include 3/8 in. (9.53×10^{-3} m) diameter hole, at 1.5 in. (3.81×10^{-2} m) radially inward from existing mounting hole. This is to provide clearance for a Nylon filament during loading.

(e) Place compressor-end carrier in housing and attach with 12 screws, P/N 699233-10, torqued to 12-14 in-lb (1.37-1.59 m.N). Take care to prevent damage to curvic couplings of the shaft assembly and to the bores of the bearing carriers.

(f) Install capacitance probes A(X_C) and B(Y_C) and their mating shims in the compressor-end bearing carrier. Use requisite number of screws, P/N 699231-6, torqued to 9-11 in-lb (1.03-1.25 m.N).

(g) Remove the outboard plate, P/N 5829, the foil lock, P/N 5850, and 2 foil clamps, P/N 5853, from the compressor-end carrier and insert the foil (coated sectors facing journal) as illustrated in Fig. 40.

Caution: Extreme care should be exercised to prevent surface and edge damage to foil. Foil should be free of dents and creases.

Insure that pairs of clearance holes in the foil, at foil lock and at point of loading, are perfectly aligned.

(h) Install the outboard plate and torque six No. 4-40 x 1/4 UNC socket-head screws to 9-11 in-lb (1.03-1.25 m.N).

(i) Attach 2 foil clamps, P/N 5853, with twelve No. 2-56 x 5/8 UNC socket-head screws, and attach the foil-lock, P/N 5850, with a No. 6-32 x 3/8 socket-head bolt. Do not tighten screws and bolt, so that clamps and foil locks remain loose.

(j) Rotate assembly-stand to "turbine-end up" position. Install capacitance probes C(Y_T) and D(X_T) and their mating shims. Insert the foil, as described in paragraphs (g), and repeat procedure (h) and (i) at turbine-end carrier.

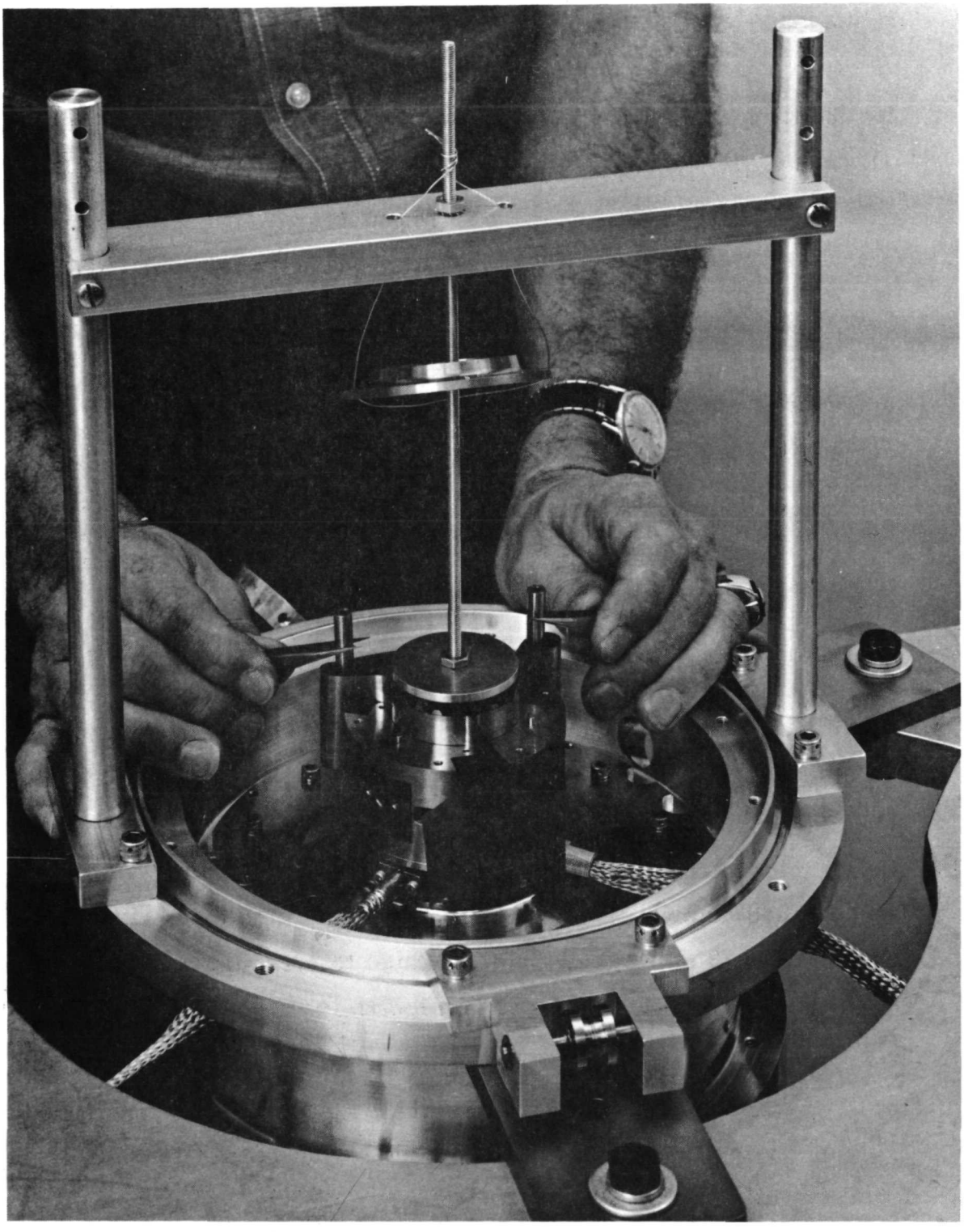

Fig. 40 Insertion of Foil into Foil-Bearing Carrier (Identical with Fig. 12)

(k) Mount rotor suspension brackets, Fig. 41, on the housing flanges, at right angles to foil locks. Suspend shaft assembly by means of threaded rod, inserted through bore of shaft assembly. Use Delrin inserts to protect curvic couplings. Position shaft assembly approximately midway between the rotor shrouds, with nuts finger-tight on threaded rod. The shaft assembly is now ready for centering without interference from rotor shrouds.

(l) Attach loading pulleys to housing flanges at each foil lock. (Loading pulleys are marked T and C for turbine and compressor ends respectively.)

(m) Insert a 3/16 in (4.77×10^{-3} m) diameter pin through one hole at the end of the foil. Slide reinforcing washers over ends of pin and cement washers to foil with quick-drying cement (Eastman 910, or equivalent). Remove pin when cement is dry. Repeat procedure at other end of foil. Secure loose foil-ends at convenient location with masking tape to avoid damage. The foregoing procedure is identical for both foils.

(n) The bores of the outboard plates provide a reference for centering the journals. The centering procedure is identical for both journals. Insert a 0.005 in (1.27×10^{-4} m) Mylar shim in the annulus between the journal and the outboard plate. This shim takes up only part of the available space. Next insert a 0.0015 in (0.38×10^{-4} m) metal shim in the remaining space, Fig. 42.

Caution: Insertion of metal shim is a tight fit. Shims should not be pushed into bores to a depth greater than 0.25 in (0.64×10^{-2} m) in order to avoid damage to edges of foils.

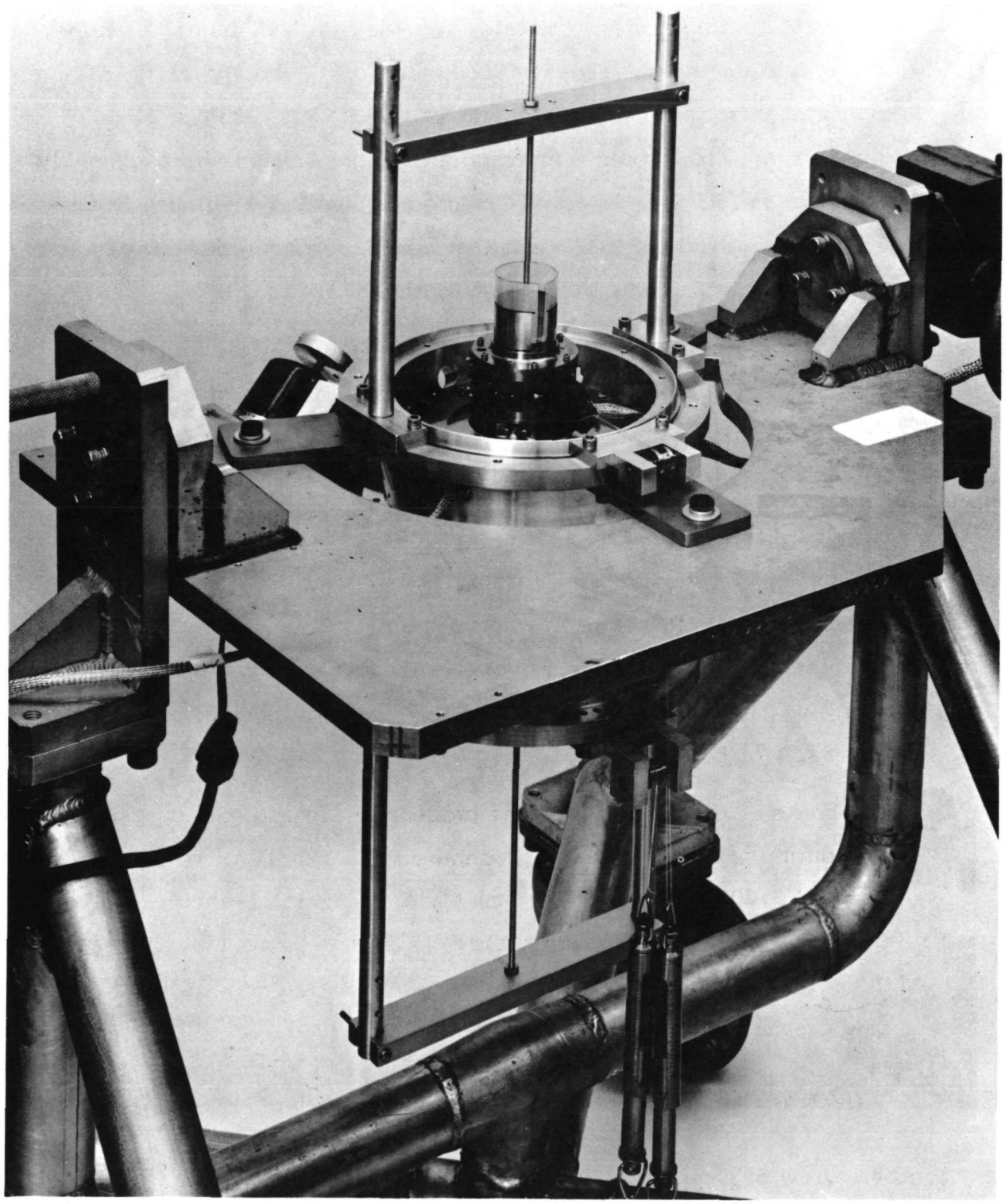

Fig. 41 Centering of Journals by Shims and Tensioning of Foil. Rotor Suspension-Brackets and Loading Pulleys Bolted to Housing (Identical with Fig. 13)

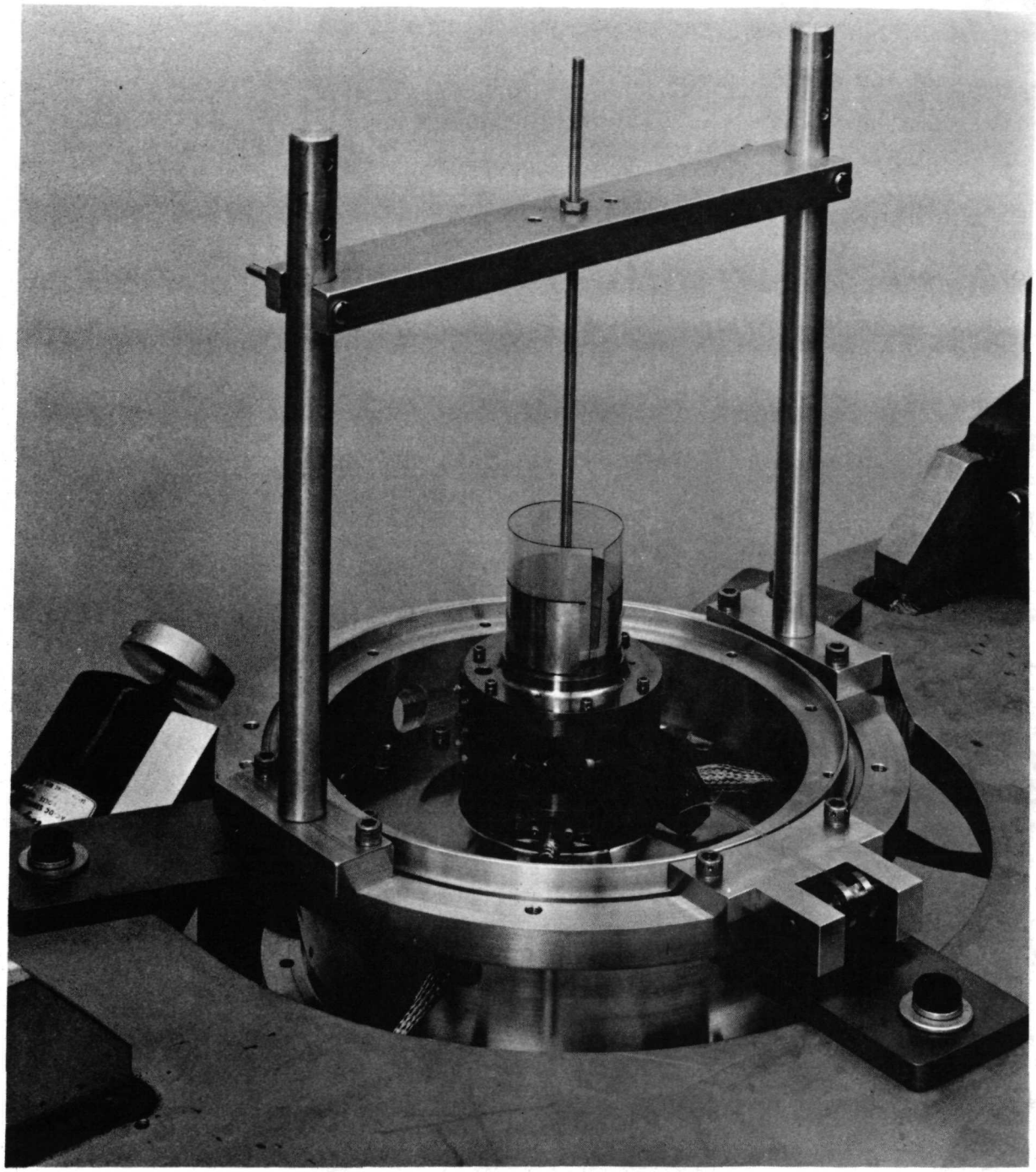

Fig. 42 View of Centering Shims Extending from Foil-Bearing Carrier

(o) Attach vibrator* at any convenient location, close to the midplane of the housing. Connect probes A, B, C and D (X_C, Y_C, Y_T and X_T in the nomenclature of this report) for orbit displays on an oscilloscope. Shake down structure with vibrator and record readings of displacement meter. Repeat shakedown and note again meter readings. The change in these readings should be negligibly small.

(p) Apply a total load of 7.5 lb (33.3N) to the free ends of each foil. Tie ends of Nylon filaments to reinforcing washers of foils, thus forming slings through which load is applied (and shared equally by foil extremities). Shake down structure to achieve partial equalization of tension.

(q) Remove centering shims and note displacement of journals from concentric reference-position. Insert Allen wrenches into sockets of free guides, P/N 5851, as shown in Fig. 43. Rotate guides in small increments until meter readings return to reference values. Shake down structure to insure that meter readings remain unchanged. Secure foils at free guides by means of clamps, P/N 5853. Torque six screws of each clamp progressively and equally to 3-5 in-lb (0.339-0.564 m.N). Secure locking bar, P/N 5850, with a torque 19-21 in-lb (2.17-2.40 m.N) applied to the bolt. Shakedown structure and read displacement meters to insure that concentric position of journals is maintained.** The centering is carried out simultaneously at both foil bearings.

---

* The vibrator is an eccentric disc, attached to the spindle of a small, variable speed motor. A speed range to 5000 rpm and an imbalance the order of 0.032 in-oz (2.26×10^{-4} m.N) are adequate.

** Experience has shown that concentricity of journals, referenced to bores of outboard plates of carriers, can be readily maintained within 100 μin (2.54×10^{-6} m). If eccentricity is excessive, repeat centering procedure and check again.

(r) Release load and sever protruding ends of each foil close to edge of locking bar.

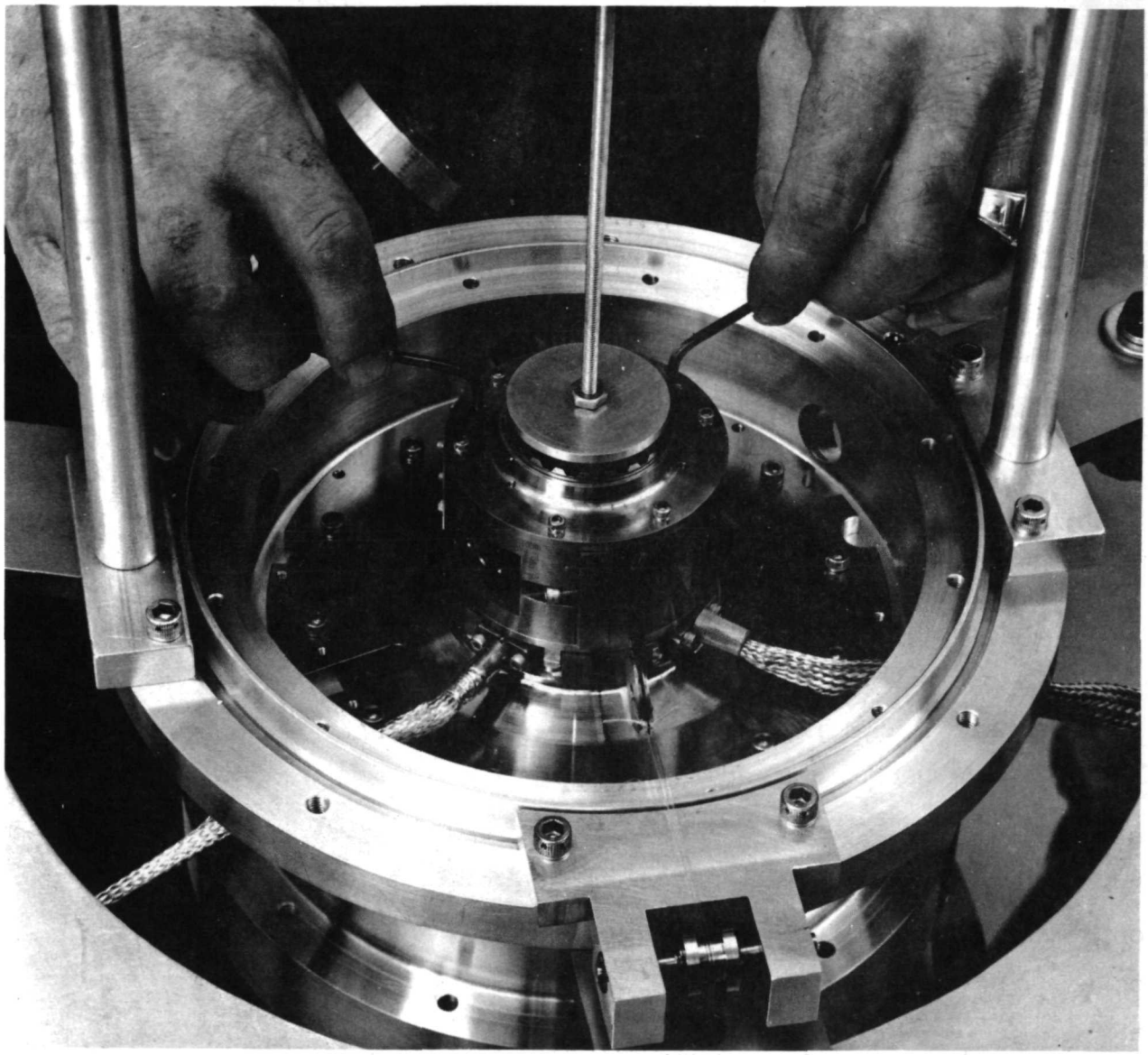

Fig. 43 Manipulation of Free Foil-Guides to Return Journals to Reference Position (Identical with Fig. 14)

APPENDIX 2

GUIDE TO SELECTION OF FOIL-BEARING METALS OF COMPATIBLE THERMAL EXPANSIVITIES*

Since temperature differences between various parts of the foil-bearing assembly are unavoidable, the coefficients of thermal expansion of constituent metals of the bearing support represent important design parameters. Ideally, it would be desirable to make the operating clearance h^* and, therefore, the tension T independent of the expansion of journal and foil-bearing components. One can approach this ideal condition by a judicious choice of metals from the point of view of thermal expansivity.

In order to simplify the problem, we lump the foil journal-bearing into three zones of unequal, but uniform temperatures:

a) The journal and the copper shunt; temperature τ_j.
b) The length of the foil between lines of tangency with the foil guides; temperature τ_f.
c) The foil guides and supports, that is the structure surrounding the foil sectors and the journal; temperature τ_g.

Furthermore, assuming Couette flow in the clearance h^*, Fig. 44, and simple conduction through the stagnant gas in the annulus δ, we can determine τ_f if τ_j and τ_g are prescribed. The temperature in the clearance h^* is governed by the equation [1]:

*The results presented in this appendix preceded the work contained in reference [9]. Selection of foil-bearing materials was based on contents of this appendix.

$$\frac{d^2\tau}{dy^2} = -\frac{\mu}{\lambda}\left(\frac{du}{dy}\right)^2 = -\frac{\mu}{\lambda}\frac{U^2}{h^{*2}}, \tag{1}$$

or $$\tau'' = -\frac{\mu}{\lambda}\frac{r_0^2\omega^2}{h^{*2}}. \tag{2}$$

Integrating and applying the boundary conditions:

$$\left.\begin{aligned} \tau &= \tau_f \quad at \quad y = 0 \\ \text{and } \tau &= \tau_j \quad at \quad y = h^*, \end{aligned}\right\} \tag{3}$$

we obtain:

$$\tau = -\frac{\mu}{2\lambda}\frac{r_0^2\omega^2}{h^{*2}}y^2 + C_1 y + C_2, \tag{4}$$

in which:

$$\left.\begin{aligned} C_1 &= \frac{\mu}{2\lambda}\frac{r_0^2\omega^2}{h^*} - \frac{\tau_f - \tau_j}{h^*}, \\ \text{and } C_2 &= \tau_f. \end{aligned}\right\} \tag{5}$$

*Note that for many gases the ratio μ/λ remains nearly constant over a wide range of temperatures.

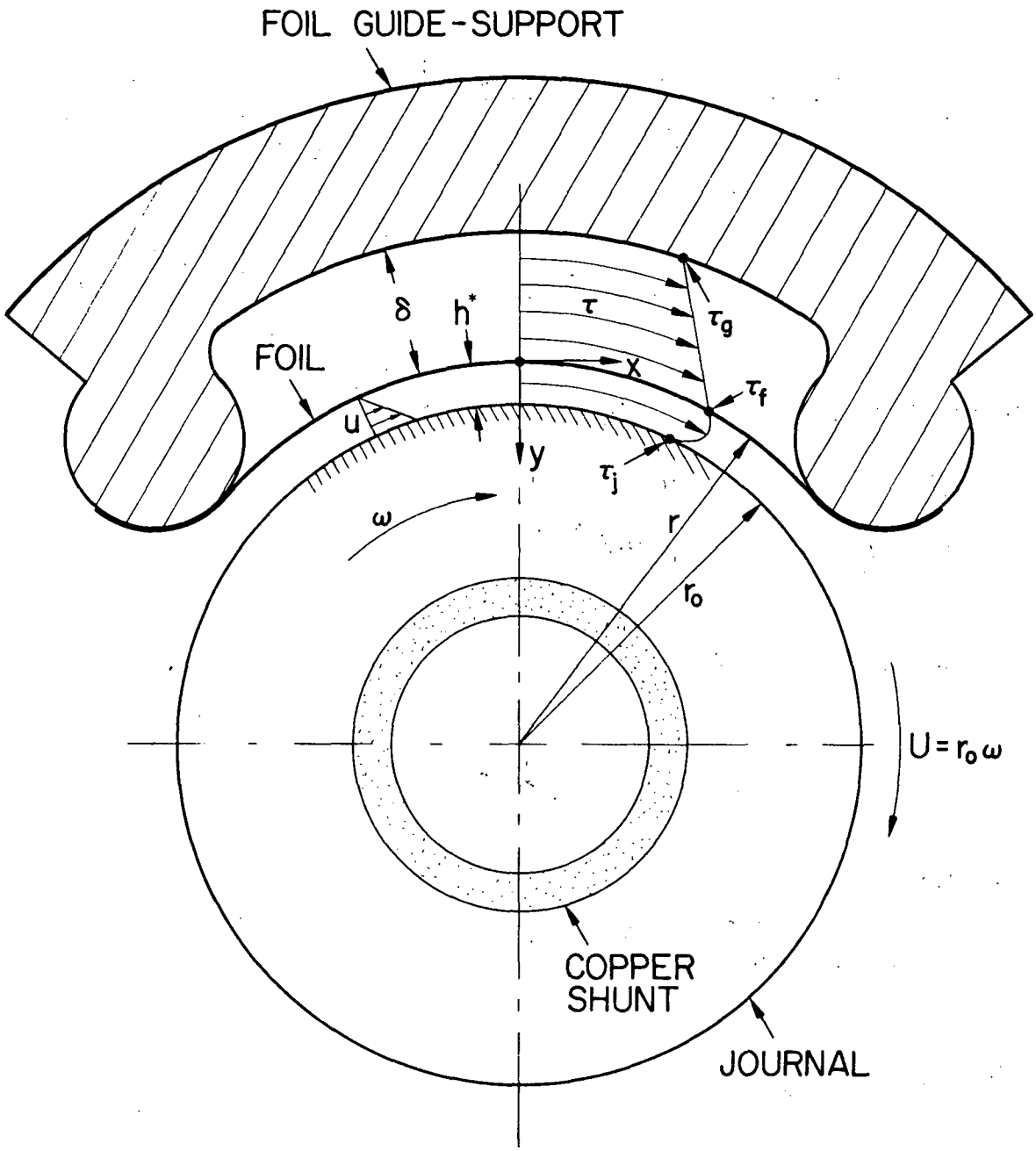

Fig. 44 Schematic Diagram of Temperature Distribution in Foil Bearing

We may also assume a linear temperature gradient $(\tau_f - \tau_g)/\delta$ across the gas film δ, and that the thin metal foil offers negligible resistance to transverse heat conduction. Consequently, we may write:

$$\left.\frac{d\bar{\tau}}{dy}\right|_{y=0} = C_1 = \frac{\mu}{2\lambda}\frac{r_0^2\omega^2}{h^*} - \frac{\bar{\tau}_f - \bar{\tau}_j}{h^*} = \frac{\bar{\tau}_f - \bar{\tau}_g}{\delta} \tag{6}$$

Solving for τ_f, we obtain:

$$\bar{\tau}_f = \frac{\bar{\tau}_j}{1+(h^*/\delta)}\left(1 + \frac{h^*}{\delta}\frac{\bar{\tau}_g}{\bar{\tau}_j} + \frac{\mu r_0^2\omega^2}{2\lambda\bar{\tau}_j}\right). \tag{7}$$

The orders of magnitude of ratios in eq. (7), at rated speed and at equilibrium operating conditions, are:

$$h^*/\delta \sim 5\times10^{-2};\quad \bar{\tau}_g/\bar{\tau}_j \sim 1.0 \text{ and } \mu r_0^2\omega^2/2\lambda\bar{\tau}_j \sim 10^{-2}$$

so that for the case at hand, and to the order of approximation compatible with the lumped-temperature model of the foil bearing:

$$\bar{\tau}_f \approx \bar{\tau}_j \tag{8}$$

The relationships about to be developed involve the calculation of increase in length of foil segments between lines of tangency at the guides and lines of tangency at the terminal of wrap. In the case of the perfectly flexible foil, these foil segments are straight. In the case of foils of finite stiffness, the segments are S-shaped, but the deviation from plane surfaces are small everywhere. A schematic representation of the reference state of a foil-bearing sector at uniform temperature τ_o is given in the left

half of Fig. 45. The state corresponding to a nonuniform temperature distribution is illustrated in the right half of the same figure. Since the postulated change of state is subject to the constraint $h^* = \text{constant}$ and, therefore, T = constant, it is more than plausible to assume that the change in distance between the terminals of the S-shaped sector $\overline{Bb}$ is nearly identical with that of the straight sector $\overline{Aa}$. We make this assumption in the development which follows, i.e. we consider a geometry consisting of circular arcs and straight lines only. We also neglect frictional constraints at the guides.

Referring now to Fig. 46, the foil length $\ell = \overline{MN}$, is given by:

$$\ell = 2r(\pi/3 - \beta) + 2r_g(5\pi/6 - \beta) + 2b, \tag{9}$$

in which:

$$b = [R^2 - (r + r_g)^2]^{1/2}, \tag{10}$$

$$R^2 = [r/\cos\beta + r_g \tan(\pi/4 - \beta/2)]^2 + r_g^2. \tag{11}$$

The increase in ℓ can be expressed as:

$$\delta\ell = 2(\pi/3 - \beta)\delta r + 2(5\pi/6 - \beta)\delta r_g + 2\delta b - 2(r + r_g)\delta\beta, \tag{12}$$

and also as the thermal elongation of the foil sector $\overline{MN}$ at constant tension, i.e.:

$$\delta\ell = 2[r(\pi/3 - \beta) + b]\alpha_f \Delta\tau_f + 2r_g(5\pi/6 - \beta)\alpha_f \Delta\tau_f . \tag{13}$$

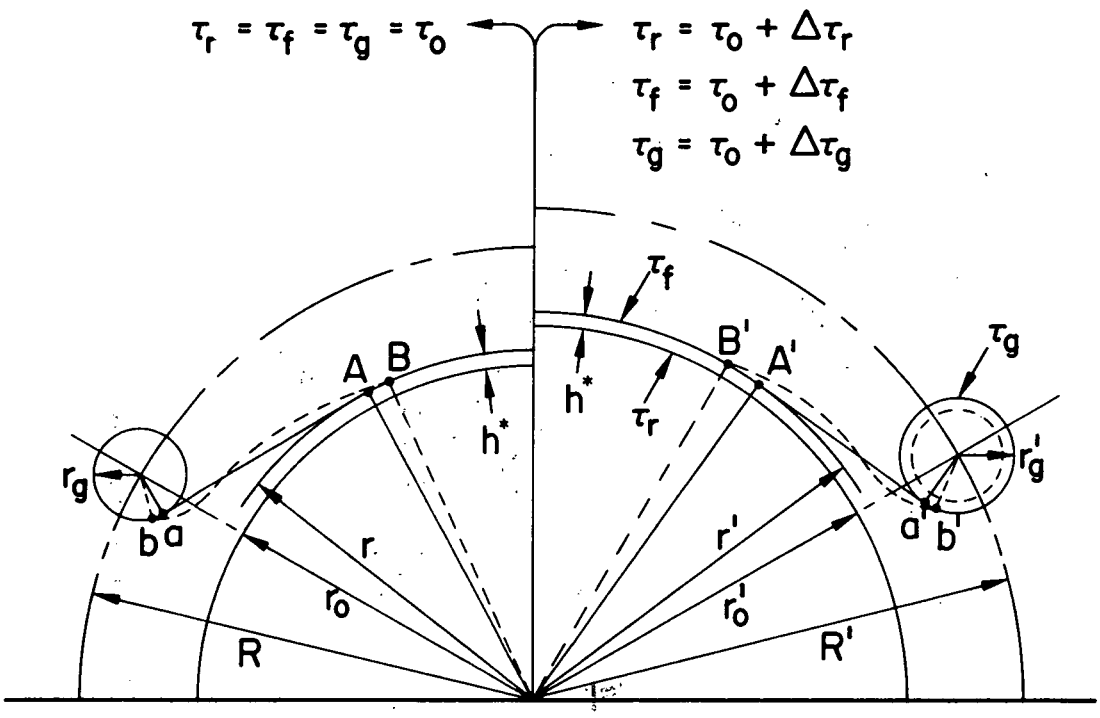

$$R' = R(1 + \alpha_g \Delta\tau_g)$$
$$r' = r(1 + \alpha_r \Delta\tau_r)$$
$$r_g' = r_g(1 + \alpha_g \Delta\tau_g)$$
$$r = r_o + h^*$$

$$\overline{B'b'} - \overline{Bb} \approx \overline{A'a'} - \overline{Aa} = \alpha_f \Delta\tau_f (\overline{Aa}) \; ; \; h^* = \text{CONSTANT}$$

Fig. 45 Schematic Representation of Thermal Expansion of Foil Bearing (h* = Constant)

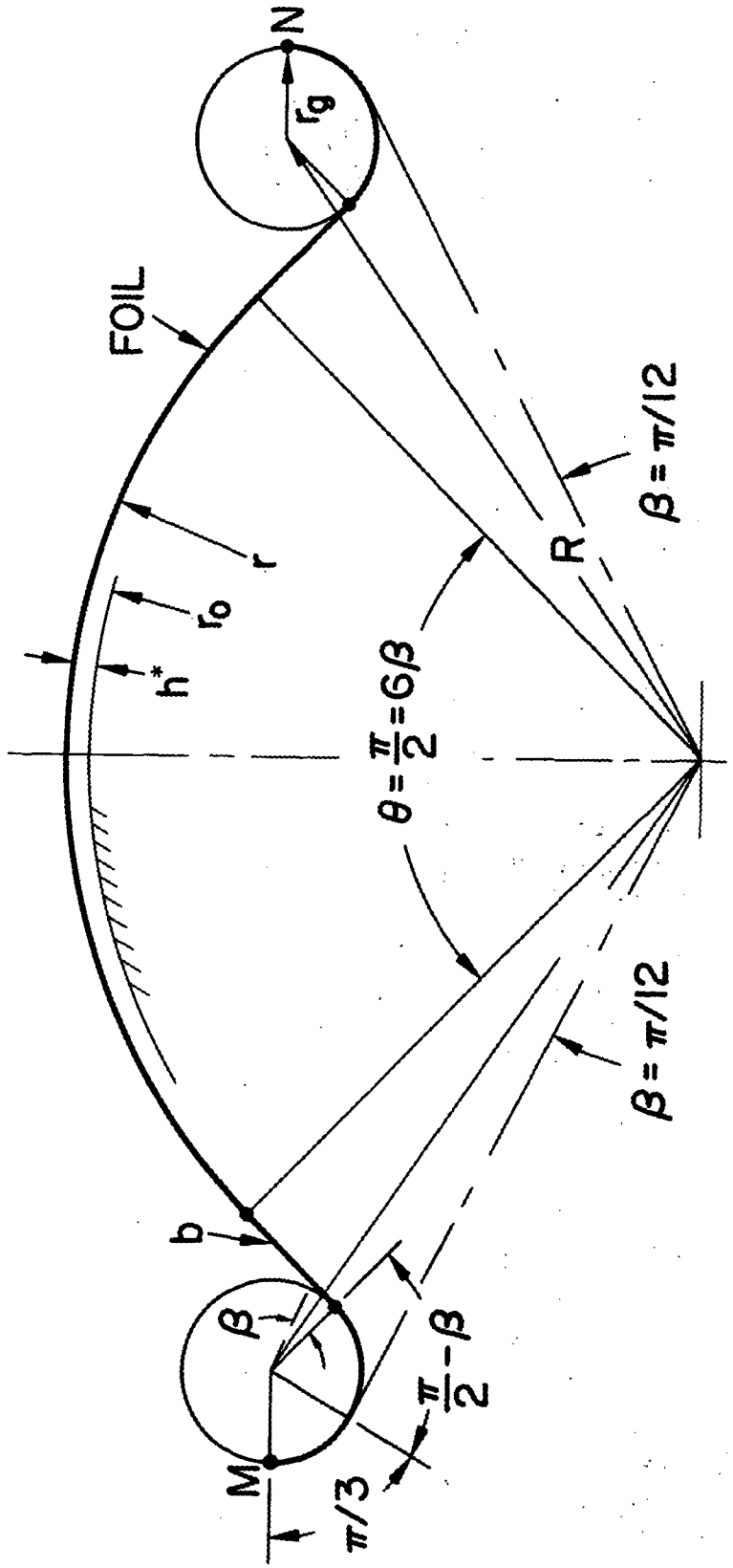

Fig. 46 Geometry of Foil-Bearing Sector

In addition, with h* = constant, and with

$$\left.\begin{aligned} \delta r \approx \delta r_0 &= r_0 \alpha_j \Delta\tau_j \,, \\ \delta r_g &= r_g \alpha_g \Delta\tau_g \,, \\ \delta R &= R \alpha_g \Delta\tau_g \,, \end{aligned}\right\} \tag{14}$$

we obtain:

$$\delta b = \left[R\delta R - (r+r_g)\delta r - (r+r_g)\delta r_g\right] \Big/ \left[R^2 - (r+r_g)^2\right]^{1/2}$$

$$= \left\{\left[R^2 - (r+r_g) r_g\right]\alpha_g \Delta\tau_g - r(r+r_g)\alpha_j \Delta\tau_j\right\} \Big/ \left[R^2 - (r+r_g)^2\right]^{1/2}, \tag{15}$$

and

$$\delta\beta = \frac{(R\delta R - r_g \delta r_g)/(R^2 - r_g^2)^{1/2} - \tan\tfrac{1}{2}(\pi/2 - \beta)\delta r_g - \delta r/\cos\beta}{(r\tan\beta/\cos\beta) - r_g/(1+\sin\beta)}$$

$$= \frac{\left[(R^2 - r_g^2)^{1/2} - r_g(1-\sin\beta)/\cos\beta\right]\alpha_g \Delta\tau_g - r\alpha_j \Delta\tau_j/\cos\beta}{(r\tan\beta/\cos\beta) - r_g/(1+\sin\beta)} \,. \tag{16}$$

Substituting the explicit expressions for δr, δr_g, δb and $\delta\beta$ in eq. (12) and combining eq.'s (12) and (13), we obtain:

$$(\pi/3-\beta)r + (5\pi/6-\beta)r_g \frac{\alpha_g}{\alpha_j}\frac{\Delta T_g}{\Delta T_j}$$

$$- \frac{(r+r_g)r}{[R^2-(r+r_g)^2]^{1/2}} + \frac{R^2-(r+r_g)r_g}{[R^2-(r+r_g)^2]^{1/2}}\frac{\alpha_g}{\alpha_j}\frac{\Delta T_g}{\Delta T_j}$$

$$+ \frac{(r+r_g)r}{r\tan\beta - r_g\cos\beta/(1+\sin\beta)} + \frac{(r+r_g)[(R^2-r_g^2)^{1/2}\cos\beta - r_g(1-\sin\beta)]}{r\tan\beta - r_g\cos\beta/(1+\sin\beta)}\frac{\alpha_g}{\alpha_j}\frac{\Delta T_g}{\Delta T_j}$$

$$= \left\{r(\pi/3-\beta) + [R^2-(r+r_g)^2]^{1/2}\right\}\frac{\alpha_f}{\alpha_j}\frac{\Delta T_f}{\Delta T_j} + (5\pi/6-\beta)r_g\frac{\alpha_f}{\alpha_j}\frac{\Delta T_g}{\Delta T_j} . \quad (17)$$

Eq. (17) can be written in the form:

$$1 + A_g\Lambda_g\phi_g = A_f\Lambda_f\phi_f + A_{fg}\Lambda_f\phi_g , \quad (18)$$

in which A_f, A_g and A_{fg} are constants involving the bearing geometry only, and

$$\Lambda_g = \alpha_g/\alpha_j \; ; \; \Lambda_f = \alpha_f/\alpha_j ,$$
$$\phi_g = \Delta T_g/\Delta T_j \; ; \; \phi_f = \Delta T_f/\Delta T_j .$$

In the foregoing, we have assumed that the coefficients of thermal expansion α have been selected so that that expansion takes place with the foil-bearing clearance (h*) and, therefore, the foil tension (T) unaffected by temperature changes. If the operating temperatures and the selected coefficients of thermal expansion are such that the left hand side of eq. (18) becomes larger than the right hand side, then $\delta h^* < 0$

and $\delta T > 0$. This "strangulation" of the journal, however, is mitigated by the ability of the foil to extend with increasing tension. A combination of temperature levels and coefficients of expansion, which makes the right hand side of the eq. (18) largest and produces "relaxation," i.e. $\delta h^* > 0$ and $\delta T < 0$, is also partly offset by contraction of the foil with decreasing tension.

The simple analysis presented herewith does not involve directly the bearing clearance, or stiffness. It does, however, permit a judicious choice of materials to minimize variations of the foregoing quantities within a range of anticipated temperature levels, so that a determination of clearance and stiffness at room temperature may suffice.

For the present foil-bearing configuration, eq. (18) becomes:

$$1 + 0.520\,\Lambda_g \Phi_g = 1.105\,\Lambda_f \Phi_f + 0.394\,\Lambda_f \Phi_g \qquad (19)$$

Since the journal (4340 steel) contains a copper shunt, the effective coefficient of expansion α_j may be obtained by considering an interference fit [14] between coalescing surfaces of cylinders made of different metals and heated uniformly. The derived expression is:

$$\alpha_j = \alpha_s \left\{ 1 + r^2 \left(\frac{\alpha_c}{\alpha_s} - 1 \right) \Big/ E_s (r_o^2 - r_c^2) \left[\frac{(1+\nu_c) r_i^2 + (1-\nu_c) r^2}{E_c (r^2 - r_i^2)} + \frac{(1+\nu_s) r_o^2 + (1-\nu_s) r^2}{E_s (r_o^2 - r^2)} \right] \right\}, \qquad (20)$$

in which the coefficients of expansion, moduli of elasticity, Poisson's ratios, and radii of the composite journal are indicated in Fig. 47.

We consider average values of coefficients of thermal expansion, applicable approximately in the range of temperatures 75 °F - 400 °F (24 °C - 205 °C). The values fixed by the existing rotor are:

$\alpha_s = 6.7\times10^{-6}$ in/in/°F (12.0×10^{-6} m/m/°C); 4340 steel,

$\alpha_c = 9.8\times10^{-6}$ in/in/°F (17.6×10^{-6} m/m/°C); copper,

so that by means of eq. (20):

$\alpha_j = 1.09\alpha_c = 7.3\times10^{-6}$ in/in/°F (13.1×10^{-6} m/m/°C).

Also, for materials selected in the present design, we have:

$\alpha_g = 5.6\times10^{-6}$ in/in/°F (10.1×10^{-6} m/m/°C); 416 stainless steel,

$\alpha_f = 6.3\times10^{-6}$ in/in/°F ($11.\times10^{-6}$ m/m/°C); 17-4 PH steel.

The above values give: $\Lambda_g = 0.767$,

$\Lambda_f = 0.864$,

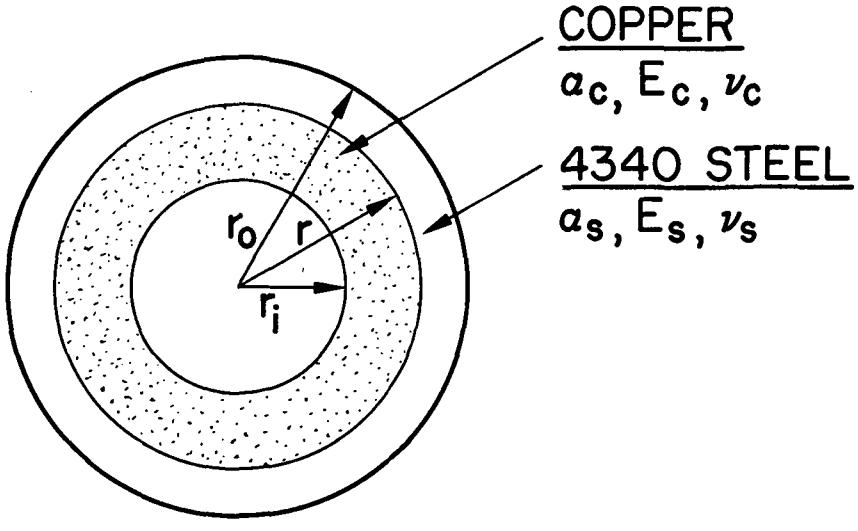

Fig. 47 Key of Symbols in Equation 20 (Expansion of Journal and Copper Shunt)

so that division of one side of eq. (19) by the other gives:

$$Q = \frac{0.955 + 0.340\,\phi_g}{1 + 0.399\,\phi_g} \tag{21}$$

It can be seen from eq. (7), that for a wide range of temperatures τ_j and τ_g, $\tau_f \approx \tau_j$ and $\varphi_f \approx 1$, so that for $0.5 < \varphi_g < 1.0$ the ratio in eq. (21) is:

$$0.925 < Q < 0.935 < 1.0 \;, \tag{22}$$

indicating that a slight decrease of clearance with increasing temperatures may be anticipated.

In the case of Inconel foils, $\alpha_f \approx 7.7 \times 10^{-6}$ in/in/°F (13.9×10^{-6} m/m/°C) and $\Lambda_f \approx 1.055$, so that the ratio in eq. (21) becomes:

$$Q = \frac{1.165 + 0.340\,\phi_g}{1 + 0.415\,\phi_g} \;, \tag{23}$$

showing that a slight increase in clearance with rising temperatures can be expected, since:

$$1.0 < 1.065 < Q < 1.105 \;. \tag{24}$$

Perfect matching of coefficients of thermal expansion for all transient and steady-state temperature distributions is hardly feasible, but the simplified analysis presented herewith has served as a useful guide in achieving a compromise in the selection of metals used in foil-bearing construction.

APPENDIX 3

THERMAL EFFECTS ON MEASUREMENTS OF FOIL-BEARING CLEARANCE AND POSITION OF ROTOR JOURNALS

It was pointed out in Section 3.1 that reliable gap measurements could be obtained only under "cold" running conditions, that is during rapid acceleration and immediately following coastdown. The effect of differential thermal expansion of measuring probes under these conditions were minor.

The location of the stainless-steel capacitance probes, used in the determination of clearance measurement, is shown in Fig. 10. It can be seen, that while both probes were mounted in a common holder, attached to one of the support-guides, the stem of the foil probe (F) was located in the interior of the support, while the stem of the journal probe (J) was adjacent, but not entirely surrounded by the support. Assuming the mean temperature of the foil probe to be at least 12.5°F (6.95°C) higher than that of the journal probe, an active probe-length of 0.75 in (1.9×10^{-2} m), and a coefficient of thermal expansion of 9.6 in/in/°F (17.3 m/m/°C), the error in the determination of clearance at thermal equilibrium may be of the order of 90 μin (2.28×10^{-6} m).

Shown in Fig. 48 (a) is a composite oscillogram, which contains scans of clearance and of foil temperature-rise above ambient versus time. The scans were obtained during a 2-hour run to thermal equilibrium, with the time-scale expanded during coastdown. The reader will note that the clearance increases to approximately h = 435 μin (11×10^{-6} m) during the brief period of acceleration. This measurement is correct within limits of experimental error, but the apparent increase of clearance with time in

approaching the state of thermal equilibrium is fictitious. At the end of coastdown, following the 2-hour run, a new reference line was established, but the magnitude $h' = 420$ μin (10.7×10^{-6} m) does not represent a true clearance measurement and is subject to an error resulting from differential expansion of probes.*

The left-hand column of oscilloscope photographs in Fig. 48 represents true gap measurements obtained during rapid acceleration and subsequent coastdown, in essentially cold state of the system. Note the superposition of acceleration and deceleration traces in Fig. 48(c), recorded by means of a storage oscilloscope. The scans of h', Fig. 48(e) and 48(f), were obtained during coastdowns from the state of thermal equilibrium. Although the magnitudes of h and h' in Fig. 48 do not differ appreciably, it is estimated that the true clearance corresponding to h' may have been smaller. This is partly substantiated by the increase of the resonant speed in the warm condition, attributed to a moderate clearance contraction and stiffening of the foil bearing. Another comparison of h and h' is contained in Fig. 49. These scans were recorded after 1000 start-stop cycles, in the cold condition (h) and during coastdown from a state of thermal equilibrium (h').

Referring to Fig. 48(g) the oscilloscope photograph contains a series of journal orbits, recorded in the d.c. mode during coastdown. The appearance is that of the rotor center translating along a line of symmetry through the foil lock and approaching the central reference position as the speed decreases from 720, through 600, 450 and 300 rps to zero. Actually, the translation of the rotor center resulting from residual dissymmetry in tension and geometry represents only a minor contribution. The major

*Probes of identical geometry have since been manufactured from Invar, which has an extremely low coefficient of thermal expansion.

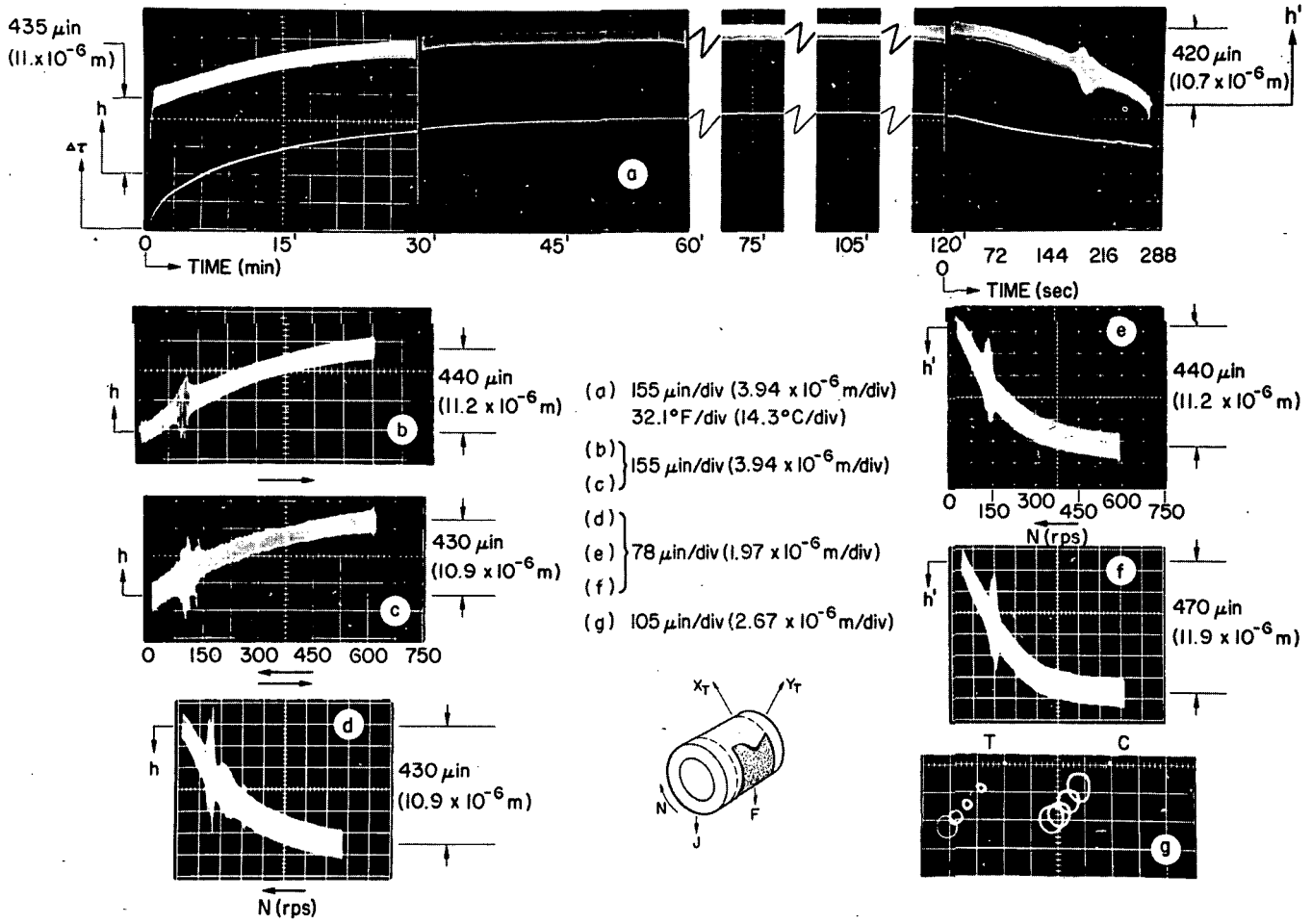

Fig. 48 Determination of Clearance and Effect of Temperature on Measurement. Time-Scan of Foil Temperature Above Ambient, ΔT, and Differential Output of Gap Probes (J-F), (a). Frequency Scans of Gap, h = J-F: Rapid Acceleration (b), Coastdown Trace Superimposed on Acceleration Trace (c), and Coastdown after 1007-th Start-Stop (d), All Near Ambient Temperature Conditions. Frequency Scans of Output (J-F) During Coastdown from Thermal Equilibrium Temperatures: Prior 100-th Start-Stop (e) and after 1007-th Start-Stop (f). Apparent Shift in Rotor Position Reflecting Thermal and Centrifugal Journal Growth (g).

NOTE: 1) h, on extreme left of (a) and in (b,c,d), represents a nearly true gap measurement. Temperatures are nearly ambient.

2) h' on the right of (a) and in (e,f) represents the differential probe-output J-F. h' involves an error of unknown magnitude due to differential expansion of probe and probe mounts.

contribution stems from the decrease of journal diameter with both speed and temperature. This increases the gap between the monitoring probes and the journal surface and produces the same effect on probe outputs as an inward translation of the journal center. The apparent, maximum displacement of 330 μin (8.4×10^{-6} m) from the central reference position at 600 rps may be attributed, in roughly commensurate proportions, to centrifugal growth, thermal expansion, and actual translation of the journals.

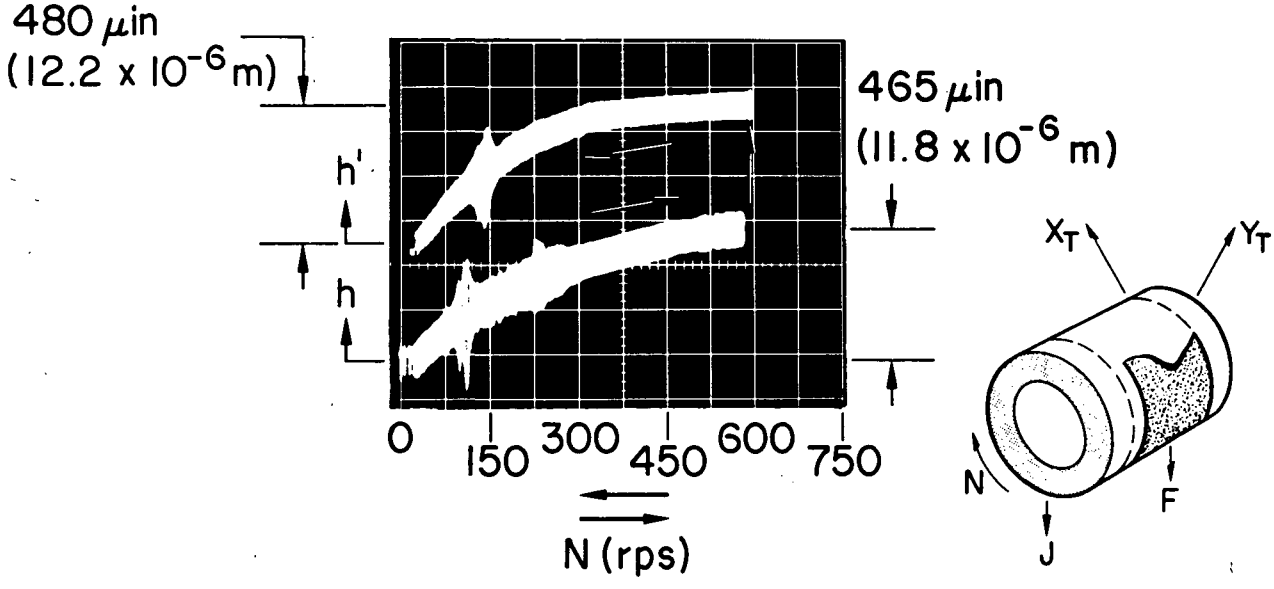

Fig. 49 Gap Measurement after 1025-th Start-Stop Cycle. Rapid Acceleration (h) and Coastdown after 2-Hour Run to Thermal Equilibrium (h') [155 μin/div (3.94×10^{-6} m/div). Note: Accuracy of h' Uncertain Because of Differential Expansion of Probes and Support]

*U.S. GOVERNMENT PRINTING OFFICE: 1973-739-029/61

NATIONAL AERONAUTICS AND SPACE ADMINISTRATION
WASHINGTON, D.C. 20546

OFFICIAL BUSINESS
PENALTY FOR PRIVATE USE $300

SPECIAL FOURTH-CLASS RATE BOOK

POSTAGE AND FEES PAID
NATIONAL AERONAUTICS AND SPACE ADMINISTRATION
451

U.S.MAIL

POSTMASTER: If Undeliverable (Section 158 Postal Manual) Do Not Return

"The aeronautical and space activities of the United States shall be conducted so as to contribute . . . to the expansion of human knowledge of phenomena in the atmosphere and space. The Administration shall provide for the widest practicable and appropriate dissemination of information concerning its activities and the results thereof."

—NATIONAL AERONAUTICS AND SPACE ACT OF 1958

NASA SCIENTIFIC AND TECHNICAL PUBLICATIONS

TECHNICAL REPORTS: Scientific and technical information considered important, complete, and a lasting contribution to existing knowledge.

TECHNICAL NOTES: Information less broad in scope but nevertheless of importance as a contribution to existing knowledge.

TECHNICAL MEMORANDUMS: Information receiving limited distribution because of preliminary data, security classification, or other reasons. Also includes conference proceedings with either limited or unlimited distribution.

CONTRACTOR REPORTS: Scientific and technical information generated under a NASA contract or grant and considered an important contribution to existing knowledge.

TECHNICAL TRANSLATIONS: Information published in a foreign language considered to merit NASA distribution in English.

SPECIAL PUBLICATIONS: Information derived from or of value to NASA activities. Publications include final reports of major projects, monographs, data compilations, handbooks, sourcebooks, and special bibliographies.

TECHNOLOGY UTILIZATION PUBLICATIONS: Information on technology used by NASA that may be of particular interest in commercial and other non-aerospace applications. Publications include Tech Briefs, Technology Utilization Reports and Technology Surveys.

Details on the availability of these publications may be obtained from:

SCIENTIFIC AND TECHNICAL INFORMATION OFFICE

NATIONAL AERONAUTICS AND SPACE ADMINISTRATION

Washington, D.C. 20546